FRIEDRICH-SCHILLERUNIVERSITÄT JENA Physikalisch-Astronomische Fal

Laser Engineering

winter term 2025/2026

Authors:

MARTIN BEYER

JÖRG KÖRNER

CLEMENS ANSCHÜTZ



Contents

	Introduction	3
	I.1 What is it all about?	3
	I.2 Possible applications	5
Ш	Solid state laser media for diode pumping	9
	II.1 Spectroscopic material parameters and their significance	9
	II.1.1 Pump process - energy deposition	9
	II.1.2 Laser process - amplification	10
	II.1.3 Quantum defect	11
	II.2 Einstein rate equations	13
	II.3 Line Broadening	16
	· · · · · · · · · · · · · · · · · · ·	17
	II.4 Füchtbauer-Ladenburg Equation	
	II.5 Reciprocity Relation (McCumber Relation)	20
	II.6 Application of FL-Method and MC-Relation in Spectroscopy	24
	II.7 Influence of the Laser Host Material	27
	II.8 Unwanted Effects	30
	II.9 Overview on Some Solid State Laser Ions	31
	II.9.1 Atomic doping concentrations	32
	II.9.2 Rare earth metals	33
	II.9.3 Transition metals	34
	II.10 Temperature dependence of the cross sections	35
Ш	Laser Amplification Process	37
	III.1 Level schemes and rate equations	37
	III.2 Pumping	39
	III.2.1 Pump saturation intensity	40
	III.2.2 Numerical solutions of the rate equations	42
	III.2.3 Storage efficiency	44
	III.3 Amplification	47
	III.3.1 Small signal gain	47
	III.3.2 Saturation fluence	49
	III.3.3 Frantz Nodvik solution	51
	III.3.4 Saturation corrected gain	54
	III.3.5 Reduction of the small signal gain	55
1\ /	/ Passanators and good sources	5 7
IV	Resonators and seed sources	57
	IV.1 Basics of the ABCD Matrix method	57
	IV.1.1 Stable Laser Resonator and ABCD matrix	59
	IV.2 Stable laser resonator with Gaussian beams	62
	IV.2.1 Gaussian beams	62
	IV.2.2 Stability condition and <i>q</i> -Parameter	63
	IV.2.3 Limitations of beam size	64

	IV.3	Unstable Cavities	66
		IV.3.1 Hard-edge resonator	66
		IV.3.2 Graded reflectivity mirror resonator	68
		IV.3.3 Gain modulation resonator	69
	IV.4	The Active Cavity	71
		IV.4.1 Q-switch operation	74
		IV.4.2 Cavity Dump	76
		IV.4.3 Mode Locking	77
		IV.4.4 Single Mode Operation	79
V	Λ	1:6:	01
V		nplifiers	81
	V.1	Regenerative amplifiers	83
	V.2	Multi-pass amplifiers	83
		V.2.1 Butterfly	os 83
	V.3	Design limitations	os 86
	v.3	V.3.1 Amplified spontaneous emission (ASE)	86
		V.3.2 Laser Induced Damage Threshold	90
		V.3.3 Nonlinear effects	92
		V.3.4 Beam Distortions	94
		V.3.5 Thermal lensing	96
		V.3.6 Air breakdown	98
		v.s.o All bicardown	50
VI	Die	ode lasers as pump source	99
	VI.1	Laser diode basics	99
		VI.1.1 Electrical characteristic	100
		VI.1.2 Output spectrum	100
	VI.2	Power scaling	101
	VI.3	Beam shaping	103
		VI.3.1 Homogenization with an imaging micro-lens array (MLA)	103
		VI.3.2 compaction	105
١/١	L D.	am Characterization	107
VI			107
	V11.	Spatial characterization	
		VII.1.1 Beam parameter product	
		VII.1.3 Beam quality factor - M ²	
		VII.1.3 beam quanty factor - M	
	ип	2Temporal characterization	
	V 11.2	VII.2.1 Pulse length	
		VII.2.2 Pulse contrast	
	улт з		113
	V 11.	•	114
		VII.3.1 Spectral intensity	
		vii.o.2 opectiai piiase	110
Α	Ар	pendix - Frantz-Nodvik calculations	119
		•	119
			121

Preface and structure

Since I was a university student myself, I have missed accompanying literature in many lectures. Professors often write long texts on the board and the entire lecture consists of copying them down, or a PowerPoint presentation is given. My goal is to summarise all the lecture content in detail in a script that students can use during the lecture to get an overview of the topic at hand. At the same time, I want to highlight the most important points on the board so that the central content of the lecture can be reinforced by copying it down. It is also important to me to relate all the material to the lecture and discuss it in detail. Only then can the learning process take place effectively. A PowerPoint presentation should only be used as a support, but should not make up the entire lecture.

As this script now exceeds 100 pages in length, it is important to clearly highlight the key content and findings. To this end, the script contains several types of boxes in different colours, which are explained below.

Equation: Einstein rate equations

$$\frac{\partial N_1}{\partial t} = -\frac{\partial N_2}{\partial t} = (B_{21}N_2 - B_{12}N_1) \cdot \varrho(v) + A_{21}N_2$$

This box is used to highlight the most important equations throughout the script.

Key point: Lecture box

This is a box to summarize the relevant points of a section with important key notes.

Mathematical derivation

In this box we show the mathematical derivation of a formula for the sake of completeness. The derivation itself is generally not important for the lecture but is still shown for students who are interested.

Example: Showing an example

Here we show an example of some previously introduced concept.

Comment: Comment box

This box is used to introduce notations or conventions (especially if they differ from cited literature) or comment on caveats of a specific physical concept.

I. Introduction

This book is intended for students of laser physics who want expand their theoretical knowledge of lasers with the engineering aspects of designing a laser system. We will divide the book into several sections.

In chapter II we will start with an in-depth characterization of solid-state laser materials, discussing the significance of their spectroscopic properties and how to measure them experimentally.

We will then discuss the laser amplification process in chapter III by solving a system of rate equations and consider saturation and reabsorption effects.

In chapter IV we will move the discussion to different types of resonators and to the different sources of generating a laser pulse. Chapter V deals with different kinds of amplifiers and their limitations in generating high power laser pulses.

Diode lasers are the most power-efficient pump sources for a high intensity laser system with great overlap to the absorption spectrum of typical solid-state laser materials. Their working principle and beam shaping techniques are therefore discussed in chapter VI.

Finally, we want to mention different kinds of techniques in chapter VII to spatially measure a high-power laser pulse and characterize its spectral and temporal domain.

In the introduction of this book we want to provide a short overview about the special properties of solid-state lasers, especially Ytterbium as the dopant material, as it will be the main point of discussion and compared to other laser materials in this book.

I.1. What is it all about?

The field of lasers covers a vast range of different types of lasers. In this book we will mainly discuss the basics that are needed to understand and develop a special kind of laser, the so called High Energy Class Diode Pumped Solid State Laser (HECDPSSL) with Ytterbium as its active laser material. What does this mean?

- We concentrate our discussion on bulk solid state lasers. This excludes other geometries like fiber lasers, which are not suitable for high energy applications, as the damage threshold of solid state fibers is too low. Furthermore, we will focus on end-pumped systems where the pump light and laser light are collinear, which leads to highly efficient lasers with excellent beam quality. Therefore, we also exclude disc lasers from our discussion, as they are typically pumped under oblique incidence.
- We talk about diode pumped lasers, as they allow a better spectral overlap to the absorption bandwidth of the laser material than a conventional flash lamp (c. f. figure I.1). Furthermore, the diode lasers are highly efficient in the conversion of electrical to optical power (≈ 60%) and can be scaled up to high output powers (several kW) by stacking laser diode bars. Therefore, the increase in efficiency using diode lasers as a pump source is particularly interesting for high power systems.
- The goal is to realize high energy output pulses, meaning several milli-Joule to multi Joule. This means the laser will:
 - be pulse pumped (otherwise the average power will be too high) with pulse durations in the order of milliseconds.

I. Introduction

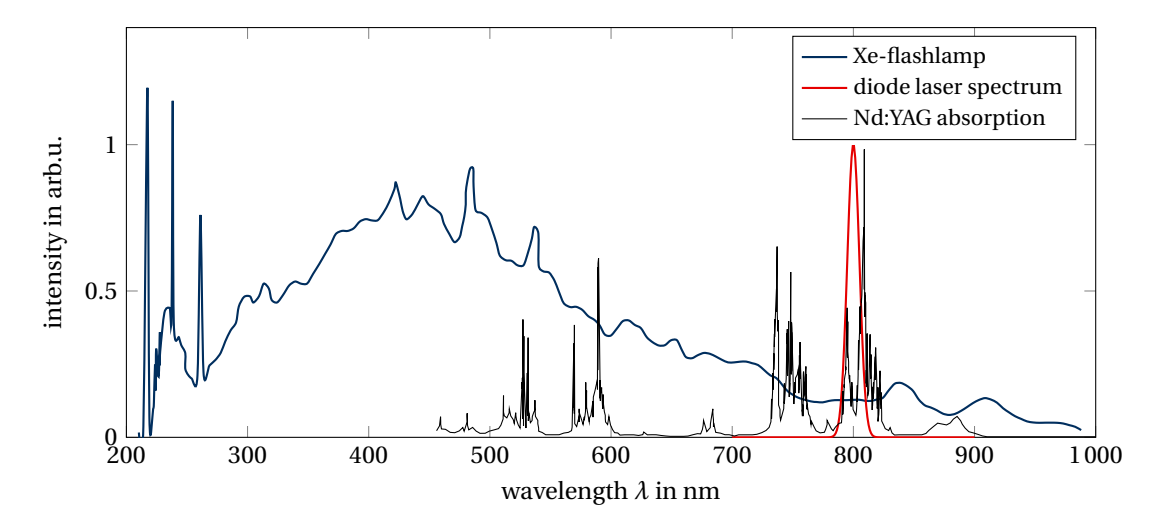


Fig. I.1.: Comparison of the emission spectrum of a Xe-flashlamp (Data taken from [Lin+99]) and a laser diode used for the pumping of a Nd:YAG laser (spectrum taken from [Zhu+13]).

- produce short output pulses depending on the type of seed source. Q-switched lasers produce nanosecond pulse durations, whereas mode-locked lasers produce femtosecond pulses.
- Based on these preconditions, most practical lasers in this field are based on materials either doped with rare earth metals such as Yb³⁺, Nd³⁺, Er³⁺, or Tm³⁺. Hence, we will focus on these materials.

The goal of this lecture is to give a basic understanding of the physics behind high energy lasers, their technical challenges and how to overcome them. We also want to explain principles (e.g. cavity designs) that set them apart from classical lasers.

I.2. Possible applications

In the following we want to discuss several possibilities of applying high energy class solid state lasers in science and industry.

Basic research

High-intensity laser systems are the new frontier to discover and study new concepts in physics such as in quantum field theory:

• *Axions*: The axion is a hypothetical elementary particle with no electric charge and zero spin. Theoretical considerations of quantum chromodynamics (QCD) require a violation of charge-parity (CP) symmetry, but this has not been observed. A CP violation would predict an electric dipole moment of up to $p = 10^{-16}$ ecm for the neutron, which has not been measured. The sofar only valid solution to the strong-CP problem predicts another pseudo-scalar particle (axion) which in many respects behaves like the neutral pion π_0 , in particular, it has a nonzero mass m and can couple to two photons $\phi \leftrightarrow 2\gamma$. The proposed experiment to test this theory is rather simple: Shine a laser onto a wall and try to observe photons behind the wall. Use a strong magnetic field to convert part of the photon wave (function) into an axion in front of the wall and back into a photon behind the wall. Since the axion is weakly interactive, it can traverse the wall in contrast to photons. The required laser intensity for this lies beyond the Petawatt regime. So far, no axions have been observed.

See: C. Robilliard et al. "No "Light Shining through a Wall": Results from a Photoregeneration Experiment". In: *Physical Review Letters* 99.19 (Nov. 2007)

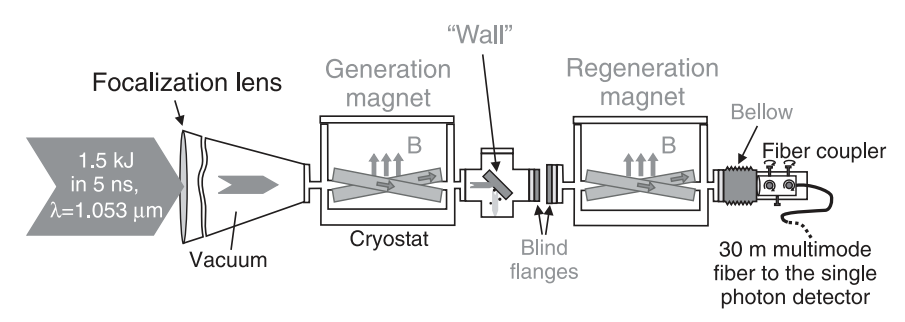


Fig. I.2.: Experimental setup by [Rob+07]. A high power laser pulse is focused onto a wall with two magnetic fields of B > 10T in front and behind the wall. Then, a detector is placed behind the wall to detect re-converted photons.

• *Vacuum birefringence*: The interaction of light an matter are described by quantum electrodynamics (QED). The QED Lagrangian couples photons to charged Dirac particles. For small photon energy but high intensity, nonlinear terms induced by QED predict pair production in a constant electric field, which is an absorptive process. This process can occur for field strengths larger than the *Schwinger-limit* given by

$$E_c = \frac{m_e^2}{e} \approx 1.3 \times 10^{18} \,\mathrm{Vm}^{-1}.$$
 (I.1)

However, the associated intensity with this field strength is $I_c = 4.4 \times 10^{29} \,\mathrm{W\,cm^{-2}}$, which is out of experimental reach for now. Alternatively, one may also observe dispersive effects like the *birefringence of the vacuum* with current laser systems. The detection of this is done by a high intensity laser pulse inducing the birefringence and a second probe beam to analyze any sort of polarization change when passing through the focus of the first pulse as shown in figure I.3.

See: [Hei+06; Kar+15]

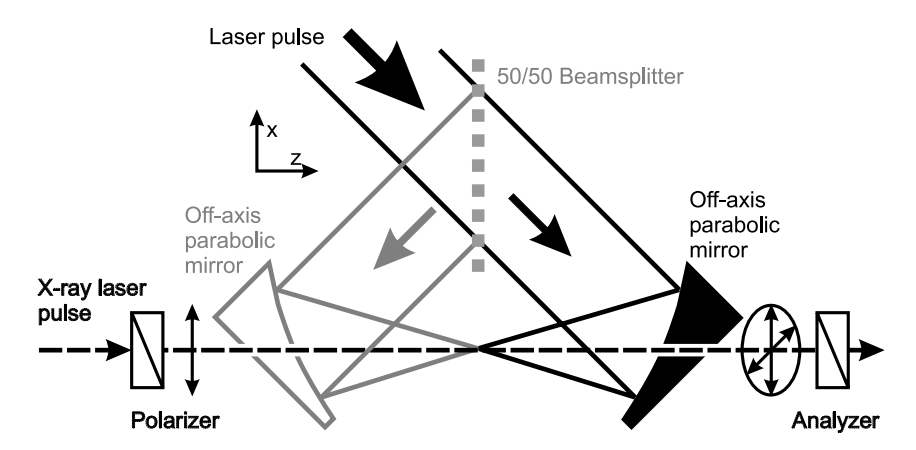


Fig. I.3.: Proposed experimental setup by [Hei+06]. A high intensity laser pulse is focused by an off-axis parabolic mirror with a drilled hole in such away that an X-ray pulse can travel through the focal region of the high intensity laser pulse. The ellipticity of the X-ray pulse may then be detected using a polarizer-analyzer pair. The setup can be extended in (grey) for a generation of a high-intensity standing wave by two counter propagating pulses which may be used for pair creation.

Secondary radiation source

High intensity laser systems can be used as a source of secondary radiation which is usually not accessible with conventional laser systems due to the lack of laser transitions in the XUV. There are different models to generate new sources of radiation which all involve high-nonlinear processes such as

• *X-ray sources and FEL*: When a high-intensity light-pulse is focused on a target (e.g. helium gas jet), a plasma is created in the target sustaining electric fields exceeding 100 GV m⁻¹. Then, using the ponderomotive forces arising from the light pressure of the intense laser field, a plasma wave is excited. This plasma wave trails behind the laser pulse at nearly the speed of light and rapidly accelerates particles to very high energies, analogous to a surfer (particle) acquiring momentum from a water (plasma) wave.

See: H-P Schlenvoigt et al. "A compact synchrotron radiation source driven by a laser-plasma wakefield accelerator". In: *Nature Physics* 4.2 (2008)

- *High harmonic generation* (HHG): When the electric field strength of the laser field approaches the atomic bonding strength of a material, extremely nonlinear optical effects start to emerge. The process of high-harmonic generation can be understood by a three-step re-collision model, comprising of tunnel ionization of an electron, free acceleration in the laser field and recombination with the atom. HHG forms the basis of attosecond science.
 - See: Shambhu Ghimire and David A. Reis. "High-harmonic generation from solids". In: *Nature Physics* 15.1 (Nov. 2018)
- Attosecond pulses: The generation of attosecond pulses requires a broad spectral bandwidth and precises spectral phase control. High-harmonic generation provides pulse trains with ultrabroad spectral bandwidths in the XUV and soft X-ray spectral region with a flat *plateau* spectrum. The high-harmonic cutoff energy is proportional to the driving laser intensity *I*. Thus, for the exploration of shorter attosecond pulses, even higher laser intensities are needed.
 - See: Michael Chini, Kun Zhao, and Zenghu Chang. "The generation, characterization and applications of broadband isolated attosecond pulses". In: *Nature Photonics* 8.3 (Feb. 2014)

Laser-particle-acceleration for medical therapy

The use of lasers for the generation of high energy ions for medical applications is a promising field of research. They are especially useful in cancer therapy as the area of effect of the radiation in biological tissue can be precisely tailored using protons instead of electrons or gamma radiation. The generation of fast ions becomes highly effective when the laser radiation reaches the petawatt power limit. Thus, the development of such lasers as a table-top systems for the purpose of creating stable ion beams would create a cost-efficient alternative of conventional accelerators.

See: SV Bulanov et al. "Oncological hadrontherapy with laser ion accelerators". In: *Physics Letters A* 299.2-3 (2002)

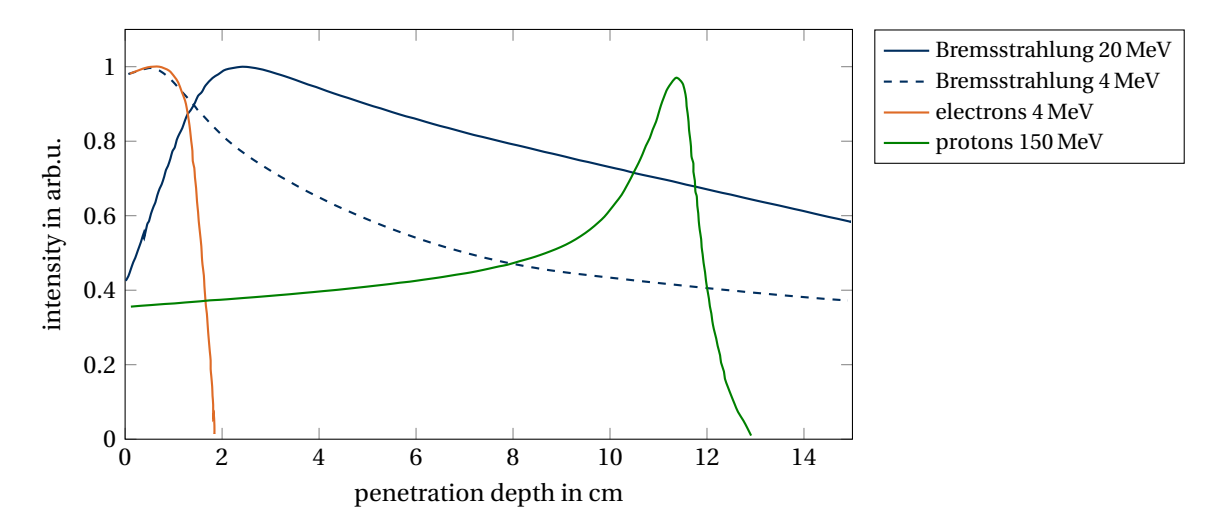


Fig. I.4.: Depth-dose curve of different kinds of radiation in tissue-like material. The dose is normalized to the maximum for all radiation sources. Protons show a narrow peak with a low surface dose which makes them ideal for the treatment of deep tumors. Adapted from [Com07].

Industry

Lasers are of course one of the widely used tool in modern industry. Some applications of high-power laser systems might be:

• Laser shock peening (LSP): A shock wave is generated using a focused laser pulse that exerts a high pressure on a material, which increases the hardness of the material without a big change in the surface structure. Laser shock peening is used to improve the lifetime, wear, crack and corrosion resistance of a material.

See: Sundar R et al. "Laser Shock Peening and its Applications: A Review". In: *Lasers in Manufacturing and Materials Processing* 6.4 (Oct. 2019)

• Laser Inertial fusion: The idea of compressing tiny targets with high-power lasers to ignite thermonuclear fuel has been developed in 1972. In the compressed core of the target, the plasma pressure induces a thermonuclear burn to produce fusion reactions (e.g. deuterium-tritium reaction) with temperatures of tens of millions of degrees to overcome the Coulomb barrier between the fusing nuclei. So far, the furthest progress has been made at the National Ignition Facility (NIF) at the Lawrence Livermore National Laboratory.

See: R. Betti and O. A. Hurricane. "Inertial-confinement fusion with lasers". In: *Nature Physics* 12.5 (May 2016)

Diagnostics

- *Plasma physics*: Study the formation and evolution of laser-induced plasmas used for particle acceleration via optical proping on a sub-picosecond level. The dynamics of an expanding over-dense plasma can be studied using shadowgraphy and then compared to a solid-state interaction model and kinetic plasma description. This provides insight into the interplay of initial ionization, collisions, and expansion of the plasma.
 - See: Yasmina Azamoum et al. "Optical probing of ultrafast laser-induced solid-to-overdense-plasma transitions". In: *Light: Science & amp; Applications* 13.1 (May 2024)
- *Particle Image Velocimetry (PIV)*: We can use ultrashort laser pulses for a time-resolved study of molecular and atomic dynamics on a picosecond level.

II. Solid state laser media for diode pumping

The laser material is the central part of a laser, as it is the place of energy deposition and extraction via stimulated emission. To understand the operation principle of a laser amplifier, the basic understanding of the laser material itself is the most important premise. In this book we focus on solid state laser materials, as they provide the most versatile radiation source, where each output parameter (output power, pulse length, repetition rate, spectral range) can be tailored, as the size, shape, doping concentration etc. can be precisely chosen.

II.1. Spectroscopic material parameters and their significance

When selecting a solid state laser medium, various parameters have to be considered. For now, we will concentrate on the spectral characteristics that define the behaviour of a material within a laser amplifier. For a start we will use simple and naive formulas to get an overview on these parameters and their influence, by modeling the material as a two-level system with a ground energy state $|1\rangle$ and an excited state $|2\rangle$.

II.1.1. Pump process - energy deposition

First of all, we will need to store energy in our material before we start the laser process. As we would like to do this in an optical way, the material should absorb our pump light. Given that the incident intensity of the pump source onto the laser material is given by I_0 , the light intensity of the pump inside the laser material $I_p(z)$ (typically given in [kW/cm²]) changes as a function of the depth z in the material. The absorption can be modeled in a first approximation by the so called Lambert Beer's law:

Equation: Lambert Beer's law

$$\frac{\mathrm{d}I_p}{\mathrm{d}z} = -\alpha \cdot I_p \quad \Rightarrow \quad I_p(z) = I_{p0} \cdot e^{-\alpha z}. \tag{II.1}$$

Here, α is the material dependent absorption coefficient. In a doped laser medium, α can be calculated by

$$\alpha = N_1 \cdot \sigma_a \tag{II.2}$$

where the variables are

- σ_a Absorption cross section (given in [cm²]). The cross section encompasses all the properties of the transition from the ground state $|1\rangle$ to the excited state $|2\rangle$, i. e. the transition probability, spectral line shape and resonance frequency. An explanation of the meaning of a cross-sectional area is given in figure II.1.
- N_1 Number density of atoms in the ground state $|1\rangle$ (given in [cm⁻³]). For now we assume this to be equal to the density of doped ions $N_1 = N_{\rm dop}$ and to be unchanged.

A high absorption cross section will result in a strong absorption, which again allows to reach a high excitation density within the laser material. It got to be further mentioned that $\sigma_a(v)$ is dependent on

$$\Delta I_p = -N_1 \cdot \sigma_a I_p \Delta z \quad \text{with} \quad N_1 = \frac{\mathcal{N}_1}{\Delta V}$$

$$\frac{\Delta I_p}{I_p} = -\mathcal{N}_1 \frac{\sigma_a}{\Delta A}$$

Fig. II.1.: For an intuitive understanding of cross sections we consider an incoming intensity I_p on a volume element $\Delta V = \Delta A \cdot \Delta z$ of the material. We can derive a ratio of the absorbed intensity to the incoming intensity, which turns out to be equal to the number of absorbing ions \mathcal{N}_1 times the cross section over the surface element ΔA . Therefore, σ_a represents an *effective* interaction area, i. e. the probability of the absorption process projected to an area. Thus, σ_a represents the cross-sectional area of the particle, if it would be perfectly absorbing (black circles).

the optical frequency v (respectively the wavelength λ), hence, the pump source and the absorption of our material should be matched.

Further, one has to consider that the excited state population, expressed by the number density of excited ions N_2 , will be depopulated over time due to spontaneous emission (there might be other processes as well, but we neglect these for now):

$$\frac{\partial N_2}{\partial t} = -\frac{N_2}{\tau_f} \quad \Rightarrow \quad N_2 = N_2(t=0) \cdot e^{-\frac{t}{\tau_f}}. \tag{II.3}$$

The time constant, in which an initial population density is reduced by a factor of 1/e is called the *fluorescence lifetime* τ_f . The fluorescence lifetime determines, how long we can store energy within the material.

II.1.2. Laser process - amplification

A laser material should amplify our incoming (seed) laser beam. Neglecting the change in the materials excitation N_2 due to the extraction process and absorption mechanisms at the laser wavelength, the beam amplification (illustrated by its intensity along the optical axis $I_l(z)$ and the incident intensity I_{l0}) can be modeled by:

Equation: Simple gain model

$$\frac{\partial I_l}{\partial z} = g \cdot I_l \quad \Rightarrow \quad I_l(z) = I_{l0} \cdot e^{gz}.$$
 (II.4)

Here, g is the material dependent gain coefficient. In a doped laser medium, g can be calculated by

$$g = N_2 \sigma_{\rm e},\tag{II.5}$$

where the variables are

- $\sigma_e(\nu)$ Emission cross section (given in [cm²]). Similar to the absorption cross section it encompasses all the properties of the transition from the excited state $|2\rangle$ to the ground state $|1\rangle$ via stimulated emission. It is a measure for the probability that the photon flux will be amplified by an excited atom. Hence, a higher gain is obtained for a higher σ_e .
- N_2 Number density of atoms in the excited state $|2\rangle$ (given in [cm⁻³]).

Furthermore we should consider that $\sigma_e(v)$ is dependent on the optical frequency v. If we want to amplify ultra short pulses the time band width product (assuming a Gaussian pulse here)

$$\Delta t \Delta v = \frac{2 \cdot \ln 2}{\pi} \tag{II.6}$$

demands a certain amplification bandwidth. Hence, σ_e should be sufficiently large and have as low as possible modulations over the entire spectral bandwidth.

Last but not least we want to be as efficient as possible with our laser. Hence, though we neglected it in our first attempt here, there got to be a significant change in the materials inversion and also its gain when extracting the energy with the seed laser pulse. To estimate the intensities involved in such processes, a parameter called *saturation fluence* $F_{\rm sat}$ is very convenient as it is directly linked to the materials cross sections. It represents the fluence in J cm⁻² needed to reduce the laser mediums gain by a factor of 1/2 (continous wave laser) or $^{1/e}$ (pulsed laser) within a single pass. For now we only want to give the definition of this parameter (it will be discussed later in section III.3.2)

$$F_{\text{sat}} = \frac{hv_l}{\sigma_{\text{a}}(v_l) + \sigma_{\text{e}}(v_l)}.$$
 (II.7)

Here, hv_l is the laser photon energy in the emission process. If we now want to be efficient, our laser should operate with an extraction fluence higher or at least in the range of $F_{\rm sat}$. But as we will discuss later on, the fluence is limited by the Laser Induced Damage Threshold (LIDT). Hence, a low saturation fluence is preferable for an efficient and safe laser amplifier (at least in pulsed mode).

II.1.3. Quantum defect

The main limit for the average power that can be achieved with a laser system is the heat generated within the active medium. Assuming an otherwise 'perfect' laser material, meaning that there are no parasitic heat sources (we may discuss such effects later), the sole source of heating is the so called quantum defect q_{QD} , which is the energetic difference between the pump and the laser wavelength:

$$q_{OD} = E(v_n) - E(v_l) = h(v_n - v_l).$$
 (II.8)

This energy is typically lost in non-radiating processes in the form of heat. Therefore, we can define the fraction of lost energy as a measure of the minimal heat fraction η_{QD} (efficiency of the laser transition) stored in the laser crystal:

Equation: Heat fraction

$$\eta_{\rm QD} = \frac{q_{\rm QD}}{E(\nu_p)} = \frac{h(\nu_p - \nu_l)}{h\nu_p} = 1 - \frac{\nu_l}{\nu_p} = 1 - \frac{\lambda_p}{\lambda_l}.$$
(II.9)

Therefore, looking for an ideal material, laser wavelength and pump wavelength should be as close together as possible. However, as we will see later, realizing this is not trivial due to re-absorption effects taking place at the laser wavelength when both transitions are too close together. Of course $\lambda_l > \lambda_p$ has to be fulfilled as otherwise the second main theorem of thermodynamics will be violated. So far it is not possible to build a laser, that is cooled by its own laser transition (at least not with optical pumping).

Example: Heat fraction of various laser ions

Table II.1.: Heat fraction of typical doping ions. For the calculation, the most commonly used laser transition and pumping wavelength was chosen. In reality, these values may differ due to the host material and the use of other available transitions.

doping ion	pump wavelength	emission wavelength	$\eta_{ m QD}$
Nd ³ +	810 nm	1064 nm	24%
Yb^3+	940 nm	1030 nm	8.7%
Er ³ +	980 nm	≈1600 nm	38.8%
Tm ³ +	≈1700 nm	≈2000 nm	15 %

Key point: The dream material

With these basic considerations we now can formulate wishes for our ideal laser material:

- long fluorescence lifetime to store as much energy in our material as possible with given pump power (especially important for diode pumping)
- huge and broad absorption and emission cross sections
- · low separation of pump and laser wavelength

We will now make a basic derivation of each of the parameters to see, whether our dreams can come true or if there are relations between those parameters that prohibit such a material.

II.2. Einstein rate equations

We will start with the derivation of the very basic formulas originally introduced by Einstein. The following derivation closely follows [Koe06, p.14].

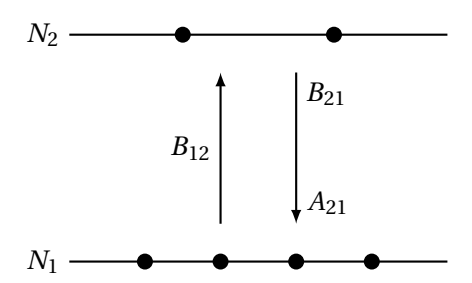


Fig. II.2.: Two level system with Einstein coefficients.

We start with a simple two level scheme with the population densities N_1 and N_2 for the lower and upper level respectively (c.f. figure II.2). The levels are non degenerated, meaning, that each atom can either be in the lower or the excited state. Hence, the total number of atoms (equaling the doping concentration of a laser medium) is obtained by:

$$N_1 + N_2 = N_{\text{dop}}.$$
 (II.10)

Transitions between those levels are done either by emitting or absorbing radiation with the according energy difference:

$$E_2 - E_1 = hv = \frac{hc}{\lambda}.\tag{II.11}$$

Here $h = 6.626 \times 10^{-34}\,\mathrm{J}\,\mathrm{s}$ is the Planck constant, $c = 3 \times 10^8\,\mathrm{\frac{m}{s}}$ the speed of light, v the frequency, and λ the wavelength of the according radiation. For now we will only consider single photon transitions. Multi-photon transitions or non-radiating transitions will be neglected.

There are two possible interactions with incoming radiation: absorption and amplification, and one process generating radiation, the spontaneous emission.

Absorption

When an incident electromagnetic wave with matching energy and the spectral radiation energy density $\varrho(v) = [J/(m^3 s)]$ interacts with an atom in the ground state it is absorbed and excites the atom. A measure for the probability is the Einstein coefficient B_{12} :

$$\frac{\partial N_1}{\partial t} = -B_{12} \cdot \varrho(v) \cdot N_1. \tag{II.12}$$

Stimulated emission

This is the inverse absorption process and the one that will allow us to achieve amplification later on. It is described in the same way as the absorption with B_{21} as coefficient:

$$\frac{\partial N_2}{\partial t} = -B_{21} \cdot \varrho(v) \cdot N_2. \tag{II.13}$$

The emitted radiation is in phase with the external radiation.

Spontaneous emission

This process describes the spontaneous decay of an excited state. As a statistical process, there is no phase relationship between each individual emission process, the radiation is incoherent. The probability of emission is proportional to the upper state population. The probability factor is A_{21} .

$$\frac{\partial N_2}{\partial t} = -A_{21}N_2 \tag{II.14}$$

Solving this differential equations results in:

$$N_2(t) = N_2(t=0) \cdot e^{-A_{21}t}$$
 (II.15)

At the time where $t = 1/A_{21}$ the initial number of excited atoms is reduced by a factor of 1/e. We will define this time constant as the radiative lifetime $\tau_{\text{rad}} := [s]$ of the transition.

$$\tau_{\rm rad} = \frac{1}{A_{21}}.\tag{II.16}$$

This is the first accessible characteristic property of our laser material. It can be obtained e.g. by measuring the decay curve of an excited material (cf. figure II.3). The retrieved lifetime from such a measurement is τ_f , which can be considered equal to $\tau_{\rm rad}$ as long as no parasitic defects contribute.

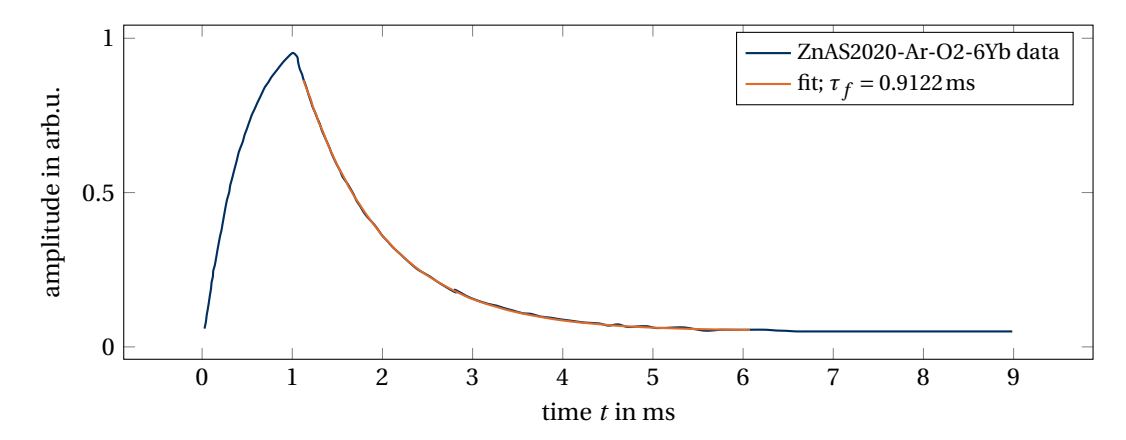


Fig. II.3.: Measurement of the excitation and decay curve for a Yb³⁺-doped glass under pulsed excitation. The orange line indicates the fitting curve used to determine the lifetime.

We now combine all three processes:

Equation: Einstein rate equations

$$\frac{\partial N_1}{\partial t} \stackrel{\text{(II.10)}}{=} - \frac{\partial N_2}{\partial t} = (B_{21}N_2 - B_{12}N_1) \cdot \varrho(v) + A_{21}N_2 \tag{II.17}$$

In thermal equilibrium there are no net changes in the population. Hence $\frac{\partial N_1}{\partial t} = 0$:

$$A_{21}N_2 + B_{21}N_2 \cdot \rho(\nu) = B_{12}N_1 \cdot \rho(\nu)$$
 (II.18)

Further in thermal equilibrium the ratio of the excited vs. the unexcited atoms is given by Boltzmann's law:

$$\frac{N_2}{N_1} = \frac{d_2}{d_1} e^{-\frac{E_2 - E_1}{kT}} \tag{II.19}$$

Note that if the degeneracies d_1 and d_2 of the lower and the upper level are different, we would have to add this to our equation. However, for simplicity we will neglect this in our simple model (and add the correction at the end) and can transform equation (II.18):

$$e^{-\frac{E_2 - E_1}{kT}} \cdot (A_{21} + B_{21}\varrho(v)) = B_{12}\varrho(v)$$

$$\Rightarrow \varrho(v) \cdot \left[B_{12} - e^{-\frac{E_2 - E_1}{kT}} \cdot B_{21} \right] = e^{-\frac{E_2 - E_1}{kT}} \cdot A_{21}$$

$$\varrho(v) = \frac{e^{-\frac{E_2 - E_1}{kT}} \cdot A_{21}}{B_{12} - e^{-\frac{E_2 - E_1}{kT}} \cdot B_{21}}$$

$$\varrho(v) = \frac{A_{21}}{B_{12} \cdot e^{\frac{E_2 - E_1}{kT}} - B_{21}}$$

$$\varrho(v) = \frac{A_{21}}{B_{21}} \frac{1}{\frac{B_{12}}{B_{21}} \cdot e^{\frac{E_2 - E_1}{kT}} - 1}$$
(II.20)

This can be compared with Plank's law (in a frequency interval dv):

$$\varrho(v) = \frac{8\pi h v^3}{c^3} \cdot \frac{1}{e^{\frac{hv}{kT}} - 1}$$
 (II.21)

Hence we obtain the so called Einstein relations

Equation: Einstein relations

$$\frac{A_{21}}{B_{21}} = \frac{8\pi h v^3}{c^3}$$
 and $\frac{d_2}{d_1} \cdot B_{21} = B_{12}$. (II.22)

From this equation we can deduce a very important fact: The higher the spontaneous emission at a given wavelength, the higher the stimulated emission will be. In other words, the longer the radiative lifetime $\tau_{\rm rad}$ of the upper state is, the lower the stimulated emission will be. We will see later why this may cause problems in our quest to find an ideal laser material.

Comment: Einstein relations

- 1. The relation between both processes can be understood by noting that both involve the quantized interaction of atoms with photons. Stimulated emission is directly related to the external field, while spontaneous emission is a result of vacuum fluctuations, derive from quantum electrodynamics.
- 2. The given speed of light in these equations is within the host material! Hence, if we want to use the vacuum speed of light $c_0 = cn$ the refractive index n got to be included:

$$\frac{A_{21}}{B_{21}} = \frac{8\pi h n^3 v^3}{c_0^3} \tag{II.23}$$

- 3. If the degeneracies $d_{1/2}$ of the levels are different, the ratio between B_{21} and B_{21} is not 1.
- 4. The Einstein relations also explain, why the operation of lasers at lower wavelengths (e.g. in the UV-regime) is much harder as for IR-lasers, because the spontaneous emission starts to dominate over the stimulated emission.

II.3. Line Broadening

In real materials the energy difference of a specific transition, and hence also the wavelength, is not a discrete value. This is also called line broadening. We do not want to discuss the details of different line broadening mechanisms here, but rather give some basic ideas by following [Koe06, ch.1.3.1] In principle there are two different types of line broadening:

homogeneous The broadening is generated by each single atom. Examples are:

- lifetime broadening: Fourier Transform Limit (FTL) pulse length
- collision broadening (gases): The emission is discontinued due to atomic collisions → FTL
- dipolar broadening: interaction of magnetic / electric fields of neighboring atoms, results are similar to collision broadening
- thermal broadening: caused by the influence of lattice vibrations of the host medium on the transition

The resulting frequency line shape $g(v, v_0)$ in this case is a Lorentz distribution:

$$g_{\rm L}(\nu, \nu_0) = \frac{\Delta \nu}{2\pi} \cdot \left[(\nu - \nu_0)^2 + \left(\frac{\Delta \nu}{2} \right)^2 \right]^{-1}$$
 (II.24)

inhomogeneous The spectrum of individual atoms is shifted vs. one another:

- Doppler Broadening: caused by movement of atoms
- inhomogeneity: Atoms are situated in different environments (glasses, inhomogeneous crystals).

The resulting frequency line shape in this case is a Gaussian distribution:

$$g_{\rm G}(v, v_0) = \frac{2}{\Delta v} \cdot \sqrt{\frac{\ln 2}{\pi}} \cdot \exp\left[-4\ln 2\left(\frac{v - v_0}{\Delta v}\right)^2\right]$$
 (II.25)

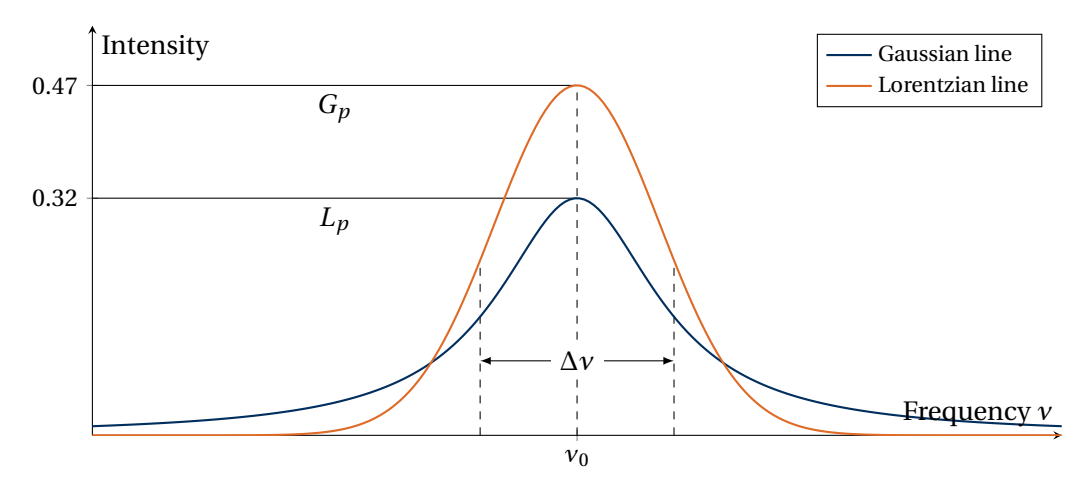


Fig. II.4.: Normalized Gaussian and Lorentz distribution with same width Δv Full Width at Half Maximum (FWHM). G_p and L_p are the peak intensities.

Both spectral shapes are displayed schematically in figure II.4. In a real laser material we will see a combination of all these effects. Therefore, for the description of real materials the broadening of the transition lines is better described by a *Voigt*-profile, which is given by a convolution of the Gaussian and Lorentz distribution

$$g(v, v_0) = \int_{-\infty}^{\infty} g_{G}(v', v_0) g_{L}(v' - v, v_0) dv.$$
 (II.26)

This integral has no analytical solution, which complicates the process of fitting the line function to a measured line spectrum. However, it has been proposed [SC97] to use a pseudo-voigt function to approximate the line function of *n*-transitions in the following way:

$$g(v) = \sum_{k=1}^{n} A_k \left[\xi_k \frac{\Delta v_k^2}{4(v - v_k)^2 + \Delta v_k^2} + (1 - \xi_k) \sqrt{\frac{4\ln(2)}{\pi}} \exp\left(-\frac{4\ln 2}{\Delta v_k} (v - v_k)^2\right) \right].$$
 (II.27)

Here, A_k is the oscillator strength, Δv_k the line width, v_k the center frequency and ξ_k a parameter which contains the relative contributions of Lorentz- and Gaussian broadening. The form of the constant amplitude A_k for each line was chosen in such a way that it is independent on the width of the spectra, because Δv_k vanishes in the case of $v = v_k$.

II.4. Füchtbauer-Ladenburg Equation

As we have just discussed, in real materials there are no discrete spectral lines. Hence we have to modify our rate equation (II.18). For this we will assume that for a transition we have a certain probability following the atomic line shape¹ to match the energy (or frequency) of an incident radiation field:

$$N_2(v) = g(v) \cdot N_2 \tag{II.28}$$

As N_2 is the total number of excited states, we got to ensure, that:

$$\int_0^\infty N_2(v)dv = N_2 \cdot \int_0^\infty g(v)dv = N_2 \quad \Rightarrow \quad \int_0^\infty g(v)dv \stackrel{!}{=} 1$$
 (II.29)

The so called line function g(v) represents the spectral shape of the transition. We now consider a rate equation representing the total change in the materials inversion density combining the Einstein equations for absorption and stimulated emission (We will neglect the spontaneous emission $A_{21} = 0$). Further we use the relation $B_{21} = B_{12}$ (note that we assume no degeneracies). Then we can rewrite equation (II.2):

$$-\frac{\partial N_1}{\partial t} = \varrho(v)B_{21} \cdot (N_1 - N_2). \tag{II.30}$$

As this is only valid within a spectral range, we want to know the total number density N_{tot} of atoms that can interact with an incident light field within a certain spectral range:

$$N_{\text{tot}} dv = (N_1 - N_2) \cdot g(v) dv$$
 (II.31)

With this we make the following changes to the rate equation:

$$\rho(v) \to \rho(v) dv$$
 (II.32)

$$B_{21} \cdot (N_1 - N_2) \to B_{21} \cdot (N_1 - N_2) \cdot g(v)$$
 (II.33)

¹Since for real materials we cannot describe the line-shape with a single Pseudo-voigt function but rather a collection of them, we will drop the parameter v_0 in the following.

Furthermore we can express the change to the population density by the change of the energy density:

$$\frac{\partial N_1}{\partial t}hv = \frac{\partial(\varrho(v)dv)}{\partial t} \tag{II.34}$$

With these modifications our rate equation (II.30) now reads:

$$-\frac{\partial(\varrho(v)dv)}{\partial t} = hv\varrho(v)dvB_{21} \cdot (N_1 - N_2) \cdot g(v)$$
 (II.35)

Assuming a small line width of the radiation field we obtain by integrating both sides:

$$-\frac{\partial \varrho(v)}{\partial t} = hv\varrho(v)B_{21} \cdot (N_1 - N_2) \cdot g(v)$$

$$-\frac{\partial \varrho(v)}{\partial z} \frac{\mathrm{d}z}{\mathrm{d}t} = -\frac{\partial \varrho(v)}{\partial z} c = hv\varrho(v)B_{21} \cdot (N_1 - N_2) \cdot g(v)$$
(II.36)

If we solve this differential equation we obtain:

$$\varrho(v) = \varrho_0(v) \cdot \exp\left[\frac{hv}{c}B_{21} \cdot (N_1 - N_2) \cdot g(v) \cdot z\right]$$
 (II.37)

If we compare this with the "naive" equation for the gain $(N_1 = 0)$ we can identify:

$$\sigma_{\rm e} = \frac{hv}{c} B_{21} \cdot g(v) \tag{II.38}$$

We now include the Einstein equations:

$$B_{21} = \frac{A_{21}c^3}{8\pi h v^3}$$
 and $A_{21} = \frac{1}{\tau_{\rm rad}}$ \Rightarrow $\sigma_{\rm e} = \frac{c^2}{8\pi \tau_{\rm rad} v^2} \cdot g(v)$. (II.39)

If we finally include the refractive index n of the material and we express the line-function in terms of wavelengths, we obtain the so called Füchtbauer-Ladenburg (FL) equation:

Equation: Füchtbauer-Ladenburg equation

$$\sigma_{\rm e} = \frac{\lambda^2}{8\pi n^2 \tau_{\rm rad}} \cdot g(\lambda) \quad \text{with} \quad g(\lambda) = \frac{\lambda^3}{c} \frac{I_{\lambda}}{\int \lambda I_{\lambda} \, d\lambda}. \tag{II.40}$$

The line-function g can be determined using a spectral fluorescence measurement I_{λ} . So what does Füchtbauer-Ladenburg (FL) tell us?

Key point: Results from Füchtbauer-Ladenburg (FL)

- $\sigma_e \propto \frac{1}{n^2}$. The emission scales inversely with the refractive index, because the wavelength shortens inside the material compared to the vacuum.
- $\sigma_e \propto \frac{1}{\tau_{rad}}$. The longer the radiative lifetime is, the smaller the emission cross section becomes. This follows directly from the Einstein equations which relate spontaneous and stimulated emission.
- The absolute value σ_e is limited by the bandwidth, as g(v) is normalized!

Hence, we have to say goodbye to our dream material. However, the question remains if we can at least rescue the as low as possible quantum defect as an universal optimization parameter?

Determining of the line-function

In equation (II.40) we give a formula, how to calculate the line-function $g(\lambda)$ from a spectral fluorescence measurement $I(\lambda)$. In the following, we want to derive this formula. We note that the spectral intensity I_v is proportional to the photon energy hv times the spectral line function, which can be written as

$$I_{\nu} = \mathcal{C} \cdot h\nu \cdot g(\nu)$$
 with $\int g(\nu) \, d\nu = 1$. (II.41)

Here, \mathscr{C} is an unknown proportionality constant. Using the normalization of g(v) we can get rid of \mathscr{C} and find an expression for g(v):

$$1 = \int g(v) \, dv = \int \frac{Iv}{\mathscr{C}hv} \, dv \quad \Rightarrow \quad \mathscr{C} = \int \frac{I_v}{hv} \, dv \quad \Rightarrow \quad g(v) = \frac{I_v}{\cancel{h}v \int \frac{I_v}{\cancel{h}v} \, dv}. \tag{II.42}$$

Finally, we need to express g(v) as a function of wavelength using $I_{\lambda} = I_{\nu} \frac{dv}{d\lambda} = I_{\nu} \cdot \frac{c}{\lambda^2}$

$$g(\lambda) = \frac{\lambda^2}{c} \frac{I_{\lambda}}{\frac{1}{\lambda} \int \lambda \cdot \frac{\lambda^2}{c} I_{\lambda} \cdot \frac{c}{\lambda^2} d\lambda} = \frac{\lambda^3}{c} \frac{I_{\lambda}}{\int \lambda I_{\lambda} d\lambda} \quad \text{with} \quad dv = \frac{c}{\lambda} d\lambda$$
 (II.43)

II.5. Reciprocity Relation (McCumber Relation)

We now want to look at how the absorption and emission cross sections relate to each other. This is useful to determine the emission cross section from an absorption measurement. The following derivation follows [Pay+92]. According to McCumber [McC64] we can calculate the overall cross sections of a transition using:

$$\sigma_{e}(v) = \sum_{ij} d_{j} \left[\frac{\exp\left(-\frac{E_{j}}{kT}\right)}{Z_{u}} \right] \sigma_{ji}(v) d_{i}$$
 (II.44)

$$\sigma_{a}(v) = \sum_{ij} d_{i} \left[\frac{\exp\left(-\frac{E_{i}}{kT}\right)}{Z_{l}} \right] \sigma_{ij}(v) d_{j}$$
 (II.45)

The variables are the:

 $\sigma_{ij/ji}(v)$ cross section of single transition incl. line shape. The total line shape of the material is then a supercomposition of the single transition lines (cf. figure II.5).

 d_i, d_i degeneracies of the according levels

 E_i , E_j energy of sub levels measured from the lowest multiplet level

 $Z_{u/l}$ partition function of upper (u) and lower (l) manifold:

$$Z = \sum_{k} d_k e^{-\frac{E_k}{kT}} \tag{II.46}$$

k,T Boltzmann factor, temperature

The factor in square brackets represents the fractional thermal occupation of the j'th or i'th level, of the upper and lower multiplets. Hence, we assume that the occupation of the sub-levels is always in thermal equilibrium. Note that the partition functions also depend on temperature (c.f. figure II.7).

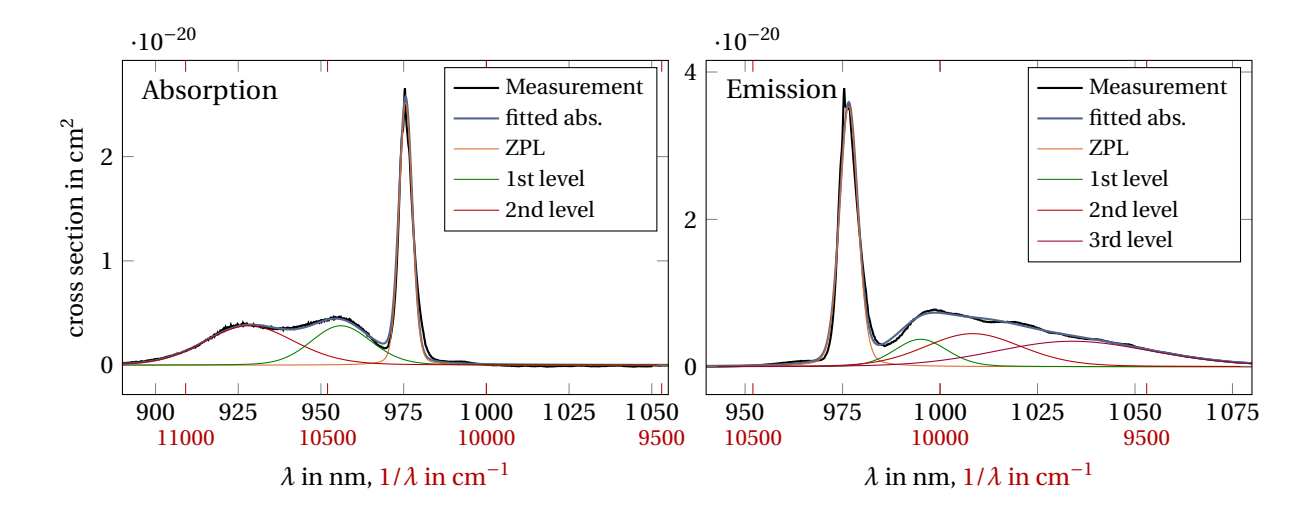


Fig. II.5.: Composition of real spectra from single lines for Yb:FP15 glass at $T = 100 \, \text{K}$. In the absorption case, the spectrum is determined by the three line transitions from the ground state to the three states in the upper manifold.

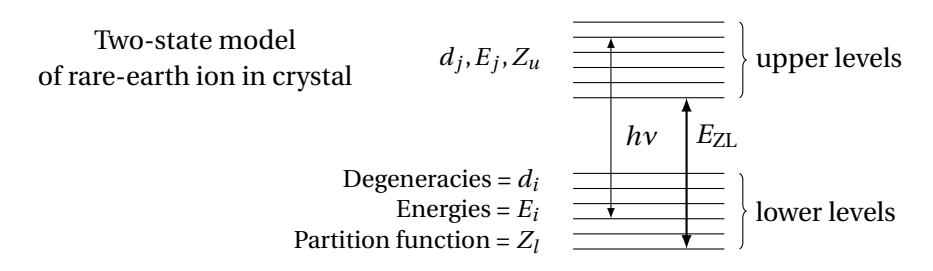


Fig. II.6.: Generic representation of the crystal field levels of the ground and excited states of a rare-earth impurity ion. The degeneracies (d) and energies (E) of the levels of the lower (i) and upper (j) electronic states are indicated, as well as the partition functions, Z_l and Z_u . The cross section between the i-th and j-th levels is equal to σ_{ij} (or σ_{ji} , by reciprocity). The energy of the zero-line between the lowest crystal field components of the electronic states is E_{ZL} . Adapted from [Pay+92].

In a high temperature limit, they simply represent the sum of the degeneracies of each manifold. A representation of the level scheme is displayed in figure II.6.

We can replace the energy difference using a particular transition (or energy hv) and the Zero Phonon Line (ZPL) (this is the transition between the lowest energy levels of both manifolds):

$$E_j - E_i = h\nu - E_{\text{ZPL}} \tag{II.47}$$

$$\rightarrow E_j = E_i + h\nu - E_{ZPL} \tag{II.48}$$

Dividing the cross sections and using the reciprocity ($\sigma_{ij} = \sigma_{ji}$) results in:

$$\frac{\sigma_{e}(v)}{\sigma_{a}(v)} = \frac{Z_{l}}{Z_{u}} \cdot \frac{\sum_{ij} d_{j} \exp\left(\frac{-E_{j}}{kT}\right) \sigma_{ji} d_{i}}{\sum_{ij} d_{i} \exp\left(\frac{-E_{i}}{kT}\right) \sigma_{ij} d_{j}}$$
(II.49)

$$= \frac{Z_l}{Z_u} \cdot \frac{\sum_{ij} d_j \exp\left(\frac{-E_i}{kT}\right) \exp\left(\frac{E_{ZL} - h\nu}{kT}\right) \sigma_{ji} d_i}{\sum_{ij} d_i \exp\left(\frac{-E_i}{kT}\right) \sigma_{ij} d_j}.$$
 (II.50)

Equation: McCumber relation

$$\Rightarrow \frac{\sigma_{\rm e}(\nu)}{\sigma_{\rm a}(\nu)} = \frac{Z_l}{Z_u} \cdot \exp\left(\frac{E_{\rm ZPL} - h\nu}{kT}\right). \tag{II.51}$$

Therefore, the emission and absorption cross sections are related via an temperature dependent inverse exponential function, the ZPL and the lower Z_l and upper Z_u state partition functions. This means that for wavelengths below the ZPL wavelength (higher frequency), the absorption cross section dominates and vice versa. So what does McCumber (MC) mean for our laser materials? The ZPL is in principle the transition between the high absorbing and high emitting areas of the spectrum. If we want to build a laser, normally our pump absorption bands will have a higher energy than our amplification bands. Furthermore, the closer our laser emission is to the ZPL, the higher is the underlying absorption, which again is disadvantageous for our laser. On the other hand, the closer our absorption band gets to the ZPL (or even beyond), the lower gets the absorption and the higher the emission, which strongly limits our absorption efficiency as well as the achievable inversion and gain. Nevertheless, the steepness of the transition between absorption and emission is increased for lower temperatures, which would allow us to temper a bit with this limitation. This effect is explained by the change in the thermal occupation of the lower laser levels and responsible for the more popular operation of low quantum defect materials at cryogenic temperatures (cf. figure II.7).

Key point: Sayonara to our dream material!

We have entirely destroyed our dream of the perfect laser medium. There will always be tradeoffs. These are

- The cross section bandwidth is proportional to the inverse maximum cross section.
- The radiative lifetime is proportional to the inverse maximum cross section. This explains why for example Ti:Sa has much higher cross sections than Yb^{3+} -doped materials, because the radiative lifetime is just in the order of μ s compared to ms lifetimes in Yb^{3+} .
- n^2 is proportional to the inverse maximum cross section.
- λ^2 is proportional to the emission cross section and inverse proportional to the absorption cross sections
- There will alway be a trade-off between a low quantum defect vs. low re-absorption. This problem can be tackled with cryogenic cooling.

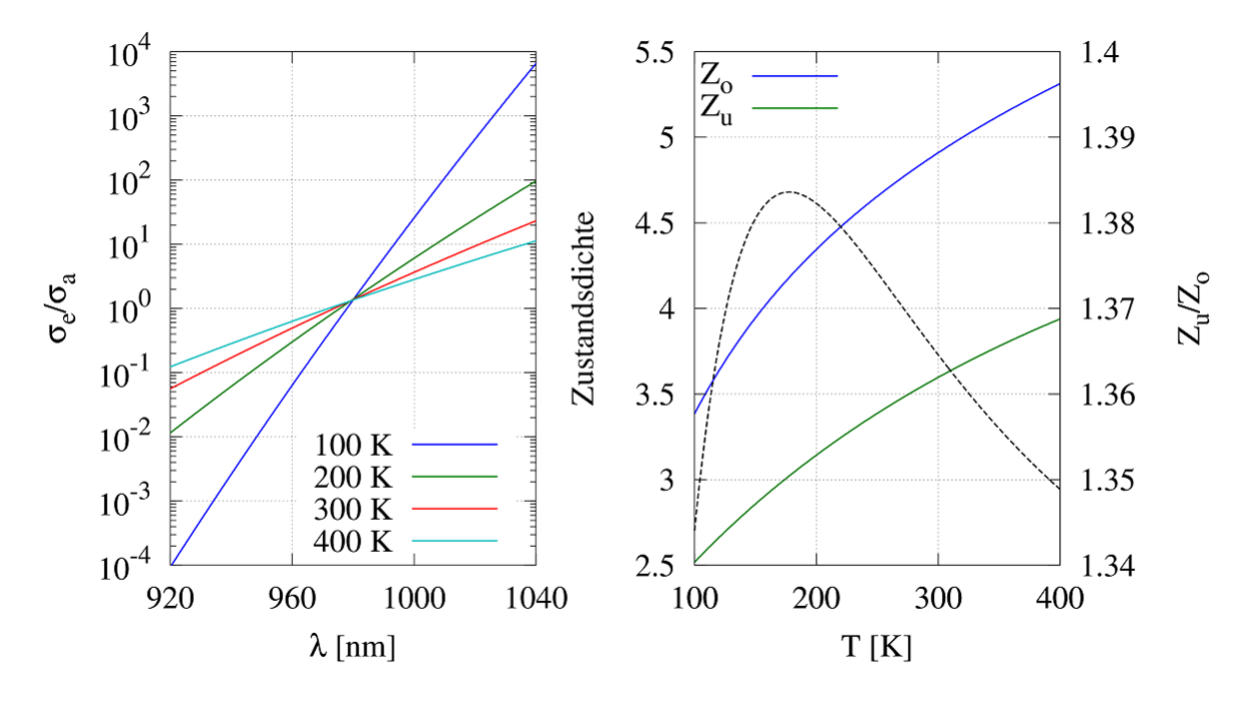


Fig. II.7.: Left: Ratio of the emission- and absorption cross section as a function of wavelength λ for different temperatures. For lower temperatures, the steepness rises which allows the effective use of low quantum defect materials without significant reabsorption. Right: Temperature dependence of the partition functions (solid lines) and their ratio (dashed line, right axis). The ratio corresponds to the ratio of the absorption and emission cross section at the ZPL. Both calculations were done for a laser medium with a ZPL at 980 nm (Yb:CaF₂). Taken from [Kör14].

Example: Field levels in Ytterbium

We want to give an example of the field levels of the ground and excited state of different Ytterbium doped host materials in figure II.8. Ytterbium is split into two sub-manifolds, the ZPL lies around 980 nm. The laser process typically occurs between the first level $E_{5/2}^1$ of the upper and the second level $E_{7/2}^2$ of the lower manifold at a wavelength of around 1030 nm. The material is

YAG CaF_2 LiMgAS FP15 $E [cm^{-1}]$

typically pumped with laser diodes at around 940 nm and not at the ZPL (which is also possible).

 $\label{eq:Fig.II.8.:} \textbf{Energy levels of the ground and excited state for Yb:YAG [Koe+12], Yb:CaF_2 [Koe+12], Yb:LiMgAS and Yb:FP15 [K\"{o}r+11].}$

Comment: Applicability of McCumber

We want to note that the McCumber relation is only applicable for laser materials with two distinct laser manifolds and negligible quenching effects (e.g. multiphoton absorption, energy transfer up-conversion). Thus, Ytterbium is well suited for McCumber, whereas Neodynium is not.

II.6. Application of FL-Method and MC-Relation in Spectroscopy

The determination of exact cross sections is fundamental for any laser calculation or simulation, but literature values are very sparse and often inaccurate, especially if temperature dependence is concerned. The derived methods now allow for the determination of the absorption and emission cross sections from measurements (or to derive missing values if only absorption or emission is known, and also to cross check the validity of spectral data). Here, we present a spectroscopic setup depicted in figure II.9 and used in several publications [Kör+11; Koe+12; Jam+13]. The setup allows for a retrieval of the absorption as well as the fluorescence data in a single run. If needed, the material can be cooled in a liquid nitrogen driven cryostat to obtain the cross sections down to temperatures of 100 K. In the following, we will discuss how absorption and emission measurements are performed.

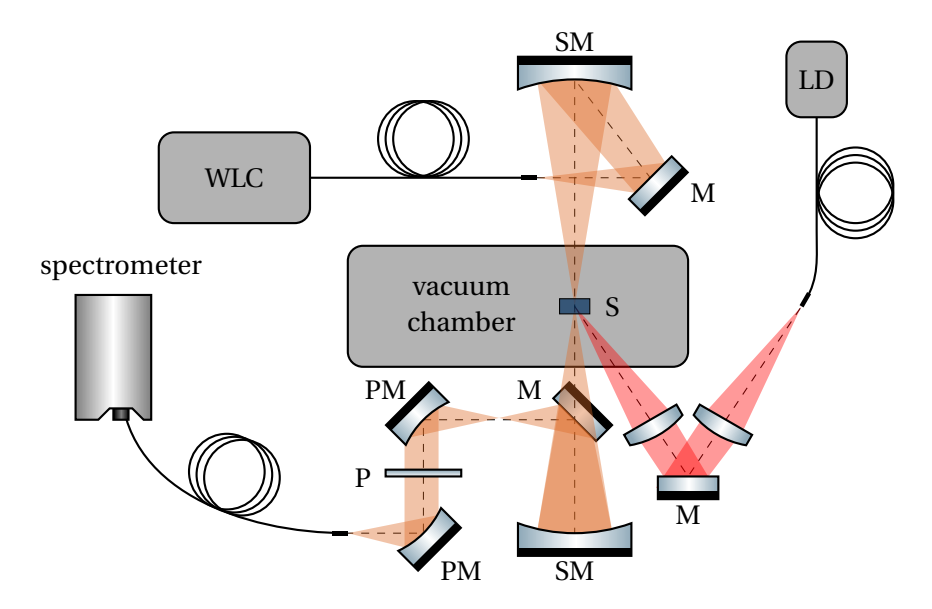


Fig. II.9.: Schematic of the measurement setup: fiber coupled Laser Diode (LD), M: plane mirror, P: polarizer, PM: off axis parabolic mirror, S: sample (mounted in cryostat), SM: spherical mirror with radius of 300 mm, WLC: fiber coupled white light source. The setup can be switched between fluorescence and absorption measurement by just switching the source. The White Light Continuum (WLC) source is used for absorption measurements, whereas the LD is used for the fluorescence measurement.

Absorption measurement

To record absorption data, a fiber coupled WLC source, focused through the sample, can be used (c. f. orange path in figure II.9). These absorption measurements can be directly related to the absorption cross section via Lambert Beer's law

Equation: Absorption cross section from spectroscopic measurements
$$\sigma_{\rm a}(\lambda) = \frac{1}{N_{\rm dop} \cdot d} \ln \biggl(\frac{I_{\rm ref}(\lambda)}{I_{\rm out}(\lambda)} \biggr). \tag{II.52}$$

Here, d is the thickness of the sample, $I_{\rm out}$ the transmitted intensity and $I_{\rm ref}$ a reference measurement taken without a sample to characterize the emission of the light source. As the absorption near the zero phonon line is very high, it is advisable to use a thin sample to measure this spectral region and relate the results to a measurement of a thicker sample to increase the spectral dynamic. In order to determine the absorption cross section, the doping concentration $N_{\rm dop}$ is needed, which is often not

exactly known.

Fluorescence measurement

The retrieval of the fluorescence data is more complicated. Here, the sample is excited by a fiber coupled laser diode (c. f. red path in figure II.9) which is then focused onto the surface of the sample. The same spot is then imaged onto the fiber of the spectrometer. This is done to reduce the effects of re-absorption, which influence the emission spectrum in regions of high absorption (especially near the zero-phonon line). Ideally, we would use a very thin sample to further mitigate re-absorption, but those are not always available. In order to suppress the influence of scattered light from the laser diode, the measurement is repeated for two different diode wavelengths (i.e. diode temperatures) to clear residual peaks from the diode light.

After the measurement of absorption and fluorescence we can calculate the emission cross sections via two different paths:

Key point: How to obtain the emission cross section?

Füchtbauer Ladenburg

- Input: fluorescence spectrum + radiative lifetime
- *Advantage*: This method works well when the absorption is low. An absorption measurement is not needed for the calculation.
- *Problems*: As only the fluorescence lifetime is experimentally obtainable, the radiative liftime might differ from the experimental value due to re-absorption or non-radiative decay. Furthermore, the fluorescence spectrum is deformed due to re-absorption.

McCumber relation

- Input: absorption cross sections + Energy levels
- *Advantage*: This method works well when the absorption is high and the energy levels and doping concentration are well characterized. No life-time measurement is needed.
- *Problems*: The absorption signal is low for wavelengths much longer than ZPL, especially at low temperatures. Therefore, a large noise makes the extraction of useful emission data nearly impossible. Furthermore, exact knowledge of energy levels is often not available and is often only determined at low temperatures in literature.

A combination of both methods allows to widely compensate for insecurities especially like re-absorption and radiative lifetime (cf. figure II.10), by using each method in its spectral area of best validity.

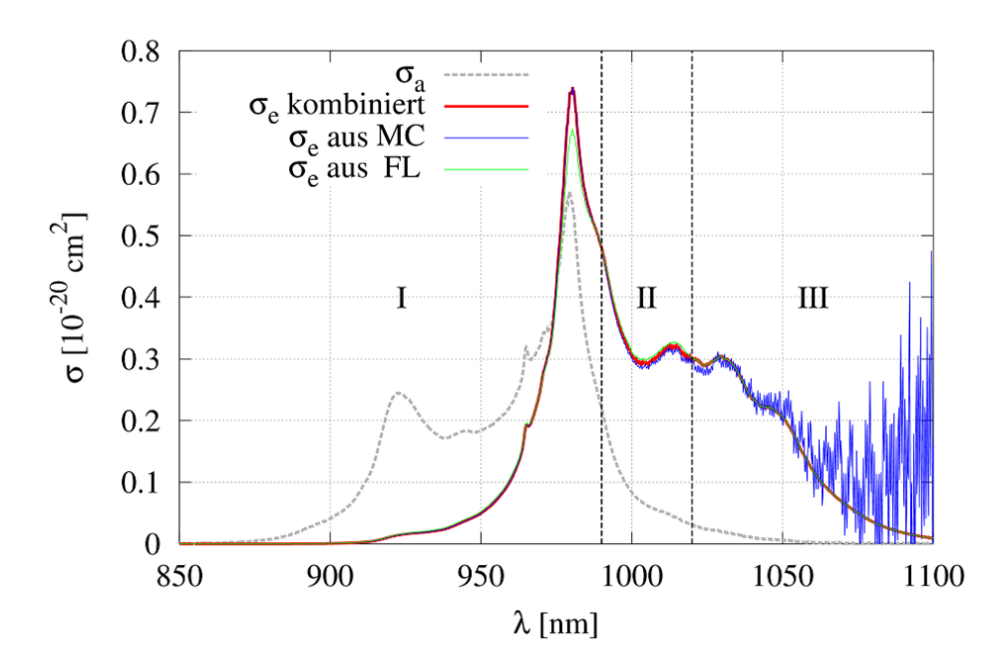


Fig. II.10.: Comparison of the emission spectra calculated with FL-method and MC-relation from spectral measurements on Yb:CaF $_2$ at $T=293\,\mathrm{K}$. The resulting curve (red) was taken from the MC-relation in domain I, and from the FL-method in domain II. In domain II the arithmetic mean of both methods is used. Taken from [Kör14].

II.7. Influence of the Laser Host Material

Besides the actual laser ion, the major influence on the spectral shape of a laser material is generated by the host material. As its internal fields influence the exact separation of the individual energy levels it determines the position of the individual absorption and emission lines. Based on the electronic structure (c. f. for example figure II.8), a relatively simple spectrum would be expected, consisting of a total of $m_l \cdot m_u$ individual lines corresponding to the electronic transitions. Here, m_l, m_u denote the number of sub-levels in the lower and upper manifold. The spectrum of Yb³⁺-doped materials shows a significant higher number of transition lines, which are cause by a coupling of phonons (lattice vibrations) to the host material. These vibration levels are positioned symmetrically to the electronic transition levels. This also leads to a temperature dependent broadening of the transition lines. Therefore, these broadening mechanisms also depend on the type of host material.

Crystals

The doped ions sit in fixed crystal positions, hence they all rather see the same environment. This results in *homogeneously* broadened spectra with rather *sharp lines*, whose bandwidth is reduced for lower temperatures (e.g. Yb:YAG). Crystals have a higher thermal conductivity than glasses due to their ordered atomic structure, which facilitates efficient heat transfer with phonons (lattice vibrations). Crystals are good for:

- · high gain amplifiers due to large cross sections
- long pulses (usally > 10 ps)
- high average power (good thermal conductivity)

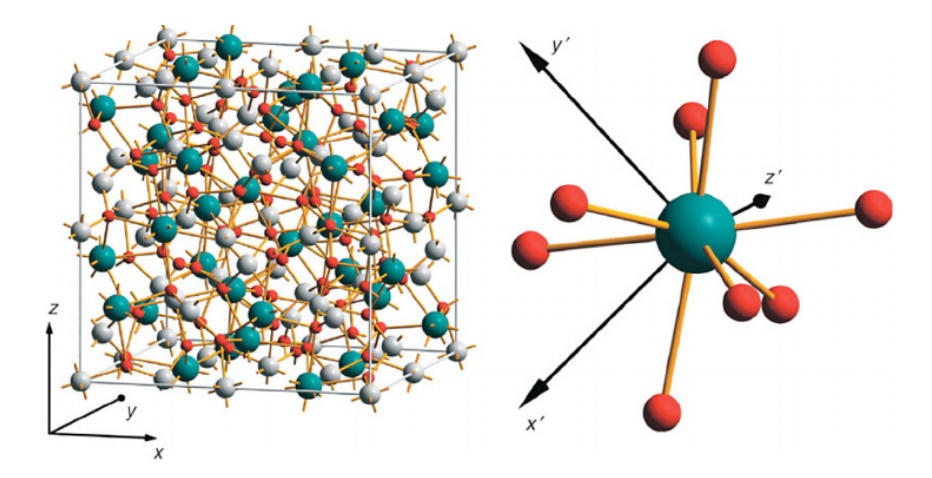


Fig. II.11.: Unit cell of a YAG crystal. Green: Yttrium, Red: Oxygen, White: Aluminium. A unit cell contains eight molecular units $Y_3Al_5O_{12}$. In the doping process, the laser active ion replaces the Yttrium site. The right side show the local surrounding of one Yttrium site. Figure taken from [Kos+15].

Example: Typically used laser crystals

Most crystalline laser materials are oxides, however, there also exist chalcogenides (semiconductor materials) like ZnS or ZnSe. We will focus on oxides [Koe06]:

- **Sapphire** (Al₂O₃): hard with high thermal conductivity, doped with transition metals like titanium (TiSa) and chromium (ruby), anisotropic
- Garnets like Y₃Al₅O₁₂ (YAG), Gd₃Sc₂A₃O₁₂ (GSGG): stable, hard, optically isotropic with

good thermal conductivity

- **Vandates** like YVO₄ and GdVO₄: typically doped with Nd₃⁺, these crystals have high absorption and emission cross sections
- **Alexandrite** (Cr:BeAl₂O₄): large emission bandwidth, low crystal symmetry and thus high polarization dependence
- **Fluorides** like YLiF₄ (YLF): polarization dependent emission wavelength, lower thermal conductivity and fracture resistance, long upper-state lifetime and high UV transparency [Pas05a]

Glasses

The doped ions sit in statistical positions, hence, they all see a different environment. This results in *inhomogeneously* broadened spectra with rather *broad bands* (but lower cross sections due to FL equation). The emission line bandwidth is nearly unchanged for lower temperatures. However, they possess the practical advantage compared to crystals in their size capability for high energy applications. Whereas crystals are difficult to grow in large sizes, glass rods can be easily fabricated up to metre lengths with high optical quality. Glasses are good for:

- high peak power amplifiers (material availability)
- ultra short pulses (<100 fs possible)
- low average power (low thermal conductivity)

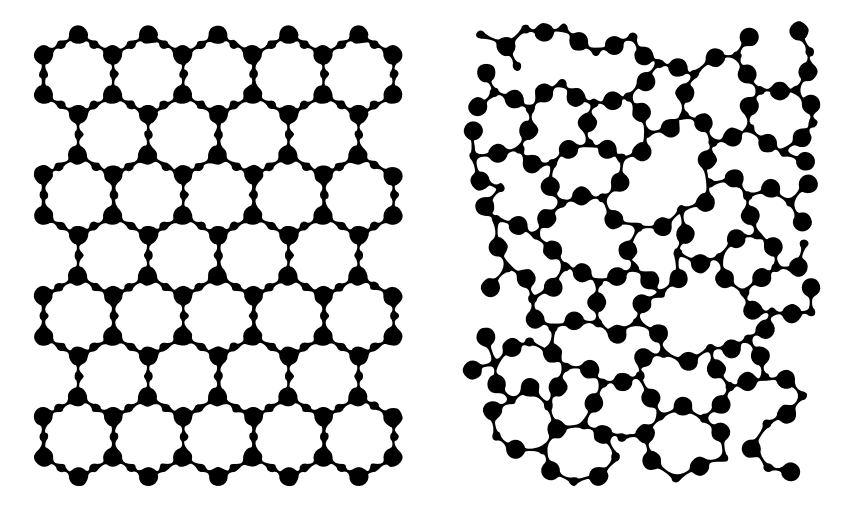


Fig. II.12.: Comparison of a crystal and glass structure. In a crystal, the molecules form an ordered and rigid lattice, however, glass has disordered molecules like a liquid but is still solid.

Crystals (no matching positions)

The doped ions sit in several positions and may cluster, hence they see multiple environments. This results in a combination of homogeneously and inhomogeneously broadened spectra with mostly broad lines, whose bandwidth is slightly reduced for lower temperatures (e.g. CaF_2 or $CaWO_4$). They are good for:

• high peak power amplifiers (material availability)

- ultra short pulses (< 100 fs possible)
- medium average power (medium thermal conductivity)

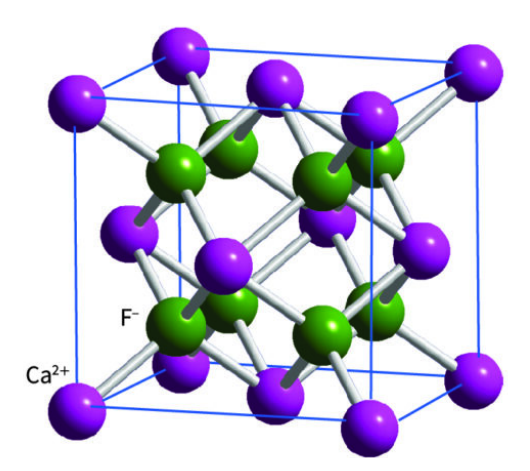


Fig. II.13.: Lattice structure of a face-centered cubic CaF₂ crystal. Three of the Ca²⁺ ions are substituted by two Yb³⁺ ions for charge neutrality. Due to these substitution ratios, the incorporation of the doping ions into the crystal lattice is not trivial. Based on the surrounding lattice structure, the spectral characteristics vary. Figure taken from www.chemtube3d.com.

II.8. Unwanted Effects

Besides the desired laser and pump transitions in a real material other transitions as well radiating as non-radiating can occur. Here are just some examples.

excited state absorption: excited atoms absorb another pump photon. This happens when there are a single or multiple higher-lying energy levels in suitable distance above the excited state level.

multi phonon relaxation: excited atoms are de-excited by multi phonon interaction (non radiative)

- · direct transfer into heat!
- decay rate adds to normal decay rate for radiative decay:

$$\frac{1}{\tau_f} = \frac{1}{\tau_{\text{rad}}} + \frac{1}{\tau_{\text{MP}}}$$

$$\rightarrow \tau_f = \frac{\tau_{\text{rad}} \tau_{\text{MP}}}{\tau_{\text{rad}} + \tau_{\text{MP}}}$$
(II.53)

• In general, the fluorescence lifetime is therefore shorter than the radiation lifetime $\tau_f < \tau_{\rm rad}$

Energy transfer upconversion:

a more complicated scheme:

- two excited ions are de-excited, while exciting another ion to a higher energy level
- this level can than be de-excited, either by radiative decay at other wavelengths or fast non-radiative decay back to the original excited level
- depends on the density of excited ions!:

$$\frac{\partial N_2}{\partial t} = -\frac{N_2}{\tau_f} - \alpha N_2^2 \tag{II.55}$$

• prominent e.g. in Tm³⁺ doped media

The so called quantum efficiency can be used to summarize such effects. It denotes how many photons on the laser transition are generated by one pump photon. In special schemes also quantum efficiency greater unity is possible (e.g. Tm³⁺, cross relaxation)

In an actual laser amplifier such effects are usually unwanted. Optimization is usually possible due to variation in the host material or reduced doping.

II.9. Overview on Some Solid State Laser Ions

It can be seen that the general trade-offs we derived before cannot be tricked. E.g. in the case of Ti:Sa, the material yields high cross sections with a huge bandwidth, but has a very short lifetime. In this way, Ytterbium doped materials are some kind off trade off that is well suited for the special case of diode pumped operation (cf. next chapter). The absorption and emission cross sections with the respective life times of the upper laser level are shown in figure II.14.

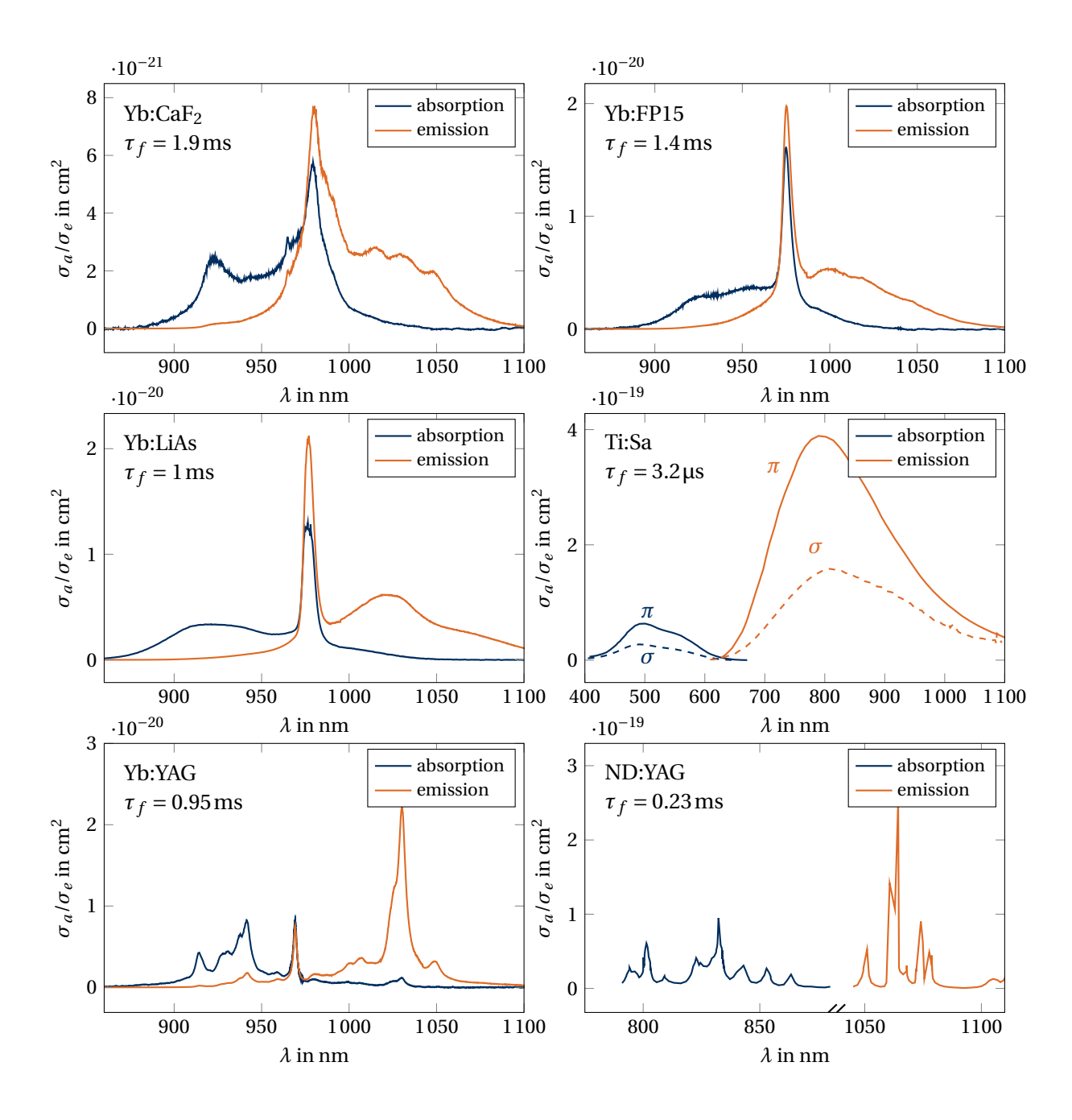


Fig. II.14.: Absorption (blue) and emission (orange) cross sections of different Ytterbium doped laser materials, measured by Jörg Körner. As a comparison, the cross sections of Ti:Sa (adapted from [Sor04]) and Nd:YAG (adapted from https://4lasers.com) are also shown.

II.9.1. Atomic doping concentrations

In the literature, doping concentrations of various laser materials are typically given in atomic percentage, which describes the fraction of ions in the host material that have been replaced by the laser active ion. However, for our calculations we need the number density of the laser active ions. For the determination of the doping concentration, the material density ρ , atomic mass units and the number of laser active ions ξ that replace the host material ions must be known. From that we can calculate the number density of laser active ions for a given percentage of atomic doping. An overview of different laser host materials is shown in Table II.2.

Table II.2.: Number density of laser active rare earth ions RE₃⁺ for different host materials. The factor ξ indicates how many atoms are replaced by how many dopant ions.

host	formula	ϱ [gcm ⁻³]	$m_{ m unit}$	ξ	N _{dop} at 1 %
YAG	$Y_3Al_5O_{12}$	4.55			$1.38 \times 10^{20} \mathrm{cm}^{-3}$
YVO_4		4.24	$3.38 \times 10^{-22} \mathrm{g}$	1	$1.25 \times 10^{20} \mathrm{cm}^{-3}$
YLF	$LiYF_4$	3.99	U		$1.40 \times 10^{20} \mathrm{cm}^{-3}$
CaF_2		3.18	U		$1.63 \times 10^{20} \mathrm{cm}^{-3}$
SrF_2		4.24	$2.09 \times 10^{-22} \mathrm{g}$		$1.36 \times 10^{20} \mathrm{cm}^{-3}$

Example: Doping concentration of YAG

Let us consider the example of Yb-doped Yttrium Aluminium Garnet (YAG) $(Y_3Al_5O_{12})$. To convert between atomic and number density, we first need to calculate the mass of one $Y_3Al_5O_{12}$ -unit. Using the periodic table of elements we obtain

$$m_{\text{YAG-unit}} = (3 \cdot \underbrace{88.9}_{m_{\text{Y}}} + 5 \cdot \underbrace{27.0}_{m_{\text{Al}}} + 12 \cdot \underbrace{16.0}_{m_{\text{O}}}) \cdot 1.66 \times 10^{-24} \,\text{g}.$$
 (II.56)

Then, the number density of Yttrium ions can be calculated by using the material density of YAG ($\varrho = 4.55\,\mathrm{g\,cm^{-3}}$) to calculate the number of Y-ions per cm³

$$N_{\text{Yb:YAG}} = 3 \frac{\varrho_{\text{YAG}}}{m_{\text{YAG-unit}}} = 1.38 \times 10^{22} \,\text{cm}^{-3}.$$
 (II.57)
- number of Y-ions per unit cell

We have to take into account, that each unit of YAG contains three Yttrium ions, thus we have a factor of three. Finally, we need to consider, how many ions ξ of the laser active material replace the host material ions. In case of Yb:YAG the Y_3^+ -ions are replaced by Yb_3^+ in a one-to-one ratio. Then we obtain the number density of Yb:YAG for one atomic percent

$$N_{\text{Yb:YAG,1\%}} = \underbrace{\xi}_{1} \cdot N_{\text{Yb:YAG}} \cdot 0.01 = 1.38 \times 10^{20} \,\text{cm}^{-3}.$$
 (II.58)

II.9.2. Rare earth metals

Rare earth ions are a very popular choice as dopands for laser crystals and glasses. Here, the rare earth ions replace other ions of similar size and charge state (e.g. Nd^{3+} ions substitute Yttrium (Y^{3+}) in Nd:YAG crystals). We may wonder, why this is the case?

- Energy Stability: A characteristic of rare earth ions is that their electronic transition occurs within the 4f shell², which is partially shielded from the host lattice (5s and 5p orbitals). This reduces influences of the host lattice, giving them well-defined, stable emission wavelengths and bandwidths.
- Efficient Absorption and Emission: The ions exhibit strong and sharp absorption lines, enabling efficient energy absorption from pump sources like laser diodes.
- Long lifetimes: In comparison to other laser materials like Ti:Sa or gases, rare earth ions have long lifetimes in the excited state, which is beneficial for energy deposition into the material
- Low Non-radiative losses: Due to the above mentioned shielding of the 4f electrons, the energy losses through non-radiative processes is minimized.

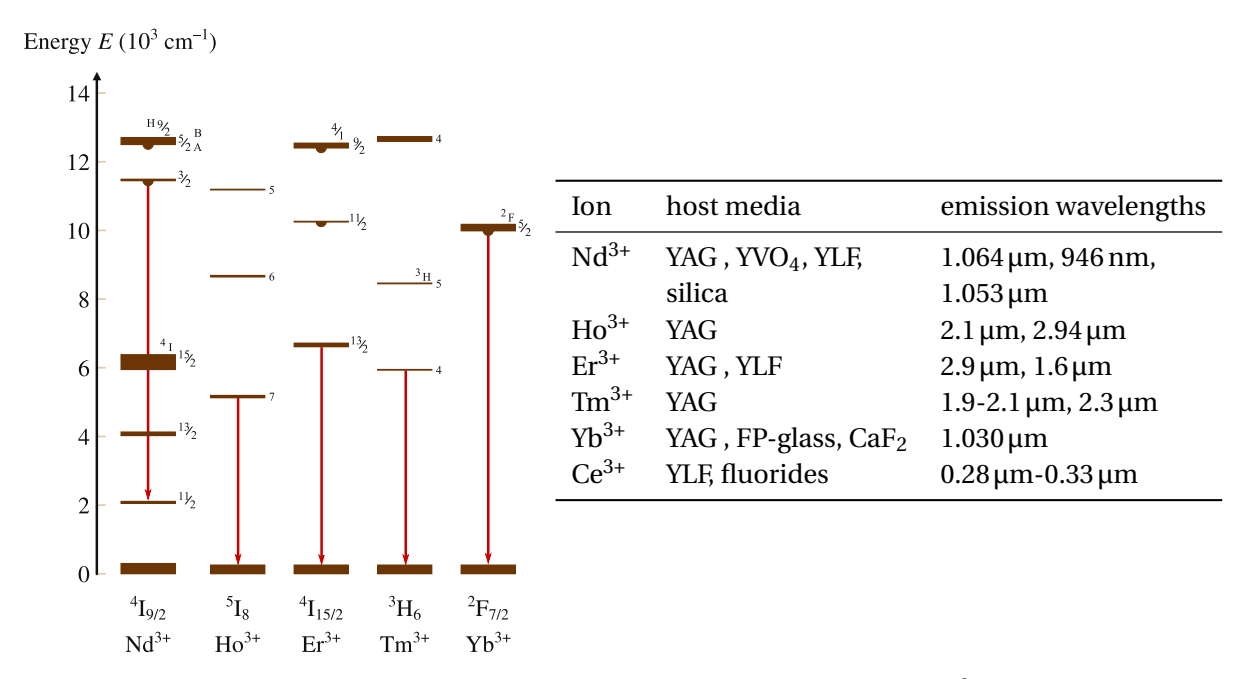


Fig. II.15.: Left: energy levels diagram of different rare earth ions of the form RE³⁺ in LaCl₃. Adapted from [Trä12, p.674].

Right: Laser-active rare earth ions and host media with typical emission wavelengths [Pas07].

Yb³⁺-materials

Ytterbium-doped laser materials possess several interesting properties which set them apart from others like Nd^{3+} -doped laser gain media [Pas05b]:

• **Simple electronic structure**: Yb³⁺ has only one excited state manifold (${}^{2}F_{5/2}$) within reach from the ground-state manifold. Here, the assumption of McCumber of a two-state system is fulfilled

²The reason that rare earth metals are placed separately in the periodic table stems from the fact that they fill up the 4f orbitals with up to 14 electrons. Thus, there are 14 lanthanoide rare earth metals. Since the 5s and 5p orbitals are energetically lower, they will be completely filled and help shielding the 4f orbitals.

and the cross sections can be calculated using the MC-relation (which is not possible for Nd^{3+}). The pumping and lasing process involve transitions between different sublevels of these two manifolds.

- **Small quantum defect**: The ability to use InGaAs-Laser diodes for pumping makes a small quantum defect possible, allowing for high power efficiencies and reducing thermal effects. However, complications may arise from the quasi-three-level behaviour.
- The simple electronic structure excludes excited-state absorption (c. f. section II.8).
- Large gain bandwidth (compared with Nd³⁺YAG-crystals). Allows for wide wavelength tuning and ultrashort pulse generation.
- Long fluorescence lifetime in the order of milliseconds
- **Quasi-three-level** behaviour: Due to the small quantum defect, we have non-neglectable emission at the absorption bands which requires high pump intensities. Furthermore, reabsorption takes place at the emission wavelength around 1030 nm.

II.9.3. Transition metals

Another group of laser active ions are the two transition metals chromium (Cr) and titan (Ti). Their electronic configuration is

Cr:
$$[Ar]3d^54s$$
 (II.59)

Ti:
$$[Ar]3d^24s^2$$
. (II.60)

- Strong influence by the host material: In their trivalent form (Cr₃⁺, Ti₃⁺) they have only electrons in the 3d orbital left, which are unshielded by outer shells in contrast to rare earth ions. Thus, their optical properties are heavily influenced by the host crystal field.
- Large gain bandwidth: The strong coupling of the electronic transition with phonons of a wide frequency range leads to broad absorption and emission bandwidths. This can be used for the generation of few-cycle pulses or tunable lasers.

Table II.3.: Laser-active transition metal ions and host media with typical emission wavelengths [Pas07].

Ion	host media	emission wavelengths
Ti ³⁺	sapphire Al ₂ O ₃	650-1100 nm
Cr ²⁺	Chalcogenides ZnS, ZnSe	$2-3.4\mu m$
Cr ³⁺	${ m rubyAl_2O_3}$	0.8-0.9 µm
Cr^{4+}	YAG	1.35-1.65 μm

II.10. Temperature dependence of the cross sections

In the following, we also want to discuss the temperature dependence of the emission and absorption cross sections for two different materials as shown in figure II.16.

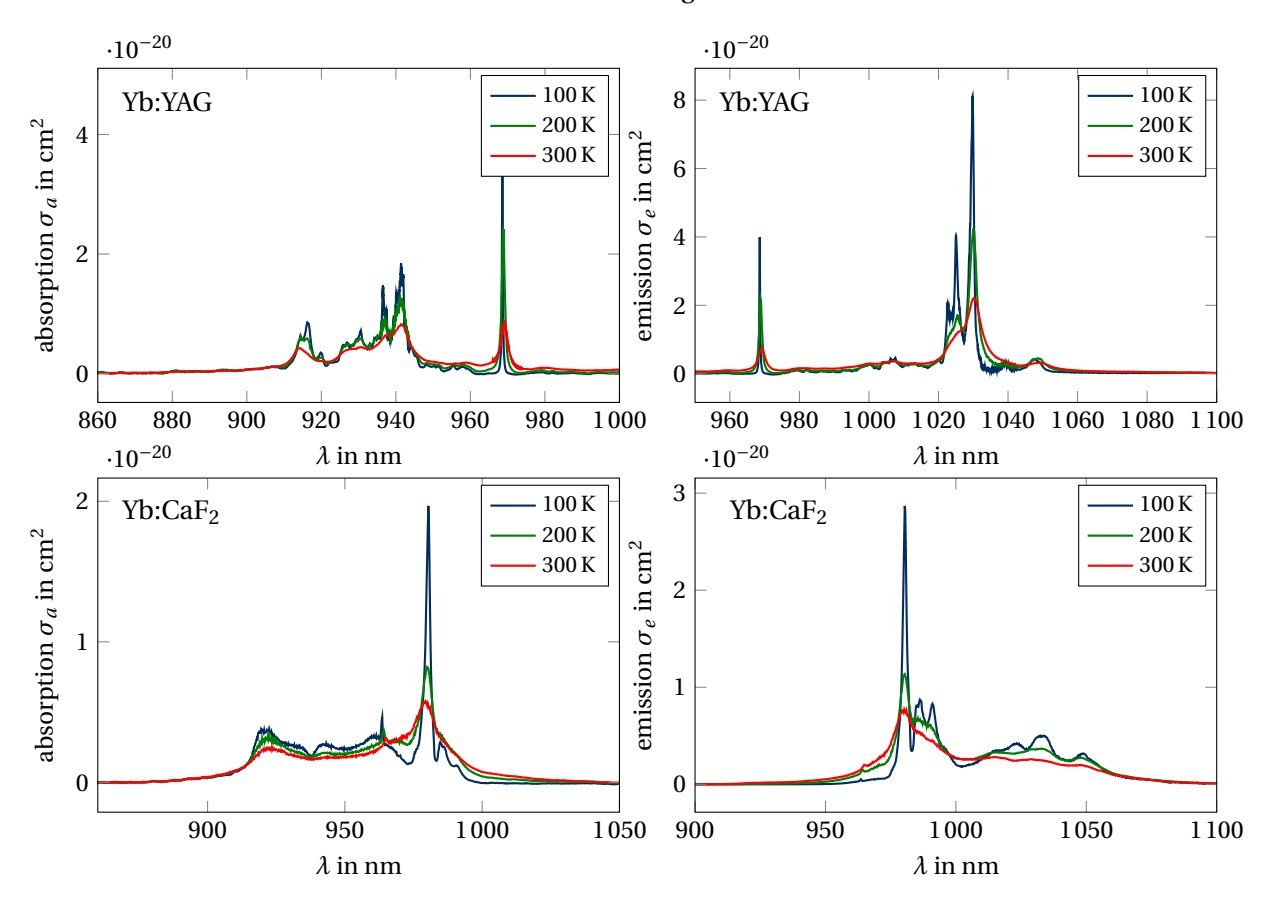


Fig. II.16.: Absorption (left) and emission (right) cross sections of Yb:YAG (top) and Yb:CaF₂ (bottom) for different temperatures. Adapted from [Kör+11].

For Ytterbium doped gain media, cryogenic cooling is necessary to set up high energy amplifiers. This is due to limitations of the thermal occupation of the lower laser levels which vanish at cryogenic temperatures. In order to efficiently extract high energies from the laser medium, the quantum defect should be as small as possible. However, at room temperatures, the re-absorption at the laser wavelength significantly reduces the possible output power and laser efficiency.

For Yb:YAG (c. f. figure II.16 top), the homogeneous broadening mechanisms exhibit a strong temperature dependence. We can observe that the re-absorption at the laser wavelength around 1030 nm becomes negligible at cryogenic temperatures, while the emission is strongly increased. However, the effective emission bandwidth is reduced significantly [Kör+11]. Therefore, cryogenic cooling is not useful for high-intensity laser systems, where short pulse lengths are required.

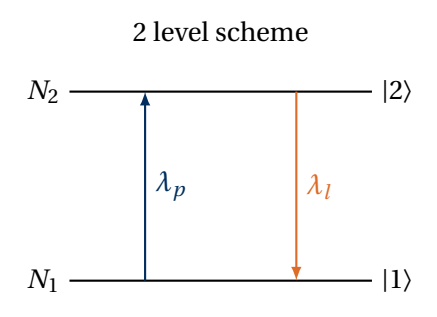
For Yb:CaF $_2$, the inhomogeneous broadening meachnisms due to the placement of the active ions in the crystal lattice are less temperature dependent. In the figure we observe that the absorption for wavelengths larger than the ZPL (980 nm) is decreasing and at 100 K, the absorption above 1000 nm is almost zero. On the other hand, the emission cross sections are increased in that spectral regions and become more structured, however, the capability of broad band amplification is preserved. At the often used pump wavelength of 940 nm, not much variation in the absorption is observed.

III. Laser Amplification Process

In this chapter we will discuss the mathematical treatment of the pump and amplification process in a laser material. We start by discussing different level-schemes of describing a laser material. For the pump process we assume a Continuous Wave (CW) pump pulse and consider the effect of spontaneous emission. For the amplification, we neglect spontaneous emission, as the extraction with the pulsed seed pulse takes place on much smaller timescales, however, we include absorption to describe 3-level materials like Yb³⁺.

III.1. Level schemes and rate equations

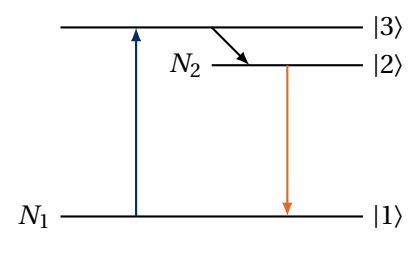
To operate a laser we will always need a so called inversion ($N_2 > N_1$), meaning that there are more ions in the excited state N_2 than in the ground state N_1 . To better understand the basic processes, we can use the following basic models:



- No laser operation is observed for optical pumping as pump and laser operate at the same wavelength.
- The inversion can at most reach equality under pumping as can be seen by rearranging equation (II.2) in steady state $(\frac{dN_2}{dt} = 0)$

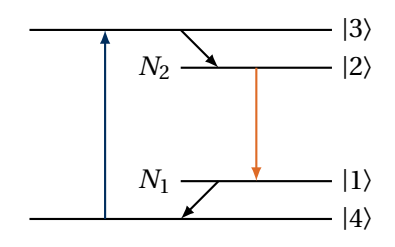
$$\frac{N_2}{N_1} = \frac{B_{12}\varrho}{B_{21}\varrho + A_{21}} < 1 \tag{III.1}$$

3 level scheme



- The pump light excites into a separate level |3> from where
 the atoms quickly relax into the meta stable laser level |2>.
 As the ground state |1> is still occupied, a certain amount of
 atoms got to be excited to achieve inversion.
- In pump pulsed mode, this can be a strong loss process.
- The 3-level scheme is often used to describe laser media with re-absorption and low quantum defect (Yb³⁺).

4 level scheme



- The laser pumps a separate level |3⟩ from where the atoms quickly relax into the meta stable level |2⟩. From there, the laser process goes to a non occupied ground level |1⟩ from which it quickly relaxes back into the ground state |4⟩.
- Inversion is already achieved with the first excited atom!
- The 4-level scheme is used to describe laser materials with high quantum defect and negligibly re-absorption (Nd³⁺).

These basic models can be thought of as some idealized laser medium. Real laser materials typically involve a much higher number of energy levels. In the following we will derive a model that takes this into account. Therefore, we use a system of 2 manifolds with a continuous level distribution in each representing a set of energy levels as shown in figure III.1. Further, for practical reasons we use the

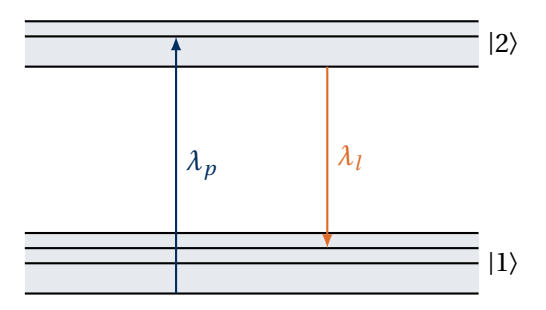


Fig. III.1.: Model of a laser material with two manifolds. In the shaded areas, intra-manifold phonon transitions are possible.

photon density Φ to describe the radiation field. Hence the rate equation for the interaction with an incident photon density reads:

$$\frac{\mathrm{d}\Phi}{\mathrm{d}z} = -\Phi \cdot (\sigma_{\mathrm{a}} N_{1} - \sigma_{\mathrm{e}} N_{2}) \tag{III.2}$$

$$\frac{\mathrm{d}\Phi}{\mathrm{d}z} = -\Phi \cdot (\sigma_{\mathrm{a}}N_{1} - \sigma_{\mathrm{e}}N_{2}) \tag{III.2}$$

$$\frac{\mathrm{d}\Phi}{\mathrm{d}z} = \frac{\mathrm{d}\Phi}{\mathrm{d}t} \frac{\mathrm{d}t}{\mathrm{d}z} = \frac{\mathrm{d}N_{1}}{\mathrm{d}t} \frac{1}{c} \quad \Rightarrow \quad \frac{\mathrm{d}N_{1}}{\mathrm{d}t} = -\Phi c \cdot (\sigma_{\mathrm{a}}N_{1} - \sigma_{\mathrm{e}}N_{2}). \tag{III.3}$$

The variables are:

 $\sigma_a(\lambda), \sigma_e(\lambda)$ wavelength dependent absorption and emission cross sections [cm²]

density of ions $[cm^{-3}]$ in the lower (1) and upper (2) manifold N_1, N_2

Photon density [cm⁻³]. The rate of change for the photon density is equal to the change Φ of ions in the manifolds.

If we now consider the pump and laser process with their appropriate cross sections for the emission and absorption, and the spontaneous emission, the rate equation for the complete laser cycle is:

$$\frac{\mathrm{d}N_2}{\mathrm{d}t} = -\frac{\mathrm{d}N_1}{\mathrm{d}t} = \underbrace{c\Phi_\mathrm{p}(\sigma_\mathrm{a}(\lambda_\mathrm{p})N_1 - \sigma_\mathrm{e}(\lambda_\mathrm{p})N_2) - \frac{N_2}{\tau_\mathrm{f}}}_{1} - c\Phi_\mathrm{l}(\sigma_\mathrm{e}(\lambda_\mathrm{l})N_2 - \sigma_\mathrm{a}(\lambda_\mathrm{l})N_1)$$
(III.4)

Here "p" denotes the parameters involved in the pumping process and "l" the corresponding ones in the laser process. The under set numbers 1 to 3 denote the parts of the equation representing the pump process (1), the spontaneous emission (2) and the amplification process (3) respectively.

For basic laser operation the steady state solution of this equation is used. Talking about high energy amplifiers, this is no option as pumping and laser amplification is described by time dependent pulses. So we got to analyze the dynamic case to understand the pulsed pump process as well as to understand the change in the temporal profile of the amplified pulse. Therefore, we will discuss efficient solution mechanisms for pumping and extraction in the following.

III.2. Pumping

During the pump process the extracting laser field will be neglected, hence we obtain:

$$\frac{\mathrm{d}N_2}{\mathrm{d}t} = c\Phi(\sigma_\mathrm{a}(\lambda_\mathrm{p})N_1 - \sigma_\mathrm{e}(\lambda_\mathrm{p})N_2) - \frac{N_2}{\tau_\mathrm{f}} \tag{III.5}$$

$$\frac{\mathrm{d}\Phi}{\mathrm{d}z} = -\Phi(\sigma_{\mathrm{a}}(\lambda_{\mathrm{p}})N_{1} - \sigma_{\mathrm{e}}(\lambda_{\mathrm{p}})N_{2}). \tag{III.6}$$

As typical for most diode pumped lasers, we will now consider an end pumped setup, meaning that the pump beam is co-propagating with the laser beam through the laser medium. For a realistic representation we got to consider as well the number densities as the photon density dependent on space. We will do so using the propagation direction z in one dimension.

Key point: Implementation of new notations

To obtain a more convenient representation of our formula we further introduce some substitutions which will be used throughout the rest of this book:

• The **inversion** $\beta(t,z)$ gives the percentage of the excited electrons in the upper manifold:

$$\beta(t,z) = \frac{N_2(t,z)}{N_{\text{dop}}}$$
 with $N_{\text{dop}} = N_1 + N_2$ (III.7)

• The **pump rate** R(t, z) [s⁻¹] states, how many electrons per second can be excited by the pumping laser field:

$$R(t,z) = \sigma_a c \Phi_P(t,z)$$
 (III.8)

• The **equilibrium inversion** (the name will become clearer looking at the final formula)

$$\beta_{\rm eq} = \frac{\sigma_{\rm a}}{\sigma_{\rm a} + \sigma_{\rm e}}.$$
 (III.9)

Using this new notation we can find an expression to describe the temporal evolution of the inversion $\beta(t, z)$ by rewriting equation (III.5) as

Equation: 1st rate equation: Time dependent inversion

$$\begin{split} \frac{\partial \beta(t,z)}{\partial t} &= \frac{R(t,z)}{N_{\rm dop}} \left(N_1 - \frac{\sigma_{\rm e}}{\sigma_{\rm a}} N_2 \right) - \frac{\beta}{\tau_f} & \frac{N_1}{N_{\rm dop}} &= \frac{N_{\rm dop} - N_2}{N_{\rm dop}} = 1 - \beta(t,z) \\ &= R(t,z) \left(1 - \beta(t,z) - \frac{\sigma_{\rm e}}{\sigma_{\rm a}} \beta(t,z) \right) - \frac{\beta(t,z)}{\tau_f} = R(t,z) \left(1 - \beta(t,z) \underbrace{\frac{\sigma_{\rm a} + \sigma_{\rm e}}{\sigma_{\rm a}}}_{:=1/\beta_{\rm eq}} \right) - \frac{\beta(t,z)}{\tau_f} \\ &= R(t,z) \left(1 - \frac{\beta(t,z)}{\beta_{\rm eq}} \right) - \frac{\beta(t,z)}{\tau_f}. \end{split} \tag{III.10}$$

From this differential equation we can already predict some interesting results. If the inversion is equal to the equilibrium inversion $\beta(t,z)=\beta_{\rm eq}$, the inversion becomes independent of the pump rate and changes only due the natural decay of the upper laser level with the time constant τ_f . This explains the naming of $\beta_{\rm eq}$ as the equilibrium inversion, because at this point the inversion is at balance (when neglecting spontaneous emission). As a second equation we would need to describe the

evolution of the pump rate during the propagation through the material. For this we utilize equation (III.6) and carry out the according substitutions to obtain:

Equation: 2nd rate equation: Space dependent pump rate

$$\begin{split} \frac{\partial R(t,z)}{\partial z} &= R(t,z)(\sigma_{\rm a}N_1 - \sigma_{\rm e}N_2) \\ \frac{\partial R(t,z)}{\partial z} &= -\alpha R(t,z) \cdot \left(1 - \frac{\beta(t,z)}{\beta_{\rm eq}(z)}\right) \quad \text{with} \quad \alpha = N_{\rm dop}\sigma_{\rm a}(z). \end{split} \tag{III.11}$$

Here, we reintroduced the absorption parameter α that we have already seen in Lambert-Beers law. In order understand the role of the equilibrium inversion in the pumping process, we can analyze the rate equation (III.11) for different inversions.

Key point: Pump process at different inversions

• low inversion: $\beta \ll \beta_{eq}$:

$$\frac{\partial R(t,z)}{\partial z} = -\alpha R(t,z) \qquad \Rightarrow \qquad R = R_0 \exp(-\alpha z). \tag{III.12}$$

At the start of the pump process, the pump rate behaves like Lambert-Beer's law.

• $\beta = \beta_{eq}$:

$$\frac{\partial R(t,z)}{\partial z} = -\alpha R(t,z)(1-1) = 0 \qquad \Rightarrow \qquad R = \text{const.}$$
 (III.13)

The material becomes transparent, as the amount of emitted and absorbed light is equal.

• $\beta > \beta_{\rm eq}$: Here we can observe that $\frac{\partial R}{\partial z} > 0$ becomes positive, therefore we have amplification.

From this we can conclude that β_{eq} is a limit of maximum inversion we can reach in the pumping process.

III.2.1. Pump saturation intensity

Before we move on to the numerical solution of the system of the rate equations, we want to start with a discussion of the steady state solution, i. e. when we have an equilibrium in the inversion. Then we can solve equation (III.10) for β as

$$0 = R(t, z) \left(1 - \frac{\beta}{\beta_{\text{eq}}} \right) - \frac{\beta}{\tau_f} \qquad \Rightarrow \qquad \beta = \frac{R}{\frac{R}{\beta_{\text{eq}}} + \frac{1}{\tau_f}} = \frac{\beta_{\text{eq}}}{1 + \frac{\beta_{\text{eq}}}{R \cdot \tau_f}}.$$
 (III.14)

Now we want to analyze the expression $\beta_{\rm eq}/(R\cdot\tau_f)$ in the denominator. We can substitute the definitions of R and $\beta_{\rm eq}$ again and obtain

$$\frac{\beta_{\text{eq}}}{R \cdot \tau_f} = \frac{\sigma_{\text{a}}}{\sigma_{\text{a}} + \sigma_{\text{e}}} \frac{1}{\tau_f} \frac{1}{\sigma_{\text{a}} c \Phi} = \frac{1}{(\sigma_{\text{a}} + \sigma_{\text{e}}) \tau_f} \underbrace{\frac{1}{c \Phi} \frac{h \nu}{h \nu}}_{I} = \frac{h \nu}{(\sigma_{\text{a}} + \sigma_{\text{e}}) \tau_f} \frac{1}{I} := \frac{I_{\text{sat}}}{I}.$$
 (III.15)

Here, we used the intensity of the pump photon field $I = c\Phi \cdot hv$ and defined the pump saturation intensity as

Equation: Pump Saturation intensity

$$I_{\text{sat}} = \frac{hv}{(\sigma_{\text{a}} + \sigma_{\text{e}})\tau_f}$$
 with $\beta = \frac{\beta_{\text{eq}}}{1 + \frac{I_{\text{sat}}}{I}}$. (III.16)

Therefore, I_{sat} describes the intensity required to reach an inversion of $\beta_{\text{eq}}/2$ (on the surface) for an infinite pump duration. The saturation intensity also indicates the order of magnitude, where saturation effects are needed to be taken into account.

Key point: Pump saturation

- $I_{\rm sat} \propto 1/\tau_f$: Saturation is inversely proportional to the fluorescence lifetime. As fluorescence is a loss mechanism, a low fluorescence lifetime increases the intensity required for saturation.
- $I_{\rm sat} \propto \beta_{\rm eq}$: When the equilibrium inversion is lower, saturation can be reached at lower pump intensities.
- $I_{\rm sat} \propto E_{\rm photon}$: Saturation is not directly proportional to the photon energy, as only the photon density Φ is important. However, since we express saturation in form of an intensity I, we need to readjust for the fact that at a higher wavelength the photon density is lower for the same observed intensity, i. e. the saturation intensity rises for smaller wavelengths, as the photon density drops.

Furthermore, we want to give some examples for typical saturation pump intensities. As the cross sections are a function of wavelength, the saturation intensity changes depending on the pumping wavelength. This is shown in figure III.2 for different pump wavelengths typically used for optical pumping with laser diodes. For Yb-doped materials, possible pump wavelengths are 940 nm and 980 nm (at the ZPL).

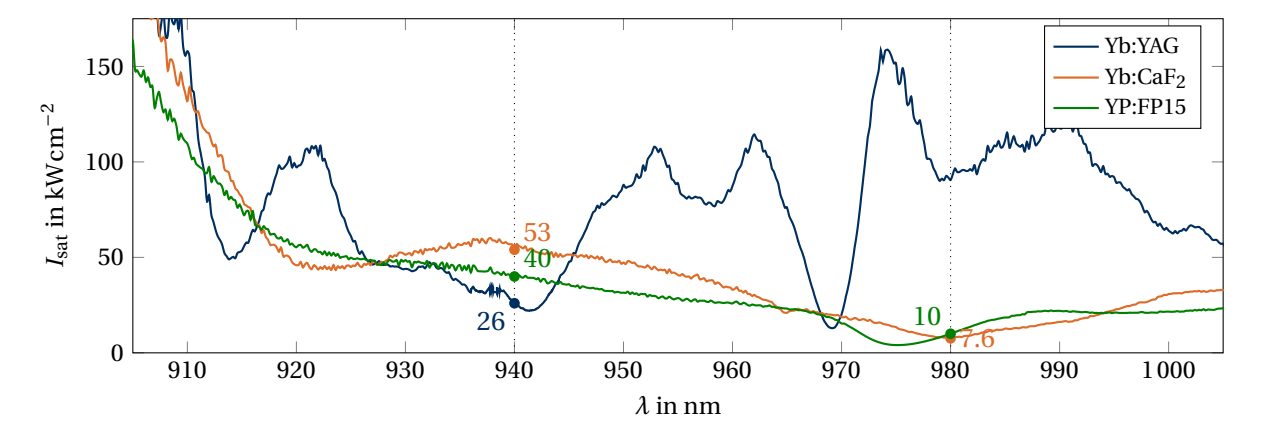


Fig. III.2.: Saturation pump intensity I_{sat} for three different Yb-doped laser materials.

In general, we aim for a low saturation pump intensity $I_{\rm sat}$ in order to pump the medium efficiently. However, we also want to achieve a high value of $\beta_{\rm eq}$ at the pump wavelength to efficiently store energy in the laser medium and a sufficiently low $\beta_{\rm eq}$ at the emission wavelength as the lasing process stops, when the equilibrium inversion is reached. The bottom right plot of figure III.3 shows, that this goal is better reached at lower temperatures and at higher quantum defects, i.e. pumping at 940 nm is better to store more energy in the crystal, however, this increases the heat fraction between pump and laser wavelength.

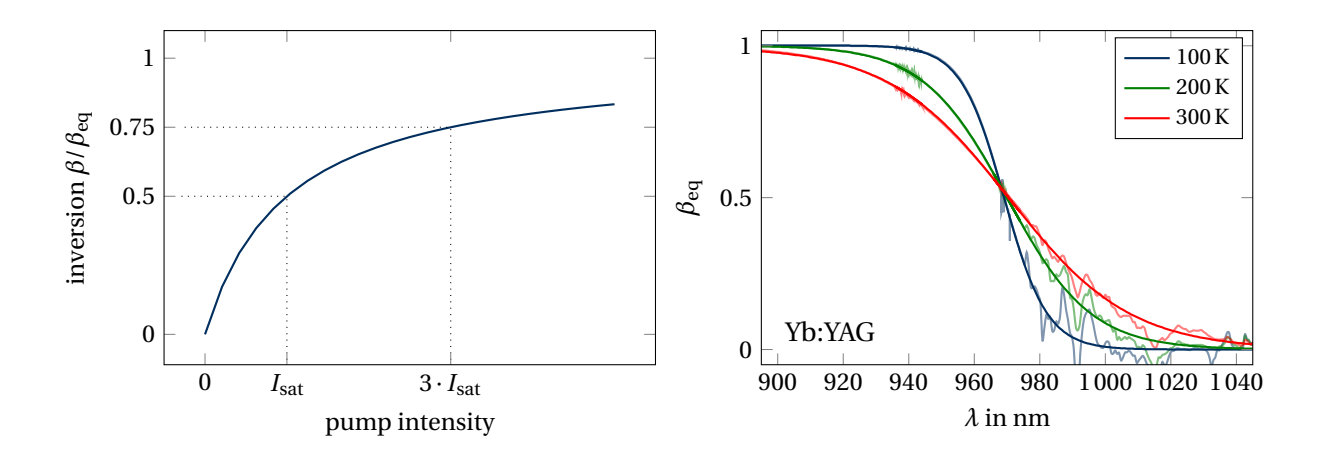


Fig. III.3.: Left: Inversion as a function of the pump intensity. Right: Equilibrium inversion β_{eq} of Yb:YAG for three different temperatures. The spectral behaviour of β_{eq} follows a logistic function, which is steeper for lower temperatures.

III.2.2. Numerical solutions of the rate equations

Derivation: Solution of the first rate equation

The time dependent rate equation (III.10) is a differential equation of the shape

$$\frac{\mathrm{d}\beta(t)}{\mathrm{d}t} + f(t) \cdot \beta(t) = g(t), \tag{III.17}$$

with the known solution (cf. e.g. [Bro13])

$$\beta(t) = e^{-F(t)} \int g(t) \cdot e^{F(t)} dt \quad \text{with} \quad F(t) = \int f(t) dt.$$
 (III.18)

Therefore, we can identify f(t) and g(t) as

$$f(t,z) = \frac{R(t,z)}{\beta_{\text{eq}}(z)} + \frac{1}{\tau_f} \quad \text{and} \quad g(t,z) = R(t,z)$$

$$\Rightarrow \quad F(t,z) = \int \frac{R(t,z)}{\beta_{\text{eq}}(z)} \, \mathrm{d}t + \frac{t}{\tau_f}. \tag{III.19}$$

Hence, using (III.18) with the initial condition $\beta(t = 0, z) = \beta_0(z)$ we obtain the solution

$$\beta(t,z) = \exp\left(-\int_0^t \frac{R(t',z)}{\beta_{\text{eq}}} dt' - \frac{t}{\tau_f}\right) \left[\int_0^t R(t'',z) \cdot \exp\left(\int_0^{t''} \frac{R(t',z)}{\beta_{\text{eq}}} dt' + \frac{t}{\tau_f}\right) dt'' + \beta_0(z)\right] \quad \text{(III.20)}$$

Further by integrating the second rate equation (III.11) by separation of variables we obtain:

$$R(t,z) = R_0(t) \cdot e^{-\alpha z} \cdot \exp\left(\alpha \cdot \int_0^z \frac{\beta(t,z')}{\beta_{\text{eq}}} \, dz'\right)$$
(III.21)

The first R_a term corresponds to the Lambert-Beer law, while the R_b term acts as a correction factor for non zero inversion.

We now derived a solution of the differential equation system in the integral form (which is ad-

vantageous as such expressions can be well handled by numerical integration). However, we cannot directly calculate the result as both equations are still linked with each other. Therefore, we have to obtain a solution based on an iterative approach.

As a start we assume two edge cases to get a lower and upper boundary for the pump rate R(t,z):

1.) zero inversion at all times

$$R_{\text{b.low}}^1 = R_{\text{b}} [\beta_{\text{low}}^0(t, z) = 0] = 1$$
 (III.22)

2.) maximum inversion at all times

$$R_{\text{b,high}}^{1} = R_{\text{b}} \left[\beta_{\text{high}}^{0}(t, z) = \beta_{\text{eq}} \right] = e^{\alpha z} = \frac{R_{0}}{R_{a}}$$
 (III.23)

Using now an iterative algorithm calculating

$$R_{\text{b,low/high}}^{m}(t,z) = R_{\text{b}} \left[\beta_{\text{low/high}}^{(m-1)}(t,z) \right]$$

$$\beta_{\text{low/high}}^{m}(t,z) = \beta \left[R_{\text{a}} R_{\text{b,low/high}}^{m}(t,z) \right]$$
(III.24)
(III.25)

and
$$\beta_{\text{low/high}}^{m}(t,z) = \beta \left[R_{\text{a}} R_{\text{b,low/high}}^{m}(t,z) \right]$$
 (III.25)

one obtains successive new estimations of minimum and maximum inversions which approach a common value representing the solution (The claim, that solutions originating from the maximum and minimum assumptions always stay maximum and minimum assumptions that are always closer to the real solution can of course be proofed. I desist from this here as it is not complicated and saves some time).

One can now numerically calculate the successive estimations for both cases together with a condition to abort the calculation as soon as the difference between both solutions is reasonably small. This then is the solution for the pump process. Solutions for successive iterations for a sample case are shown in figure III.4.

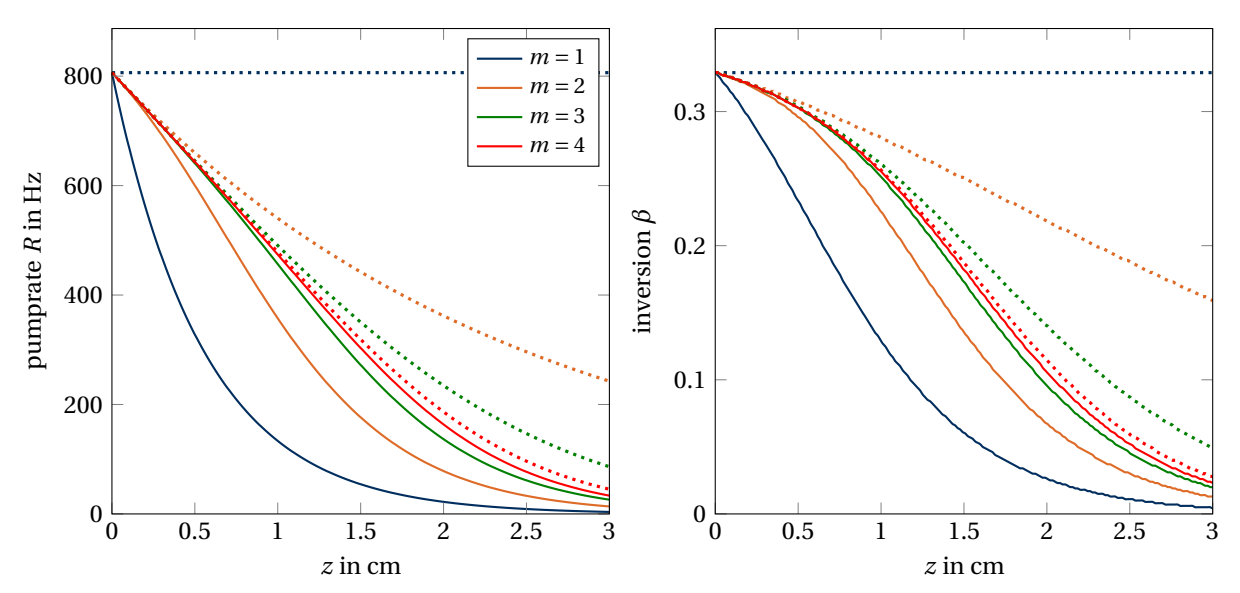


Fig. III.4.: Sample iteration steps for the calculation of the inversion in a laser medium (here Yb:CaF₂ with $N_{\rm dop} = 3.3 \times 10^{20} \, \rm cm^{-3}$ pumped at 980 nm for $\tau_{\rm pump} = 2 \, \rm ms$ with a pump intensity of 30 kW cm⁻²). The dashed lines show the upper limit assumptions and the solid lines the lower limit assumption. m denotes the iteration number.

Though this might seem like a rather complex calculation, a numerical implementation is pretty effective and accurate. The solution converges most of the time after five iteration steps.

Key point: Discussion of the Pump process

Manipulating the input parameters for the pump process, one can see several effects that are present in an actual laser material:

- For a pump duration much longer than the fluorescence lifetime ($\tau_{\rm pump} \gg \tau_f$) the introduced changes to the materials inversion are rather small. Hence, it does not make sense to pump much longer than the lifetime. In practice most lasers work with a pump duration in the range of the fluorescence lifetime. In extreme cases a maximum of twice this value is used.
- For low pump densities the pump density and, hence, the inversion follow an exponential decay as known from Lambert Beers law.
- For high pump intensities the inversion is somehow "pushed through" the material along the propagation axis (the inversion at the entrance face of the crystal stays rather constant, before it converts back to the exponential decay for later times). This can be observed in figure III.5.
- The maximum inversion, that we can achieve for high pump intensities approaches β_{eq} and therefore is strongly dependent on the wavelength (especially near the ZPL). The higher the cross sections are, the less pump intensity is needed to approach this limit.

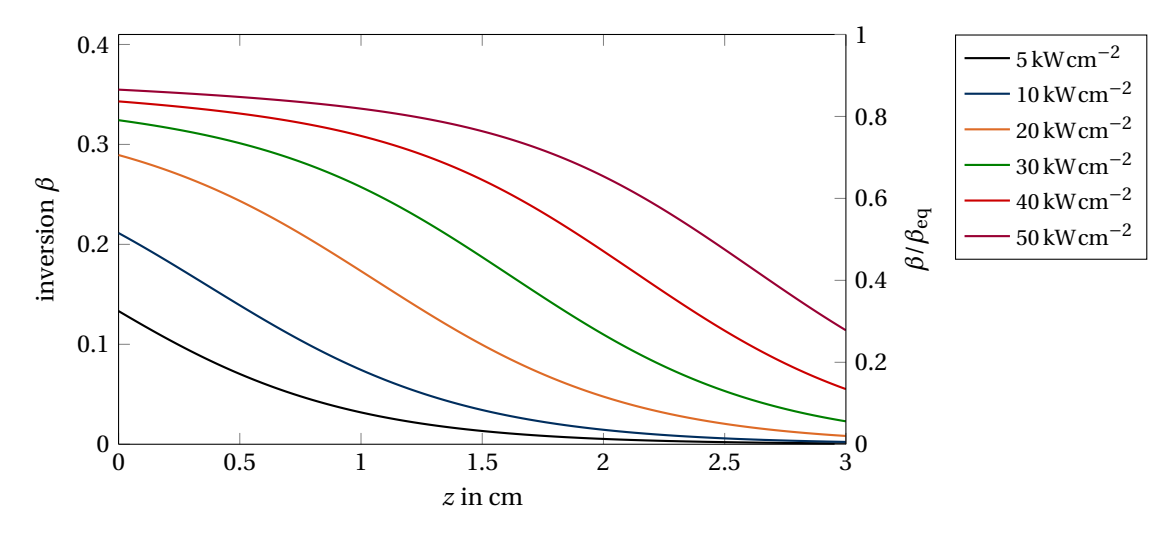


Fig. III.5.: Calculated inversion in Yb:CaF₂ with $N_{\rm dop} = 3.3 \times 10^{20} \, {\rm cm}^{-3}$ and thickness $d = 3 \, {\rm cm}$ pumped at 980 nm for $\tau_{\rm pump} = 2 \, {\rm ms}$ at varying pump intensities. The saturation intensity of Yb:CaF₂ at this wavelength is around $I_{\rm sat} = 8 \, {\rm kW \, cm}^{-2}$.

III.2.3. Storage efficiency

We now want to discuss, which pump parameters we should choose, in order to make the optical conversion from the pump to the laser process as efficient as possible. We can quantify the efficiency of the conversion by calculating the part of the pump energy that can be extracted by the laser. This is called *storage efficiency*. The problem lies within the equilibrium inversion β_{eq} at the laser wavelength λ_l . The stored inversion $\beta(z)$ inside the crystal can only be reduced to the equilibrium inversion, as the material becomes transparent at this point.

With this in mind, the maximum efficiency can be calculated directly using the stored inversion. For this, we have to calculate the maximum fluence, that can be extracted at the laser wavelength,

given by the amount of excited ions minus the amount of ions needed for transparency of the laser material per area:

$$F_{\text{ex}} = N_{\text{dop}} h v_l \cdot \int_0^l \beta(z) - \beta_{\text{eq}}(v_l) \, dz.$$
 (III.26)

We can now compare this value with the incident pump fluence simply given by the product of pump intensity I_{pump} and pump duration τ_{pump} for a rectangular pump pulse

$$F_{\text{pump}} = I_{\text{pump}} \cdot \tau_{\text{pump}} = \Phi \cdot ch \nu_{\text{pump}} \cdot \tau_{\text{pump}}. \tag{III.27}$$

This yields an expression for the maximum storage efficiency η_{store} of a laser:

Equation: Storage efficiency
$$\eta_{\text{store}} = \frac{F_{\text{ex}}}{F_{\text{pump}}} = \frac{N_{\text{dop}}h\nu_l}{I_{\text{pump}}\cdot\tau_{\text{pump}}} \int_0^l \beta(z) - \beta_{\text{eq}}(\nu_l) \, \mathrm{d}z \quad < \quad 1. \tag{III.28}$$

An example for the storage efficiency as a function of pump intensity and pump duration is given in figure III.6 and figure III.7.

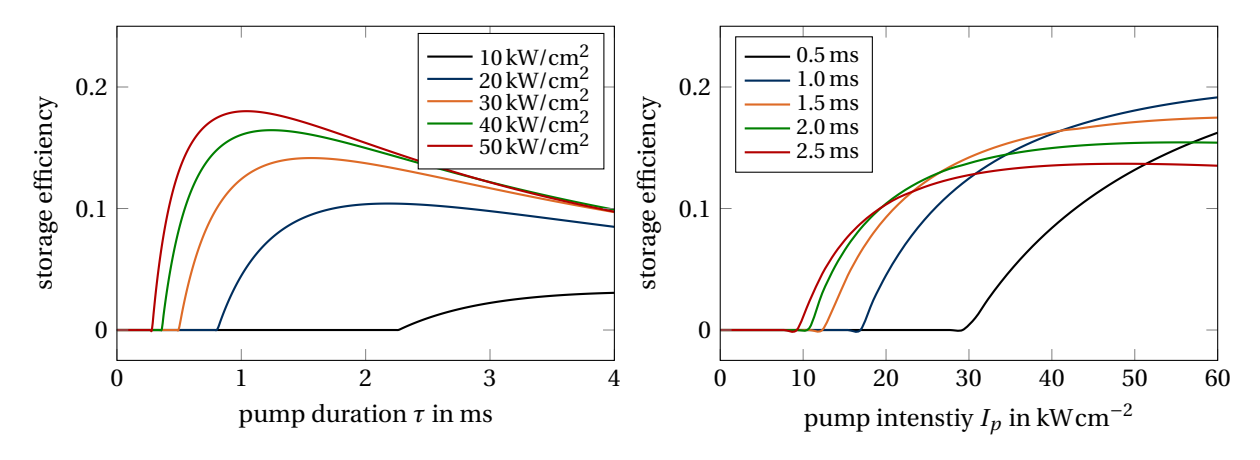


Fig. III.6.: Calculated storage efficiency of Yb: CaF_2 as a function of the pump duration (left) and pump intensity (right). In general, the efficiency rises for increasing pump intensity because the achieved inversion is higher and the equilibrium inversion at the laser wavelength becomes less relevant. The discussion of varying the pump duration is more nuanced. As a higher pump intensity is preferable it becomes clear, that shorter pump durations result in a higher efficiencies.

Key point: How to choose the pump system

From figure III.6 we can make some conclusions for the design of our pump system.

- The Efficiency increases with pump intensity (figure III.6 left).
- Efficiency increases for shorter pump pulses at high intensities (figure III.6 right). This is limited by the size of the pump engine and the thermal stress, the laser medium can take.
- As a compromise we choose the pump duration about equal the fluorescence life time: $\tau_{\text{pump}} \approx \tau_f$
- Efficiency is increased by multipass pumping, this is limited by setup.

• Efficiency increases for lower temperatures because $\beta_{eq}(\lambda_l)$ at the laser wavelength is lower which allows extraction at lower inversion.

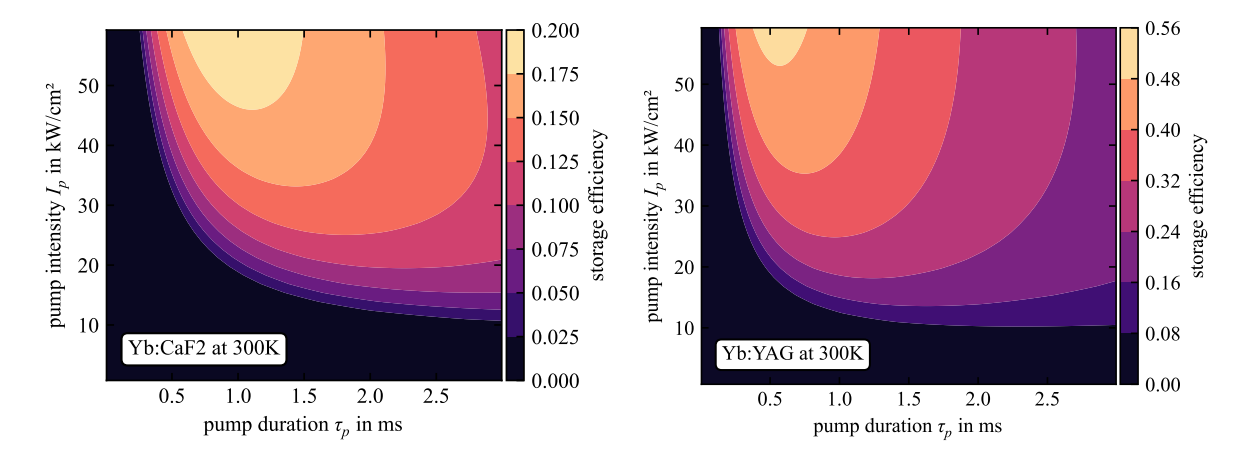


Fig. III.7.: Storage efficiency as a function of pump duration and intensity for Yb:CaF₂ and Yb:YAG. Note that the scaling of the colour bar is different for both materials. The storage efficiency of Yb:YAG is much higher due to a lower saturation intensity of $I_{\text{sat}} = 26 \,\text{kW}\,\text{cm}^{-2}$ compared to Yb:CaF₂ with $I_{\text{sat}} = 54 \,\text{kW}\,\text{cm}^{-2}$ at 940 nm (c.f. figure III.2). Furthermore, the equilibrium inversion at the laser wavelength is also lower for Yb:YAG due to a sharper absorption line.

Comment: Pump limitations

So why cant we just increase the pump intensity as far as we would like?

- LIDT: for nanosecond pulses, the extracting pulse in a cavity with a fluence of more than approx. 10J/cm² will destroy our optics.
- B-Integral: Nonlinear effects will occur. This will be discussed in section V.3.3 in more detail.
- Brightness of the pump: The higher the pump intensity the larger the opening angle will be.

III.3. Amplification

While the pump duration of rare earth ion-doped materials is in the order of the fluorescence lifetime (which is in the millisecond range), laser amplification by stimulated emission takes place at much shorter time scales. Thus, the decay of the upper laser level due to spontaneous emission can be neglected in this regime. Therefore, if we consider the amplification process, the rate equations can be simplified and now have an analytical solution. We will use the rate equation in the following form neglecting the pump radiation as well as the fluorescence:

$$\frac{\mathrm{d}N_2}{\mathrm{d}t} = -c\Phi_\mathrm{l}(\sigma_\mathrm{e}(\lambda_\mathrm{l})N_2 - \sigma_\mathrm{a}(\lambda_\mathrm{l})N_1). \tag{III.29}$$

In the following, we first want to discuss the simple case of a constant inversion β which will lead us to the small signal gain description. Later, we want to show the analytical solution under the assumption that absorption cannot be neglected.

III.3.1. Small signal gain

When we have small signal gain, the inversion is not changed by the extracting laser field and stays constant (β is constant over z).

Comment: Reminder of the substitutions

To estimate the small signal gain we can again the photon density Φ and use the same substitutions (III.7) and (III.9) as for the pump process:

• The **inversion**:
$$\beta(t,z) = \frac{N_2(t,z)}{N_{\rm dop}}$$
 with $N_{\rm dop} = N_1 + N_2$

• The **equilibrium inversion**:
$$\beta_{eq} = \frac{\sigma_a}{\sigma_a + \sigma_e}$$
.

We can use the third part of equation (III.4) and obtain a differential equation of the photon density in terms of β and β_{eq}

$$\frac{d\Phi}{dz} \cdot c = -\frac{dN_2}{dt} = c\Phi_{l}(\sigma_{e}(\lambda_{l})N_2 - \sigma_{a}(\lambda_{l})N_1)$$

$$\Rightarrow \frac{d\Phi}{dz} = \Phi_{l}(\sigma_{e}(\lambda_{l})N_2 - \sigma_{a}(\lambda_{l})N_1) \text{ with } N_{\text{dop}} = N_1 + N_2$$

$$= \Phi_{l}[(\sigma_{e} + \sigma_{a})N_2 - \sigma_{a}N_{\text{dop}}]$$

$$= \Phi_{l}N_{\text{dop}}(\sigma_{e} + \sigma_{a})\left[\beta - \frac{\sigma_{a}}{\sigma_{a} + \sigma_{e}}\right]$$

$$= \Phi_{l}N_{\text{dop}}(\sigma_{e} + \sigma_{a})(\beta - \beta_{\text{eq}}).$$

$$= \Phi_{l}N_{\text{dop}}(\sigma_{e}\beta - \sigma_{a}(1 - \beta)).$$
(III.31)

This differential equation is easily solvable, which gives us:

$$\Phi(z) = \Phi_0 \cdot e^{N_{\text{dop}}(\sigma_e + \sigma_a)(\beta - \beta_{\text{eq}}) \cdot z}$$

$$\Phi(z) = \Phi_0 \cdot e^{N_{\text{dop}}(\sigma_e \beta - \sigma_a(1 - \beta)) \cdot z}.$$
(III.33)

From this result we can deduct the small signal gain (using the length of the laser medium z = d):

Equation: Small signal gain

$$G_0 := \frac{\Phi(z)}{\Phi_0} = \exp(g) = \exp(N_{\text{dop}}(\sigma_e \beta - \sigma_a (1 - \beta)) \cdot d)$$

$$= \exp(N_{\text{dop}} \sigma(\beta - \beta_{\text{eq}}) \cdot d) \text{ with } \sigma = \sigma_a + \sigma_e.$$
(III.34)

We call G_0 the (small signal) gain and g the gain coefficient.

Comment: different equivalent forms of writing down the gain coefficient

- The first line (equation (III.34)) describes that the gain coefficient is given by the effective amount $N_{\rm dop}\sigma_{\rm e}d$ of stimulated ions (β) emitting radiation minus the effective amount $N_{\rm dop}\sigma_{\rm a}d$ of ground state ions $(1-\beta)$ absorbing radiation.
- The second line describes that a gain coefficient g > 0 is only possible if the inversion β is larger than the equilibrium inversion β_{eq} .

Emission and absorption are handled well with these equations if we assume that the inversion is spatially constant and does not change during the amplification process. Thus, we exclude saturation effects and differences in the inversion of the pumped crystal.

The small signal gain of two different Yb-doped laser media was simulated in figure III.8 using the spectral absorption and emission cross sections from figure II.14.

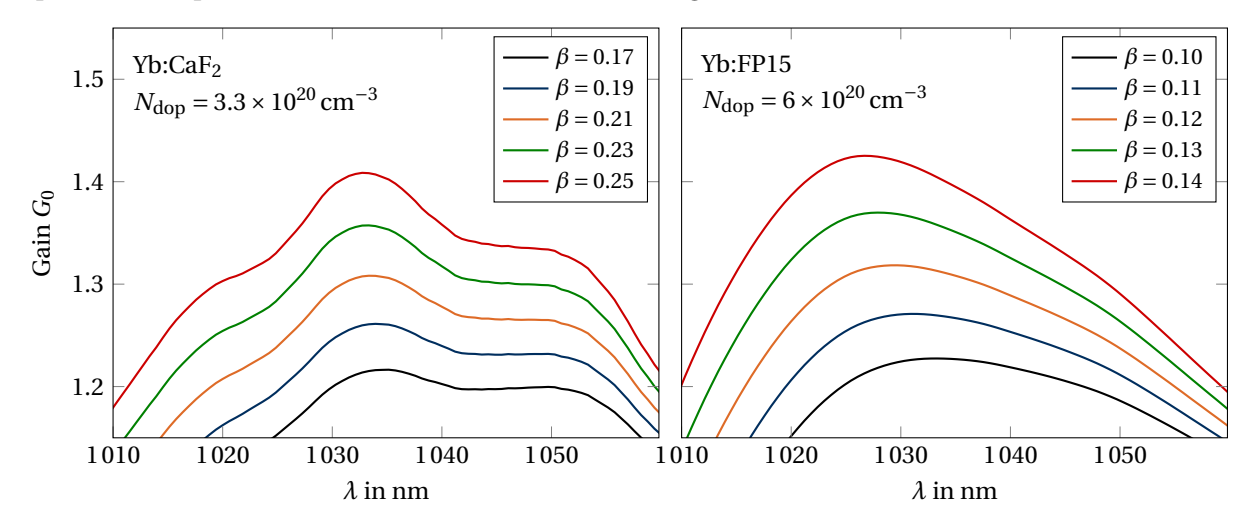


Fig. III.8.: Simulated small signal gain of Yb:CaF₂ (left) with a thickness of d = 11 mm and Yb:FP15 (right) with a thickness of d = 6 mm in a double pass setup. Since the doping concentration of Yb:CaF₂ is about half as large as for the Yb:FP15 glass, we need a higher inversion β and a thicker crystal to reach the same double pass gain values.

Key point: Small signal gain

- 1. The small signal gain G_0 increases exponentially with the inversion, however, since g is generally small, this exponential behaviour looks rather linear (c. f. figure III.8).
- 2. As stated before, there is only gain, when $\beta > \beta_{\rm eq}(\lambda_l)$ is fulfilled. This is only achievable by the fact that the equilibrium inversion at the pump wavelength is higher than at the laser wavelength $\beta_{\rm eq}(\lambda_p) > \beta_{\rm eq}(\lambda_l)$.
- 3. Due to the frequency dependence of the effective cross-sections, the gain factor becomes

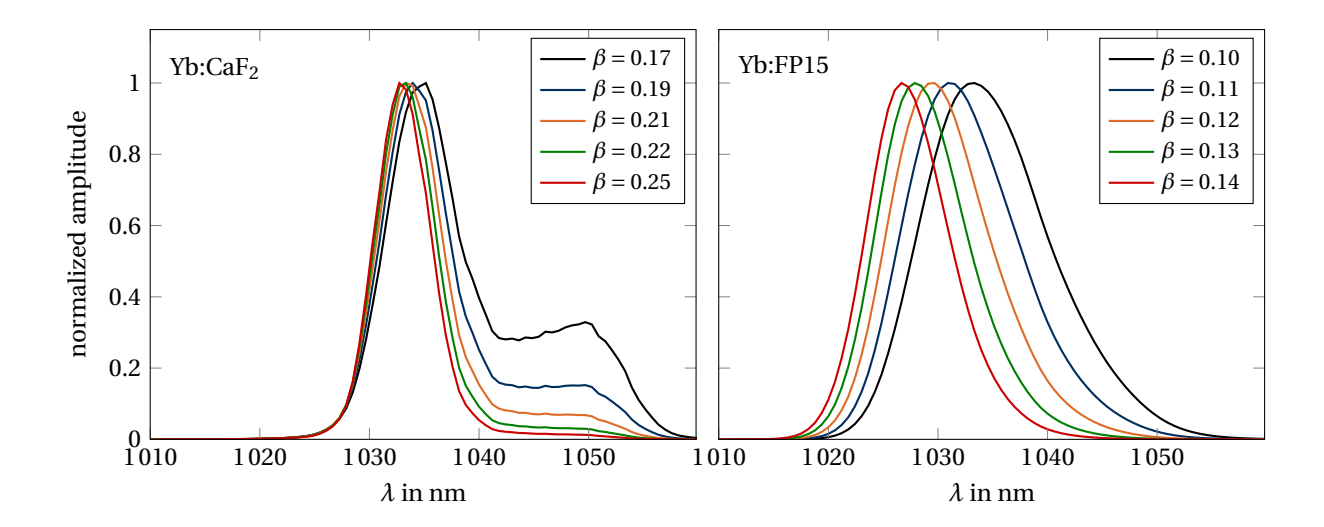


Fig. III.9.: Simulated amplified pulse shapes generated in the cavity based on the small signal gain profile calculated in figure III.8. For Yb:FP15 we observe a blue-shift of the central wavelength of the generated spectrum for higher inversions β .

frequency dependent $g_0(\lambda)$. This means that the spectrum of the amplified laser is influenced according to this spectral dependence. After several material passes, this leads to narrowing of the bandwidth, which is often referred to as "gain narrowing".

4. The "quasi-three level" characteristic of Yb-doped laser materials leads to a non-neglectable absorption in the laser emission range. For higher pump intensites (i. e. higher inversion β), this leads to a "blue"-shift of the spectral gain curve. This can be observed especially for Yb:FP15 glass in figure III.8.

III.3.2. Saturation fluence

Similar to the pump process one can define a saturation fluence which corresponds to the input fluence of an amplifier for which the small signal gain is reduced to 1/2 of its initial value. As it has been shown in the last section, the gain factor g is proportional to the inversion β in the steady state of continuous pumping

$$g = N_{\text{dop}}\sigma(\beta - \beta_{\text{eq}})d. \tag{III.35}$$

Therefore, such an extraction of laser energy (i. e. a CW seed pulse) will reduce the gain factor g in the same way as the inversion β (c. f. equation (III.16)). Thus, the gain is given by:

$$g(F) = \frac{g_0}{1 + \frac{F}{F_{\text{sat}}}},$$
 (III.36)

where F_{sat} is the saturation fluence given by

Equation: Saturation fluence
$$F_{\rm sat} = \frac{h v}{\sigma_{\rm a} + \sigma_{\rm e}}. \tag{III.37}$$

Furthermore, we can relate the saturation fluence to the maximum extractable fluence (given by

equation (III.26)). By noting, that in general *g* has to be obtained by integrating along the axis of the laser medium, we find that

$$g = N_{\text{dop}}(\sigma_{\text{a}} + \sigma_{\text{e}}) \int (\beta - \beta_{\text{eq}}) \, dz \stackrel{\text{(III.26)}}{=} \frac{\sigma_{\text{a}} + \sigma_{\text{e}}}{h\nu} F_{\text{ex}} = \frac{F_{\text{ex}}}{F_{\text{sat}}}.$$
 (III.38)

Thus, the saturation fluence limits the extractable fluence from an amplifier for a given gain coefficient *g*.

As the saturation fluence denotes an operation scheme, which significantly alters the inversion state of the active medium, it is desirable to work at fluences that are even higher, as this would mean, that the energy is efficiently extracted (the ultimate limit is the laser induced damage threshold). It should be noted that in a multi-pass amplifier the fluence is added up for every pass, which would allow extraction with higher fluences than which are applied in a single pass.

Further, as soon as one approaches these fluences, it will no longer be possible to use small signal gain. Hence a more elaborated solution for the amplification got to be used, which will be described in the following section.

Comment: Saturation fluence

- 1. Even though we defined the saturation fluence as the input fluence which reduces the gain coefficient to 1/2 of its initial value, this only true for CW seed sources. In a pulsed regime, the gain coefficient is reduced to 1/e of its initial value in the limit $g \to 0$ (c. f. figure III.12).
- 2. We want to note the similarity to the pump saturation intensity $I_{\rm sat}$ (III.16) in the pump process. Multiplying $I_{\rm sat}$ with the fluorescence life time (which is typically also the pump time of the CW laser pump diode) we obtain the same formula (different numerical value, as $\sigma_{\rm a}, \sigma_{\rm e}$ are wavelength dependent), which describes the saturation fluence $F_{\rm sat}$ at the pump wavelength.

III.3.3. Frantz Nodvik solution

For laser pulses with high photon densities, the gain factor is significantly influenced by the inversion reduction during the passage through the pumped laser material. Therefore, we cannot assume a constant small signal gain anymore as the rising edge of the laser pulse will be amplified more than the trailing edge.

The Frantz - Nodvik algorithm as given in the original paper from 1963 allows for an accurate solution but has to be modified for a three level scheme, as we have to deal with reabsorption at the laser wavelength.

Comment: Notation

For consistency reasons we will **not** use the same definition of the inversion as Frantz-Nodvik [FN63]:

$$\Delta = N_2 - N_1. \tag{III.39}$$

Therefore, the solutions we mention here look different than the solution given in the original publication.

We start with the rate equations for inversion $\beta(z,t)$ and photon density $\Phi(z,t)$. By modifying equation (III.33) we can write

$$\frac{\partial \Phi}{\partial z} = -\alpha \Phi \left(1 - \frac{\beta}{\beta_{\text{eq}}} \right) \quad \text{with} \quad \alpha = \sigma_{\text{a}} \cdot N_{\text{dop}}$$
 (III.40)

$$\Rightarrow \frac{\partial \beta}{\partial t} = \sigma \cdot c \beta_{\rm eq} \Phi \left(1 - \frac{\beta}{\beta_{\rm eq}} \right) \quad {\rm with} \quad \sigma = \sigma_{\rm a} + \sigma_{\rm e}. \tag{III.41}$$

For the second equation we used the following relations:

$$\frac{\partial \beta}{\partial t} = \frac{\partial N_2}{\partial z} \frac{\partial z}{\partial t} \frac{1}{N_{\text{dop}}} = -\frac{\partial \Phi}{\partial z} \frac{c}{N_{\text{dop}}} \quad \text{and} \quad \sigma_{\text{a}} = \beta_{\text{eq}} \cdot (\sigma_{\text{a}} + \sigma_{\text{e}}). \tag{III.42}$$

The solution of this system of equations is rather complex, so we do not want to show it here. However, you can find the derivation in the appendix A.1. The final result is:

Equation: Frantz-Nodvik solution

$$\Phi(z,t) = \Phi_0(t) \frac{S(t) \cdot G(z)}{1 + [S(t) - 1]G(z)} \quad \text{with} \quad \Phi_0 = \Phi(z = 0, t)$$
 (III.43)

$$\beta(z,t) = \beta_{\text{eq}} + \frac{\beta_0(z) - \beta_{\text{eq}}}{1 + [S(t) - 1]G(z)} \quad \text{with} \quad \beta_0 = \beta(z, t = 0)$$
 (III.44)

with
$$S(t) = \exp\left[\frac{F_0(t)}{F_{\text{sat}}}\right] = \exp\left[\sigma c \int_0^t \Phi_0(t') dt'\right]$$
 (Saturation) (III.45)

$$G(z) = \exp \left[N_{\text{dop}} \sigma \int_{0}^{z} \left(\beta_{0}(z') - \beta_{\text{eq}} \right) dz' \right]$$
 (Gain). (III.46)

- $\Phi_0(t)$ Photon density in front of the gain medium (z = 0) before interaction.
- $\beta_0(z)$ Space dependent inversion of the active medium at t = 0 before interaction.
- S(t) This expression is a saturation term which is $S \approx 1$ for the small signal gain $(F_{\rm in}/F_{\rm sat})$ or an exponentially growing function $S(t) = \exp(\sigma_c \Phi_0 t)$ for a square shaped pulse.

G(z) This is equal to the small signal Gain $G_0(z)$. For a spatially constant β_0 it reads (III.34)

$$G(z, \beta_0) = e^{N_{\text{dop}}(\sigma_e + \sigma_a)(\beta_0 - \beta_{\text{eq}})z} = G_0.$$
 (III.47)

F(t) This is the accumulated fluence (energy per area) of the laser pulse at time t:

$$F_0(t) = h v \cdot c \int_0^t \Phi_0(t') \, \mathrm{d}t'. \tag{III.48}$$

 $F_{\rm sat}$ The *saturation fluence* describes, at which fluences saturation effects start to play a role and is a wavelength dependent property. For an efficient energy extraction, an input fluence of $F(t) > F_{\rm sat}$ is desired. It is given by (III.37).

Small photon density

We can already see, that in the case of a very small photon density $F_{\rm in} \ll F_{\rm sat}$, these equations translate into the ones we already derived for the small signal gain:

$$\Phi_0 \approx 0 \Rightarrow S \approx 1 \quad \Rightarrow \quad \Phi(z, t) = \Phi_0(t) \cdot G(z) \quad \text{and} \quad \beta(z, t) = \beta_0(z).$$
 (III.49)

This means, for small input fluences the inversion remains unchanged and the photon density is amplified by the small signal gain.

High photon density

In case of a high input fluence way larger than the saturation fluence $F(t) \gg F_{\text{sat}}$ we find $S \gg 1$ and thus

$$\Phi(t) = \Phi_0(t) \frac{S(t) \cdot G(z)}{S(t) \cdot G(z)} = \Phi_0(t) \quad \text{and} \quad \beta = \beta_{\text{eq}} + \underbrace{\frac{\beta_0(z) - \beta_{\text{eq}}}{1 + [S(t) - 1]G(z)}}_{\to 0} = \beta_{\text{eq}}. \quad (\text{III.50})$$

Here, the photon density remains unchanged and the inversion approaches its equilibrium state. Thus, the medium becomes transparent.

No initial inversion

In case of no initial inversion $\beta_0 = 0$, we are not extracting energy but pump the laser active medium instead. Still, our equations apply in this case (e.g. the Gain G(z) simplifies to Lambert Beer's law $G(z) = \exp(-N_{\rm dop}\sigma_{\rm a}\cdot z)$) and we can derive an interesting formula for the output inversion

$$\beta(z,t) = \beta_{\text{eq}} - \frac{\beta_{\text{eq}}}{1 + (S-1)G} = \frac{G(S-1)}{1 + G(S-1)} \beta_{\text{eq}} = \frac{\beta_{\text{eq}}}{1 + \frac{1}{G(\exp(F/F_{\text{sat}}) - 1)}}.$$
 (III.51)

The inversion is displayed in figure III.10 (right) for different input fluences.

Since we use the Frantz-Nodvik solution, we neglect effects of spontaneous emission. Therefore, this results refers to a pumping process with a pump pulse much shorter than the life time of the medium e.g. a 100 ns (Q-switched) pump pulse for a Ti:Sa system. For fluences beyond the saturation fluence, the inversion is pushed through the laser active material.

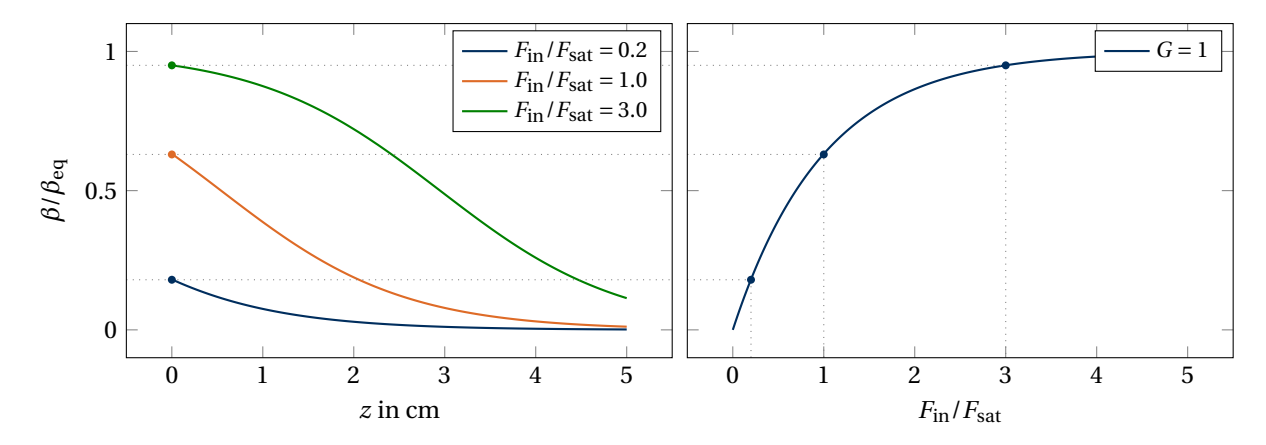


Fig. III.10.: For an initial inversion of $\beta(z,t)=0$ we do not extract energy from the system, but rather pump the laser material. However, the Frantz-Nodvik solution still applies. Left: Calculated inversion $\beta(z)$ for three different values of the pump input fluence. The gain was assumed as $G(z)=\exp(-\alpha\cdot z)$ with $\alpha=1\,\mathrm{cm}^{-1}$. Right: Inversion at the entrance of the medium as a function of the input fluence.

Comment: Comparison to the pump process

The derived equation (III.51) can be related to equation (III.16) of the pump process. For small input fluences we can write $\exp(F/F_{\text{sat}}) \approx 1 + F/F_{\text{sat}}$ which results at the front of the laser medium (z = 0) in

$$\beta(z,t) = \frac{\beta_{\text{eq}}}{1 + \frac{F_{\text{sat}}}{F}} \quad \text{with} \quad G = \exp(-N_{\text{dop}}\sigma_{\text{a}}z) = 1.$$
 (III.52)

Now this formula is identical to the solution of the pump process in equilibrium for an infinite pump duration.

Key point: Frantz-Nodvik solution

- 1. Approaching saturation, the single pass gain factor is reduced and approaches zero for high input fluence (complies with energy conservation).
- 2. As long as the gain is not saturated, the input pulse shape is maintained.
- 3. In saturation the temporal pulse shape is altered, as the leading edge sees a higher gain than the rest of the pulse (edge steepening). This effect is stronger for:
 - · higher single pass gain
 - already steep etched pulse shapes.
- 4. The edge steepening should be taken into account for all effects linked to intensity as non-linear effects and the LIDT.
- 5. Edge steepening can also occur on the spectrum in a Chirped Pulse Amplification (CPA) system, where typically a positively chirped pulse propagates through the amplifier. Here, the red part of the spectrum experiences edge-steepening.

III.3.4. Saturation corrected gain

As the pulse travels through the amplifying medium, the gain changes as saturation effects start to deplete the inversion. Therefore, we want to give a formula for the total gain after a single pass, which is independent on the pulse shape. We can define it as the ratio of the input and output fluence:

$$\mathcal{G} = \int_{-\infty}^{\infty} \Phi(t) \, \mathrm{d}t / \int_{-\infty}^{\infty} \Phi_0(t) \, \mathrm{d}t.$$
 (III.53)

Let us first find an expression for the integral of the laser fluence. We can rewrite (III.43) as

$$\Phi(t) = \Phi_0(t) \frac{S \cdot G}{1 + (S - 1)G} = \frac{1}{\sigma c} \frac{\partial}{\partial t} \ln(1 + (S - 1)G). \tag{III.54}$$

Now we can do the integration which leads to

$$\mathcal{G} = \int_{-\infty}^{\infty} \Phi(t) \, \mathrm{d}t / \int_{-\infty}^{\infty} \Phi_0(t) \, \mathrm{d}t = \frac{\ln(1 + (S - 1)G)}{\sigma c \int_{-\infty}^{\infty} \Phi_0(t) \, \mathrm{d}t}.$$
 (III.55)

Now we can use (III.48) with $F_{\rm in} = F_0(t \to \infty)$ and the definition of $F_{\rm sat} = hv/(\sigma_{\rm a} + \sigma_{\rm e}) = hv/\sigma$ to find

Equation: Saturation corrected gain

$$\mathscr{G}(z) = \frac{F_{\text{sat}}}{F_{\text{in}}} \ln \left(1 + G(z) \left[\exp \left(\frac{F_{\text{in}}}{F_{\text{sat}}} \right) - 1 \right] \right). \tag{III.56}$$

Comment:

Using a low input fluence $F_{in} \ll F_{sat}$, this will simplify to the small signal gain formula (III.34)

$$\mathcal{G}(z) \approx \frac{F_{\text{sat}}}{F_{\text{in}}} \ln \left(1 + G(z) \frac{F_{\text{in}}}{F_{\text{sat}}} \right) \qquad (\exp x \approx 1 + x)$$

$$\approx \frac{F_{\text{sat}}}{F_{\text{in}}} G(z) \frac{F_{\text{in}}}{F_{\text{sat}}} = G(z) \qquad (\ln(1+x) \approx x). \tag{III.57}$$

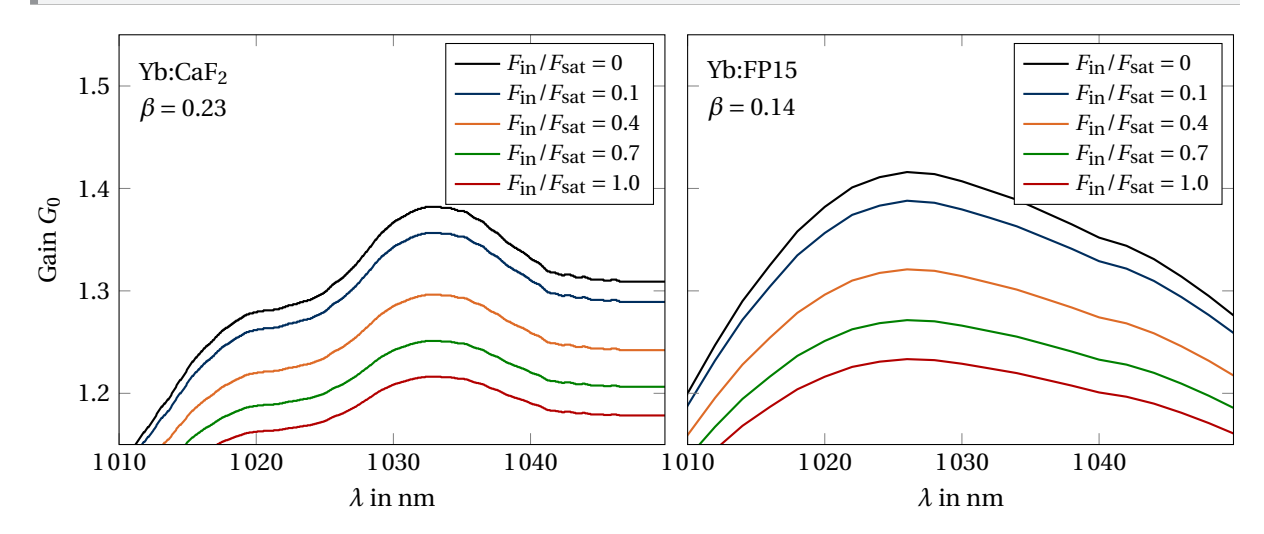


Fig. III.11.: Simulated correction of the small signal gain of Yb:CaF₂ (left) with a thickness of d = 11 mm and Yb:FP15 (right) with a thickness of d = 6 mm in a double pass setup for different input fluences F_{in} and constant inversion β .

III.3.5. Reduction of the small signal gain

In the introduction of the saturation fluence $F_{\rm sat}$ we claimed that for input fluences $F_{\rm in} = F_{\rm sat}$ the small signal gain factor g is reduced to 1/2 (CW case) or 1/e (pulsed case) of its initial value. For that let us calculate the small signal gain, after one pass in the amplifier. For that we insert the Frantz-Nodvik solution of the inversion β (III.44) into the formula of the small signal gain G_0 (III.46)

$$G_{1}(d) = \exp\left[N_{\text{dop}}\sigma \int_{0}^{d} \left(\beta_{\text{eq}} + \frac{\beta_{0}(z) - \beta_{\text{eq}}}{1 + [S(t) - 1]G(z)}\right) - \beta_{\text{eq}} dz\right]$$

$$= \exp\left[N_{\text{dop}}\sigma \int_{0}^{d} \frac{\beta_{0}(z) - \beta_{\text{eq}}}{1 + [S(t) - 1] \exp\left(N_{\text{dop}}\sigma \int_{0}^{z} (\beta_{0}(z') - \beta_{\text{eq}}) dz'\right)} dz\right]$$

$$= \exp\left[a \int_{0}^{d} \frac{f(z)}{1 + b \cdot \exp(a \cdot F(z))} dz\right] \quad \text{with} \quad f(z) = \beta_{0}(z) - \beta_{\text{eq}}, \ a = N_{\text{dop}}\sigma, \ b = S(t) - 1. \quad \text{(III.58)}$$

This integral is analytically solvable (notice that f(z) is the derivative of F(z)) and the solution is given by

$$G_{1}(d) = \exp\left[-\ln\left(1 + \frac{1}{b}\exp(-a \cdot F(z))\right)\Big|_{0}^{d}\right]$$

$$= \frac{b+1}{\exp(-a \cdot F(d)) + b} = \frac{S(t)}{1/G(d) + [S(t) - 1]} = \frac{G_{0}S(t)}{1 + G_{0}[S(t) - 1]}.$$
(III.59)

This is the same factor which appears in (III.43) to describe the change in the photon density after amplification.

Now we can have a look at the reduction of the small signal gain for an input fluence of $F_{\text{in}} = F_{\text{sat}}$ which means $S(t \to \infty) = 1$ and plot the result as a function of the small signal gain G_0 .

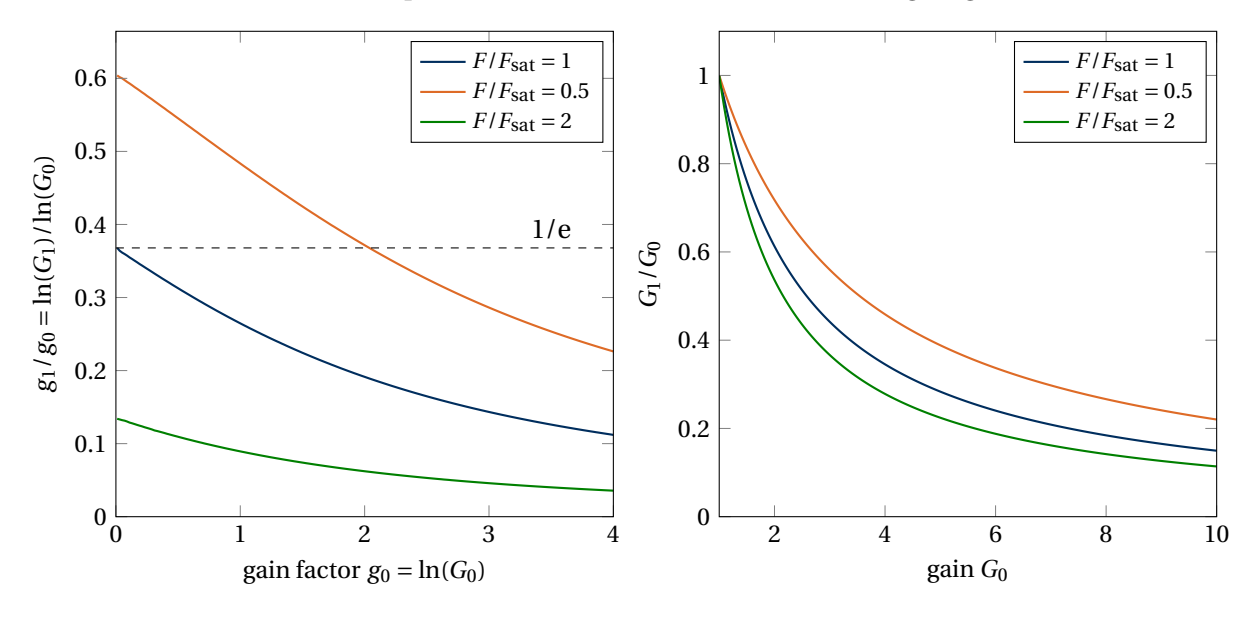


Fig. III.12.: Left: Reduction of the gain factor $g = \ln(G)$ as a function of the input small signal gain factor g_0 for different input fluences F. At $F = F_{\text{sat}}$ the small signal gain factor is reduced to 1/e of its original value in the limit of $g \to 0$. This corresponds to the often used definition of the saturation fluence. Right: Reduction of the small signal gain G as a function of the input gain as a function of the small signal gain.

IV. Resonators and seed sources

In any large high energy system, a crucial part is the so called "front end". As this generates the pulses that are sent to the amplifier chain afterwards, it also defines many parameters for the overall laser system (though some might be influenced by the amplification process):

- pulse length τ
- wavelength λ
- bandwidth $\Delta \lambda$
- · pulse shape
- · temporal contrast
- · maximum repetition rate

Furthermore, problems arising in this part of the laser will influence the whole system. In the following, we will discuss different kinds of methods to generate the pulse of the front end. In this chapter, we will have a look on the classical laser resonators and the basic principles to operate them in nanosecond and femtosecond regimes or alternatively in longitudinal single mode (though we will not go too far into detail here).

But first we will renew the knowledge about matrix optics, which we will regularly use in the following chapters to describe the different kinds of laser resonators.

IV.1. Basics of the ABCD Matrix method

For now we will start with (par-axial) geometrical optics. We can describe an arbitrary ray of our beam in any point z along the optical axis in a medium with refractive index n by its distance x from the optical axis and its angle α with respect to said axis. This can be expressed by a vector:

$$r = \begin{pmatrix} x \\ n\alpha \end{pmatrix}. \tag{IV.1}$$

If we now consider anything interacting with the beam, e.g. a lens or a translation in space, it will alter the position and angle of our beam in dependence of its original set of parameters. As we are in the *par-axial approximation* ($\tan \alpha \approx \sin \alpha \approx \alpha$), we will only consider changes that are proportional to these original parameters. This simplifies Snell's law of refraction to $n_1\alpha_1 = n_2\alpha_2$. In this regime, any setup can be expressed by a system of linear equations with the proportionality factors A, B, C and D, which can be compactified into a matrix notation

$$x' = A \cdot x + B \cdot n\alpha$$

$$\alpha' = C \cdot x + D \cdot n\alpha \qquad \Rightarrow \qquad \mathbf{r'} = \begin{pmatrix} A & B \\ C & D \end{pmatrix} \cdot \mathbf{r}$$
(IV.2)

Here are some basic matrices for standard elements we will often use [ST19, p.29]:

Equation: ABCD matrices

propagation of distance
$$d$$
 in medium n_1
$$T = \begin{pmatrix} 1 & d/n \\ 0 & 1 \end{pmatrix}$$
 (IV.3)

thin lens/curved mirror with focal width
$$f$$
 $L = \begin{pmatrix} 1 & 0 \\ -\frac{1}{f} & 1 \end{pmatrix}$ (IV.4)

refraction from plane surface
$$n_1$$
 to n_2 $R = \begin{pmatrix} 1 & 0 \\ 0 & \frac{n_1}{n_2} \end{pmatrix}$ (IV.5)

refraction at a spherical surface
$$n_1$$
 to n_2 , curvature R
$$R_L = \begin{pmatrix} 1 & 0 \\ -\frac{n_2 - n_1}{R} & \frac{n_1}{n_2} \end{pmatrix}$$
 (IV.6)

If we now have a series of optical elements we can calculate the system's matrix by a matrix multiplication of the individual elements (the sequence of elements has to be considered).

Example: Single lens with propagation

Let's take an example to learn how to read an ABCD matrix: We assume a beam, which first propagates some distance g then sees a lens with a focal length f and finally propagates again for a distance b. We first calculate the system matrix M:

$$M = T_2 \cdot L \cdot T_1 = \begin{pmatrix} 1 & b \\ 0 & 1 \end{pmatrix} \cdot \begin{pmatrix} 1 & 0 \\ -\frac{1}{f} & 1 \end{pmatrix} \cdot \begin{pmatrix} 1 & g \\ 0 & 1 \end{pmatrix}$$

$$M = \begin{pmatrix} 1 - \frac{b}{f} & g + b - \frac{gb}{f} \\ -\frac{1}{f} & 1 - \frac{g}{f} \end{pmatrix}$$
 (IV.7)

Besides being able to calculate the output ray of any input ray, what can we gain from M? Can we get more information from the matrix? Yes we can!

Imaging

If we want to image something, our output beam position shall **not** be dependent of the angular distribution of our input. Hence the B term of our matrix has got to be zero (c. f. equation (IV.2)). In the case of our single lens this means:

$$0 = g + b - \frac{gb}{f} \quad \Rightarrow \quad \frac{1}{f} = \frac{1}{g} + \frac{1}{b}. \tag{IV.8}$$

This is now just the well known lens equation!

If we further want to know the magnification V of our image in comparison to the input, we just have to look at the entry "A", which is multiplied with our input ray position:

$$V = -\frac{b}{f} + 1 \stackrel{\text{(IV.8)}}{=} -\frac{b}{g} - \frac{b}{b} + 1 = -\frac{b}{g}.$$
 (IV.9)

Hence, we can directly read the magnification factor and the orientation of our image from the matrix. This method can be applied to any optical system! Hence, we can calculate the image plane position and magnification, which will be helpful later.

Far field

An often required task is the determination of the so called far field (angle distribution) of a beam (geometrical optics!). We can use our single lens to do this, but we might wonder where we have to place the camera? To measure the angle distribution e.g. with a camera, we would need to see it in position space. Hence, the position of our output beam should only depend on our angular distribution, meaning *A* got to be zero:

$$0 = -\frac{b}{f} + 1 \quad \Rightarrow \quad b = f. \tag{IV.10}$$

We see, that the far field will always be in focal distance of our lens. Here, the far field position is independent from the distance between lens and the object plane (which is only true in the geometrical optic approximation)!

Finally, we would like to know how we can read the actual angle from the beam size. This is possible with the *B* parameter as (see equation (IV.2)):

$$x' \stackrel{\text{(A=0)}}{=} B \cdot \alpha = \left(g - \frac{gb}{f} + b \right) \cdot \alpha$$

$$x' = \left(g - \frac{gf}{f} + f \right) \cdot \alpha = f \cdot \alpha \quad \Rightarrow \quad \alpha = \frac{x'}{f}. \tag{IV.11}$$

Comment: Special matrix properties

As we have seen ABCD matrices are a very valuable tool for calculating optical systems and we will use it from time to time. Finally, we want to mention some special properties of ABCD matrices:

- *not* commutative: $M_2 \cdot M_1 \neq M_1 \cdot M_2$

- associative: $M_3 \cdot (M_2 \cdot M_1) = (M_3 \cdot M_2) \cdot M_1$

- determinant: $\det(M) = AD - BC = \frac{n_1}{n_2}$ or when no medium change is involved $\det(M) = 1$

- inverse system: $M_{\rightarrow} = \begin{pmatrix} A & B \\ C & D \end{pmatrix} \rightarrow M_{\leftarrow} = \frac{n_2}{n_1} \begin{pmatrix} D & B \\ C & A \end{pmatrix}$ (c. f. seminar for derivation)

IV.1.1. Stable Laser Resonator and ABCD matrix

If we consider a resonator, whose system matrix is represented by M, we would like to consider many round-trips to allow for amplification. Hence we have to calculate:

$$M^n = \begin{pmatrix} A & B \\ C & D \end{pmatrix}^n.$$
 (IV.12)

For this we use the transformation of the principal axis with the Eigenvalues x_i :

$$\begin{pmatrix} A & B \\ C & D \end{pmatrix}^n = W \cdot \begin{pmatrix} \lambda_1^n & 0 \\ 0 & \lambda_2^n \end{pmatrix} \cdot W^{-1}$$
 (IV.13)

Hence, for a stable cavity, the absolute values of the Eigenvalues λ_1, λ_2 got to be ≤ 1 . We can calculate

them solving the characteristic equation:

$$0 = \det(M - \lambda \cdot \mathbb{I})$$

$$0 = (A - \lambda)(D - \lambda) - BC$$

$$0 = \lambda^2 - (A + D)\lambda + \underbrace{AD - BC}_{=1}$$

$$\Rightarrow \lambda_{1/2} = \frac{A + D}{2} \pm \sqrt{\frac{(A + D)^2}{2^2} - 1}.$$
(IV.14)

And as follows from the determinant $AD - BC = 1 = \lambda_1 \lambda_2$, the only real solution that fits our criteria for a stable cavity is $\lambda_1 = \lambda_2 = 1$. Alternatively we can allow for complex values. From this we obtain the stability criterion:

Equation: Stability criterion of a laser resonator

$$\left| \frac{A+D}{2} \right| \le 1. \tag{IV.15}$$

We now want to consider a simple resonator design with two curved mirrors with radius of curvature R_1 and R_2 and distance L as shown in figure IV.1.

$$\begin{pmatrix} 1 & 0 \\ \frac{2}{R_1} & 1 \end{pmatrix} = L_1 \qquad \qquad L_2 = \begin{pmatrix} 1 & 0 \\ \frac{2}{R_2} & 1 \end{pmatrix}$$

$$\begin{pmatrix} 1 & 0 \\ \frac{1}{R_1} & 1 \end{pmatrix} = L'_1 \qquad \begin{pmatrix} 1 & 0 \\ \frac{1}{R_2} & 1 \end{pmatrix}$$

Fig. IV.1.: Top: Simple resonator design with two curved mirrors.

Bottom: Since curved mirrors and lenses are identical in the matrix formalism you can imagine the curved mirror being represented by two thin lenses which inverse focal lengths add up $\frac{1}{f_{tot}} = \frac{1}{f} + \frac{1}{f}$.

The focal lengths are given as $f_{1/2}=-\frac{R_{1/2}}{2}$. We start with the resonator matrix of half a round trip. For symmetry reasons we will replace the curved mirror with two lenses $f=1/R_1$ that, together, have the same refractive power as the curved mirror and we will start in the middle of them. Then M_{\rightarrow} is given by

$$\begin{split} M_{\to} &= L_2'(R_2) \cdot T(L) \cdot L_1'(R_1) \\ &= \begin{pmatrix} 1 & 0 \\ \frac{1}{R_2} & 1 \end{pmatrix} \cdot \begin{pmatrix} 1 & L \\ 0 & 1 \end{pmatrix} \cdot \begin{pmatrix} 1 & 0 \\ \frac{1}{R_1} & 1 \end{pmatrix} = \begin{pmatrix} 1 + \frac{L}{R_1} & B \\ C & 1 + \frac{L}{R_2} \end{pmatrix} := \begin{pmatrix} g_1 & B \\ C & g_2 \end{pmatrix}. \end{split}$$
 (IV.16)

Here, we defined the resonator parameters g_1 , g_2 as

Equation: resonator parameters

$$g_{1/2} = 1 + \frac{L}{R_{1/2}}. ag{IV.17}$$

Now we can use $det(M) = g_1g_2 - BC = 1$ to replace $C = \frac{g_1g_2 - 1}{B}$ which then yields for a full round-trip

in the resonator

$$M_{\leftarrow} \cdot M_{\rightarrow} = \begin{pmatrix} g_2 & B \\ \frac{g_1 g_2 - 1}{B} & g_1 \end{pmatrix} \cdot \begin{pmatrix} g_1 & B \\ \frac{g_1 g_2 - 1}{B} & g_2 \end{pmatrix}$$
 (IV.18)

$$M_{\leftarrow} \cdot M_{\rightarrow} = \begin{pmatrix} g_2 & B \\ \frac{g_1 g_2 - 1}{B} & g_1 \end{pmatrix} \cdot \begin{pmatrix} g_1 & B \\ \frac{g_1 g_2 - 1}{B} & g_2 \end{pmatrix}$$

$$M_{\leftarrow} \cdot M_{\rightarrow} = \begin{pmatrix} 2g_1 g_2 - 1 & 2B g_2 \\ \frac{2g_1 \cdot (g_1 g_2 - 1)}{B} & 2g_1 g_2 - 1 \end{pmatrix}$$
(IV.19)

If we apply our stability criterion we get:

$$-1 \le 2g_1g_2 - 1 \le 1$$
 or $0 \le g_1g_2 \le 1$. (IV.20)

The stability criterion forms a hyperbolic region of stable resonators in a $g_1 - g_2$ diagram as shown in figure IV.2. Some special cases can be found on the stability edges. But how can we apply this to coherent beams? Such beams are not included in geometrical optics. But this matrix method can be applied as well!

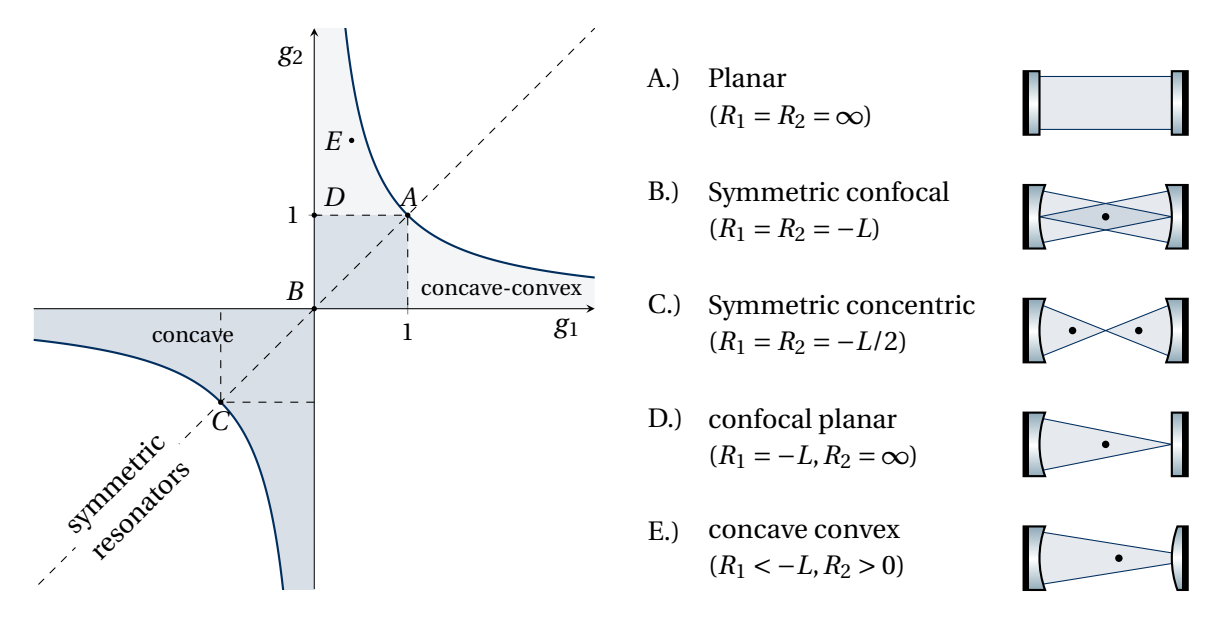


Fig. IV.2.: Resonator stability diagram: A spherical resonator is stable if the parameters $g_{1/2} = 1 + L/R_{1/2}$ lie in the shaded regions delimited by the coordinate axes. the dark shaded area indicates concave resonators, whereas the light shaded area contains conave-convex resonators. The resonator designs for each case are shown on the right (the focal points are indicated with a black dot).

IV.2. Stable laser resonator with Gaussian beams

In the previous section we have discussed criteria for a stable laser resonator. Now, we want to consider, what kinds of electromagnetic fields can propagate inside such a cavity. We assume that the light travels along the symmetry axis z of the resonator. The Helmholtz equation can then be approximated for this geometry which yields different solutions (e. g. Gaussian beams or parabolic beams).

IV.2.1. Gaussian beams

The Gaussian beam is a solution for the par-axial Helmholtz equation

$$\left[i\frac{\partial}{\partial z} + \frac{1}{2k}\left(\frac{\partial^2}{\partial x^2} + \frac{\partial^2}{\partial y^2}\right) + k\right]E(x, y, z) = 0.$$
 (IV.21)

for a given wavelength $\lambda = \frac{2\pi}{k}$. It describes the electromagnetic field for a propagating beam along its propagation axis z and is very well suited to describe laser beams. The solution of the electric field is given by

Equation: Gaussian beam

$$E(r,z) = E_0 \frac{w_0}{w(z)} \cdot \exp\left[-\frac{r^2}{w(z)^2}\right] \cdot \exp\left[i\left(-\frac{kr^2}{2R(z)} + \zeta(z) - kz\right)\right]. \tag{IV.22}$$

The variables are:

- E_0 : maximum field strength on-axis
- w_0 : beam waist radius (1/e field strength)
- w(z): beam radius at distance z from the waist
- *r*: distance from the optical axis
- R(z): wavefront radius of curvature
- r(x). Waverrolle radius of carvata

• $\zeta(z)$: Gouy phase

In the following we want to give the definitions of the various parameters that characterize a Gaussian beam.

Beam radius w(z)

The beam radius along the axis is calculated by

$$w(z) = w_0 \cdot \sqrt{1 + \frac{z^2}{z_r^2}}$$
 with $z_r = \frac{\pi w_0^2}{\lambda}$ (Rayleigh length). (IV.23)

Hence we have a quadratic dependence of the Rayleigh length and the waist diameter. For large propagation distances $z \gg z_r$ the beam radius depends linearly on z.

Radius of Curvature R(z)

The wavefront outside of the beam waist is curved. The radius of this wavefront is defined by:

$$R(z) = z \cdot \left(1 + \frac{z_r^2}{z^2}\right). \tag{IV.24}$$

Hence we have a minimal wavefront radius at $z = z_r$.

Gouy phase $\zeta(z)$

Finally we have the Gouy phase, which induces a phase shift of a Gaussian beam compared to a plane wave

$$\zeta(z) = \arctan\left(\frac{z}{z_r}\right).$$
 (IV.25)

All three beam parameters are summarized in figure IV.3 to visualize the propagation of a Gaussian beam around its waist.

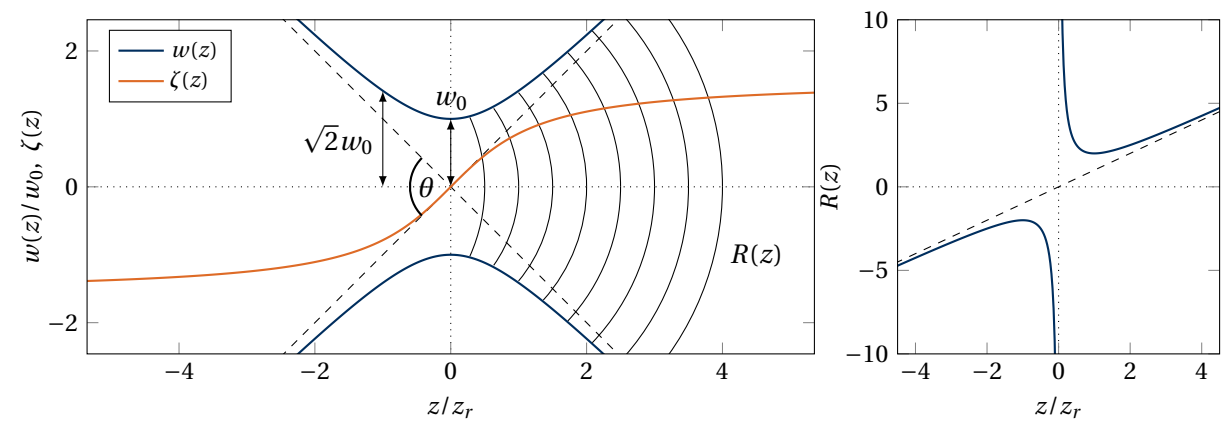


Fig. IV.3.: Gaussian beam parameters w(z), $\zeta(z)$ and R(z). The phase front is shown with black lines. The limits $R(z) \approx z$ and $w(z) \approx w_0 z/z_r$ for $z \gg z_r$ are indicated by dashed lines. They form the beam divergence angle θ , which describes the beam divergence in the farfield.

When we apply the formula of the Gaussian beam to a measured profile like a camera image, we have to use the beam intensity. As $I \propto E^2$ we can write for the intensity:

Equation: Intensity of a Gaussian beam

$$I(z) = I_0 \frac{w_0^2}{w(z)^2} \cdot \exp\left(-\frac{2r^2}{w(z)^2}\right).$$
 (IV.26)

IV.2.2. Stability condition and q-Parameter

In the following we will use a single complex beam parameter q to describe our beam:

$$q = z + iz_r. (IV.27)$$

The q-parameter contains the Rayleigh length (diffraction parameter) and the distance z to the beam waist. With this parameter, a direct application of our ABCD-matrix is possible by using [Kog79, p.179]

$$q_2 = \frac{q_1 A + B}{q_1 C + D} (IV.28)$$

If we now consider our resonator, we would be able to do an infinite number of round-trips, without changing our beam. Hence the beam parameter should reproduce after every round-trip. Hence:

$$q = \frac{qA + B}{qC + D} \implies 0 = q^{2}C + q \cdot (D - A) - B$$

$$\rightarrow q_{1/2} = -\frac{D - A}{2C} \pm \sqrt{\frac{(D - A)^{2}}{4C^{2}} + \frac{B}{C}}$$

$$q_{1/2} = -\frac{D - A}{2C} \pm \frac{1}{2C}\sqrt{(D - A)^{2} + 4CB}$$
(IV.29)

As AD - BC = 1 we get:

$$q_{1/2} = \frac{A - D}{2C} \pm \frac{1}{2C} \sqrt{(A + D)^2 - 4}$$
 (IV.30)

As there is only a Gaussian beam as long as z_r is not zero (q needs to be complex) we can find a stability criterium for a Gaussian resonator by demanding:

$$(A+D)^2 - 4 \le 0 \quad \Rightarrow \quad \frac{|A+D|}{2} \le 1.$$
 (IV.31)

Comment:

- 1. If we calculate a resonator starting at a plane end mirror, we will always get an imaginary *q* meaning we are positioned at the beam waist.
- 2. Besides the basic Gaussian mode, higher order modes are equally a solution for the resonator. Those modes are generally larger than the ground mode and have higher refraction losses (but nevertheless can still start to oscillate). Hence, they can be suppressed e.g. by introducing losses for larger beam diameters (c. f. mode apertures).
- 3. In some cases these modes are also welcome, e.g. to generate a rather tophat like beam profile. In high energy resonators for example Gaussian mirrors are used to purposefully generate higher order modes, in order to achieve a better match between pump and extracting mode (c. f. chapter IV.3.2).

IV.2.3. Limitations of beam size

To conclude this chapter we want to show the constraints of a stable cavity in relation to the size of the beam waist w_0 . As we would like to amplify our laser pulses to high energies, we would like to increase the beam size in order to keep the fluences below the laser induced damage threshold. The beam waist radius gives us an upper bound on the fluence we might encounter inside the cavity. Let us take a look how we can calculate this for a symmetric cavity $R = |R_1| = |R_2|$. We use the fact that in a stable cavity the radius of curvature on the mirror surface R(z) must match the mirror's radius of curvature. Furthermore, the beam waist is positioned in the center of the cavity, therefore we can demand R(L/2) = R which gives us

$$R\left(\frac{L}{2}\right) \stackrel{\text{(IV.24)}}{=} \frac{L}{2} \left(1 + \frac{4z_r^2}{L^2}\right) \stackrel{!}{=} R.$$
 (IV.32)

We can solve this for the Rayleigh length z_r and find an expression of the beam waist radius w_0

$$z_r^2 = \frac{R \cdot L}{2} - \frac{L^2}{4} \quad \Rightarrow \quad w_0(L) \stackrel{\text{(IV.23)}}{=} \sqrt{\frac{\lambda}{\pi} z_r(L)} = \sqrt{\frac{\lambda}{2\pi} \sqrt{L(2R - L)}}. \tag{IV.33}$$

From this we can formulate a scaling law of the beam radius as a function of the cavity length (for a fixed ratio R/L):

Equation: Beam size scaling law

$$w_0 \propto \sqrt{\lambda \cdot L}$$
 with $w_0(L) = \sqrt{\frac{\lambda L}{2\pi}} \sqrt{\frac{2R}{L} - 1}$. (IV.34)

In order to have a stable cavity, ratios of $0.5 < R/L < \infty$ are needed. We have plotted the size of the

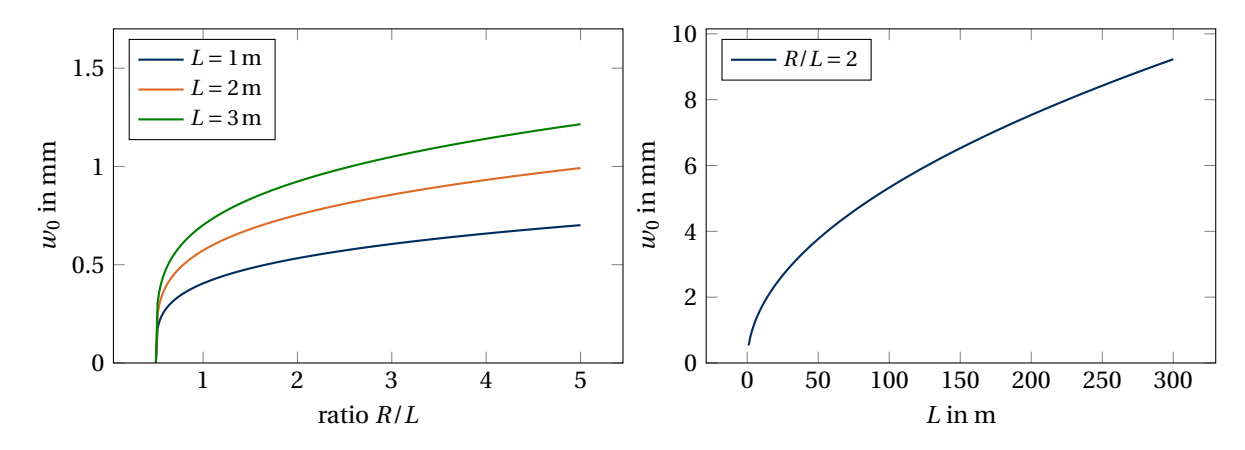


Fig. IV.4.: Left: Beam waist radius w_0 as a function of the ratio R/L for a fixed cavity length L at $\lambda = 1030$ nm. Right: Beam waist radius w_0 as a function of L for a fixed ratio R/L.

beam waist for different cavity lengths L and ratios R/L in figure IV.4. We observe that that the beam waist ratio increases for larger ratios R/L. However, we cannot increase this value arbitrarily, as the cavity is pushed towards the edge of the stability region. Thus it becomes more and more difficult to align properly for larger values of R as it becomes more sensitive to external perturbations like mechanical vibrations or temperature variations. Therefore, the only reasonable solution would be to increase the cavity length L. Suppose, we want to amplify pulses up to $10\,\mathrm{J}$ with our system, but the damage threshold of our optics is around $10\,\mathrm{J}\,\mathrm{cm}^{-2}$. Then, we would have to use a cavity of more $L > 100\,\mathrm{m}$, which is not feasible in the lab. Therefore, stable cavities cannot be used for high energy scaling.

Key point: Stable resonators

- A stable resonator allows the propagation of Gaussian beams a solution of the par-axial Helmholtz equation, which can be described by a beam radius w(z) and a radius of the curvature of phase fronts R(z).
- The propagation of Gaussian beams can be modeled using the q-parameter $q = z + iz_r$.
- The supported beam waist radius w_0 increases with the square root of the cavity length L for a fixed ration R/L. Larger beam radii require a quadratic increase in cavity length.
- Stable cavities are only feasible for output energies < 100 mJ, otherwise the damage threshold is reached inside the cavity.

IV.3. Unstable Cavities

As we have seen in the previous section, it is difficult to achieve large beam sizes in a stable cavity. To go beyond certain thresholds in energy, we can either give up the monolithic resonator and use different power amplifier schemes (c. f. chapter V.2) or give up the stability criterion which leads us to the unstable cavity.

In contrary to a stable cavity, an unstable cavity does not require that the intra-cavity beam is restored after each round-trip. Instead, the criterion for constructive interference of the laser-mode is:

The wavefront radius must be restored after each round-trip.

Besides this, the actual beam diameter can be expanded or reduced over the round-trips. The latter possibility is ruled out due to diffraction effects limiting the reduction of the beam diameter. The main advantage of such design is that in principle the beam diameter has no upper limit and therefore, high energy pulses can be generated directly in the cavity.

We will discuss the basic design rules for such layouts in the following.

IV.3.1. Hard-edge resonator

For a start we will assume a so called *hard-edge unstable resonator*:

- The output coupling is achieved by clipping on the aperture of one of the resonators end mirrors, which creates a hard edge in the output profile.
- Output profile is normally a ring/doughnut shape.
- The "stable mode" is a spherical wave that is magnified during the round-trips.
- The mid-point of the spherical wave is somewhere on the optical axis.

We use the matrix formalism to describe the cavity:

$$\begin{pmatrix} x' \\ \alpha' \end{pmatrix} = \begin{pmatrix} A & B \\ C & D \end{pmatrix} \cdot \begin{pmatrix} x \\ \alpha \end{pmatrix}.$$
 (IV.35)

The radius of curvature is obtained within the small angle approximation with:

$$R \approx z \approx \frac{x}{\alpha}$$
 (IV.36)

Hence we can describe the evolution of the spherical wave radius by:

$$\frac{1}{R'} = \frac{\alpha'}{x'} = \frac{Cx + D\alpha}{Ax + B\alpha} = \frac{C + D/R}{A + B/R}$$
 (IV.37)

The radius of curvature got to be maintained, therefore R = R'. We get:

$$\frac{1}{R} = \frac{C + D/R}{A + B/R}$$

$$\frac{A}{R} + \frac{B}{R^2} = C + \frac{D}{R}$$

$$0 = \frac{B}{R^2} + \frac{A - D}{R} - C$$

$$\Rightarrow \frac{1}{R_{1/2}} = \frac{D - A}{2B} \pm \sqrt{\left(\frac{D - A}{2B}\right)^2 + \frac{C}{B}} \text{ using: } AD - BC = 1$$

$$\frac{1}{R_{1/2}} = \frac{1}{B} \left[\frac{D - A}{2} \pm \sqrt{\left(\frac{A + D}{2}\right)^2 - 1} \right]$$
(IV.38)

The $R_{1/2}$ represent the forward and backward propagation direction. As we need a real value for the radius of curvature, we obtain the opposite criterion to equation (IV.31):

$$\left| \frac{A+D}{2} \right| \ge 1 \tag{IV.39}$$

A further very important parameter of an unstable cavity is the magnification per round-trip which is directly obtained by:

$$x' = A \cdot x + B \cdot \alpha \quad \Rightarrow \quad M = \frac{x'}{x} = A + \frac{B}{R}.$$
 (IV.40)

Now, having the unstable cavity condition and the key parameters, many versions of such cavity can be thought of. In practice mostly cavities based on two mirrors similar to the configurations shown in figure IV.5 are used. These setups are con-focal, meaning that the cavity length L is given by:

$$2L = R_1 + R_2 \tag{IV.41}$$

The magnification of these systems is:

$$M = \frac{R_2}{R_1}. ag{IV.42}$$

The reason for this, besides being relatively simple, is that such setup generates a collimated output beam which is suited well for energy extraction in a long gain medium. Hence, one of the results for equation IV.38 will be 1/R = 0 for the wavefront radius.

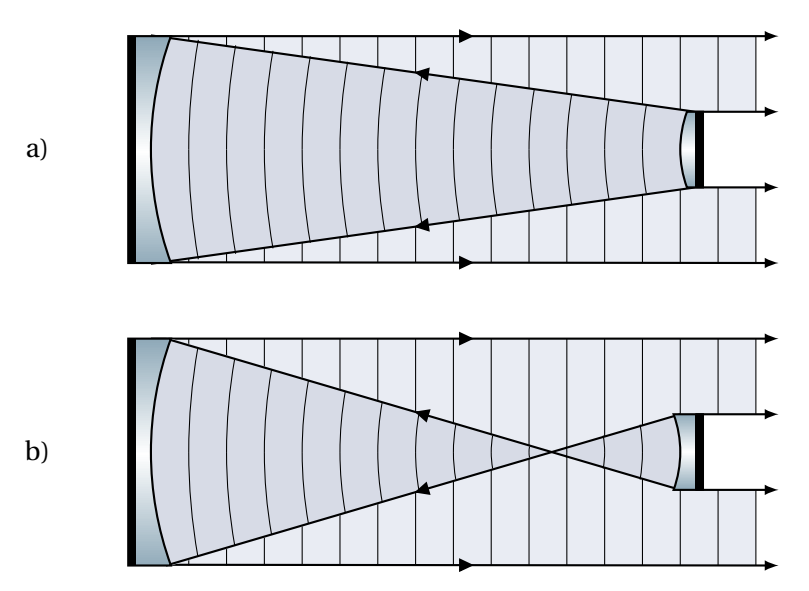


Fig. IV.5.: Practical unstable resonators: a) positive branch confocal; b) negative branch confocal resonator layout. Adapted from [Mor97, p.830].

The major disadvantage of these cavities in their original layout is, that the output beam will be doughnut like, which is often not desired. Especially, due to the sharp edges strong diffraction will deteriorate the beam profile as well. However, it has to be mentioned that the output beam wavefront is typically very good. This originates from the fact that the basic "mode" generated by such cavity is a plane wave, corresponding to an infinitely large Gaussian TEM_{00} beam, which is just spatially truncated. Furthermore, the mode discrimination with respect to higher order modes is typically quite large.

IV.3.2. Graded reflectivity mirror resonator

Hard-edge diffraction is a major issue in unstable resonators as it involves scattering energy into the de-magnifying part of the wave, which leads to energy loss and focal spots inside the cavity that might destroy the setup. We can solve this problem by introducing a so called Graded Reflectivity Mirror (GRM) as the output coupler. Such a mirror exhibits a reflectivity profile $R_{\rm GRM}$ corresponding to a super Gaussian distribution of the Gaussian Order (GO) with a maximum reflectivity R_0 on the optical axis:

$$R_{\text{GRM}}(r) = R_0 \cdot \exp\left(-2\left(\frac{|x|}{w_{\text{GRM}}}\right)^{2 \cdot GO}\right). \tag{IV.43}$$

Here, $w_{\rm GRM}$ is the $^{1/e^2}$ -radius of the reflectivity profile. Assuming a spatially constant gain, the output beam's intensity profile as function of the distance to the optical axis I(r) of such cavity can be calculated by just adding up the reflected intensities of many (in principle infinite, but the intensity distribution will converge quite fast) successive round-trips, while applying the according magnification in each cycle, starting with homogeneous intensity distribution with the intensity I_0 :

$$I_{\rm in}(r) = I_0 \cdot \prod_{k=1}^{\infty} \frac{R_{\rm GRM} \left(\frac{r}{M^k}\right)}{R_0}$$
 (IV.44)

We use equation IV.43:

$$I_{\text{in}}(r) = I_{0} \cdot \prod_{k=1}^{\infty} e^{-2\left(\frac{r}{w_{\text{GRM}}M^{k}}\right)^{2 \cdot GO}}$$

$$I_{\text{in}}(r) = I_{0} \exp\left[-2 \cdot \sum_{k=1}^{\infty} \left(\frac{r}{w_{\text{GRM}}M^{k}}\right)^{2 \cdot GO}\right] \quad \text{with} \quad \sum_{k=1}^{\infty} x^{k} = \frac{x}{1 - x}$$

$$I_{\text{in}}(r) = I_{0} \exp\left[-2 \cdot \left(\frac{r}{w_{\text{GRM}}}\right)^{2 \cdot GO} \cdot \frac{1}{M^{2 \cdot GO} - 1}\right]$$

$$I_{\text{in}}(r) = I_{0} \exp\left[-2 \cdot \left(\frac{r}{w_{\text{GRM}}} \cdot (M^{2 \cdot GO} - 1)^{\frac{1}{2 \cdot GO}}\right)^{2 \cdot GO}\right]$$

$$I_{\text{in}}(r) = I_{0} \exp\left[-2 \cdot \left(\frac{r}{\omega_{i}}\right)^{2 \cdot GO}\right] \quad \text{with} \quad \omega_{i} = w_{\text{GRM}} \cdot (M^{2GO} - 1)^{\frac{1}{2GO}} \quad \text{(IV.45)}$$

Here, we indentified ω_i as the intra-cavity intensity distribution, which has a slightly larger radius than the GRM's reflectivity profile. The intra-cavity intensity profile will as well resemble a super Gaussian beam distribution. However, due to the size mismatch, a high R_0 value will result in a suppression of the central part of the output intensity profile, which is obtained by multiplying equations IV.45 and IV.43

$$I_{\text{out}}(r) = (1 - R_{\text{GRM}}) \cdot I_{\text{in}}(r)$$

$$= I_0 \left[1 - R_0 \cdot \exp\left(-2\left(\frac{r}{w_{\text{GRM}}}\right)^{2 \cdot GO}\right) \right] \exp\left[-2 \cdot \left(\frac{r}{\omega_i}\right)^{2 \cdot GO}\right]. \tag{IV.46}$$

A condition to avoid the central part suppression, a so called flat top condition is obtained by setting the second derivative of the output beam intensity at r = 0 to zero, such that there is neither a maximum nor a minimum in the center. One obtains:

$$R_0 \le \frac{1}{|M|^{2GO}}.$$
 (IV.47)

The resulting output beam profile for different values at a given magnification M = 1.3 and GO = 2 is given in figure IV.6. Here, the flattop condition is reached at $R_0 = 35\%$.

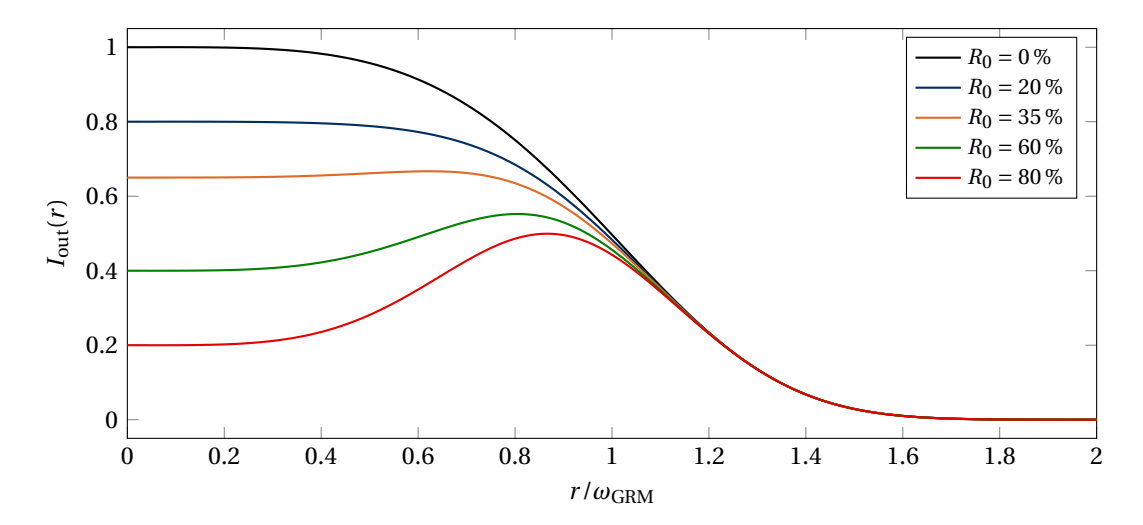


Fig. IV.6.: Output beam profile for different values of R_0 according to equation (IV.46). The values of magnification M = 1.3 and Gaussian order GO = 2 are fixed such that the flat-top condition is fulfilled for $R_0 = 35\%$. Adapted from [Mor97, p.838].

The feedback F of the cavity per round-trip, which in the end is to be balanced with the round-trip gain G_0 is given by:

$$F = \frac{R_0}{M^2}$$
 and $G_0 = \frac{M^2}{R_0}$. (IV.48)

Due to the flattop condition this so far limits unstable cavity designs to high gain laser media, especially for higher values of GO. (M cannot be made infinitely small due to stability issues. Good values are typically ≥ 1.3).

IV.3.3. Gain modulation resonator

The graded reflectivity mirror resonator has the disadvantage that the GRM has to be tailored exactly to the setup of the laser resonator, i.e. customarily designed for each setup. Therefore, we want to look at a different approach of using a spatially tailored gain profile instead of a GRM [Kör+19]. The basic working principle is similar, but instead of introducing additional losses at the beam edge to limit its spatial extension, a spatially confined gain area introduces a gain-modulation in the beam's center.

We start by assuming a super-Gaussian double pass gain distribution G(r) analogously to the GRM profile with an offset of 1, which considers that there are no losses outside the pumped region

$$G(r) = (G_0 - 1) \exp\left[-2 \cdot \left(\frac{r}{w_g}\right)^{GO}\right] + 1.$$
 (IV.49)

Here, w_g is given as the $^{1}/e^{2}$ width of the double pass gain distribution. The intra-cavity intensity can be calculated using a sufficient number of terms of the product series

$$I_{\text{in}}(r) = I_0 \prod_{k=0}^{\infty} \frac{G\left(\frac{r}{M^k}\right)}{G_0} = I_0 \prod_{k=0}^{\infty} \left[\left(1 - \frac{1}{G_0}\right) \exp\left[-2 \cdot \left(\frac{r}{w_g M^k}\right)^{GO}\right] + \frac{1}{G_0} \right]$$

If we assume a steep edge of the gain distribution, we can transform this product into a sum where each summand is defined by the lowest k exponential term contained in the product, as all higher order terms will not significantly contribute as their diameter is greater and thus they will not add additional structure inside the flat top area. Then we will find an approximation:

$$I_{\rm in}(r) \approx I_0 \sum_{k=0}^{\infty} \left[\left(1 - \frac{1}{G_0} \right) \exp \left[-2 \cdot \left(\frac{r}{w_g M^{k+1}} \right)^{GO} \right] \cdot \frac{1}{G_0^k} \right]. \tag{IV.50}$$

The resulting output profile $I_{\text{out}} = R_0 \cdot I_{\text{in}}$ has to be calculated numerically and will resemble a step pyramid as shown in figure IV.7.

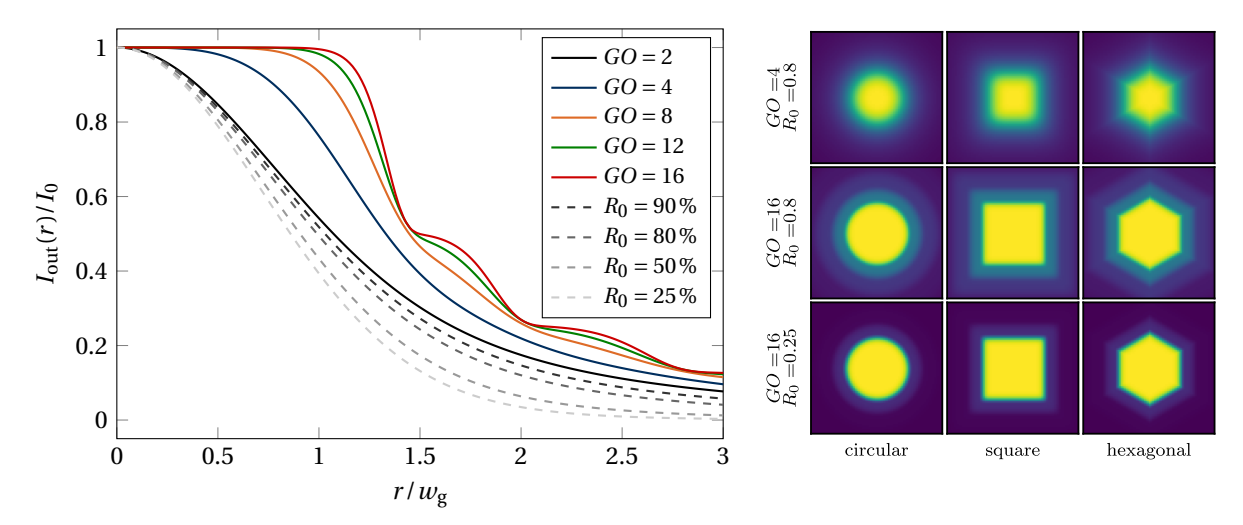


Fig. IV.7.: Left: Output intensity I_{out} for a cavity with M=1.4. For the solid graphs, the reflectivity of the output mirror was kept constant $R_0=99\,\%$, while the Gaussian order of the gain distribution was varied. The dashed lines show a GO=2 with varied reflectivity R_0 . Right: Simulated output intensity profiles for differently shaped gain distributions (circular, square, hexagonal) with M=1.4 and different GO and R_0 . Taken from [Kör+19].

Contrary to GRM layouts, an output coupling via an end mirror is not necessary without losing the intra-cavity shaping mechanism. This opens the possibility to use a variable output coupler, e.g. an electro-optical switch in combination with a polarizer and a waveplate to use the unstable cavity in a cavity dump operation mode or as an regenerative amplifier (c. f. later sections).

Additionally, this shaping mechanism will work for all shapes of tophat beams, as long as the intensity is decreasing monotonously from the center to the edges (c. f. figure IV.7 right). This covers shapes commonly used for homogenized laser diode pump beams like rectangular or hexagonal profiles.

Key point: Unstable resonators

- In contrast to a stable cavity, only the wavefront radius (not the beam radius) must be restored after a round trip in an unstable cavity.
- The magnification of the beam size is given by the ratio of the radius of curvature of both cavity mirrors.
- The most simple setup is the hard-edge resonator, which produces a doughnut like shape with sharp edges that will diffract and may deteriorate the beam profile.
- The beam profile can be improved by using graded reflectivity mirrors (Gaussian reflectivity profile) or by tailoring the shape of the pump beam (gain modulation resonator).

IV.4. The Active Cavity

We now know how to establish a cavity which allows to achieve multiple round trips with ideally no losses. During each round trip there are basically four processes to be considered:

• *Amplification*: In an oscillator under CW operation no alteration in the inversion occurs. Hence, we can assume small signal gain (c. f. equation (III.34)) in a homogeneously inverted laser medium:

$$I = I_0 \cdot \exp(N_{\text{dop}}(\sigma_e \beta - \sigma_a \cdot (1 - \beta)) \cdot d) = I_0 \cdot e^{g \cdot d}$$
 (IV.51)

• *Output coupling* is realized through the reflectivity R_1 (or transmission T_1 respectively) of an output coupling mirror or other element in the cavity

$$R_1 = 1 - T_1. (IV.52)$$

- *Amplification losses* α that are linked with the amplification process .
- *Round-trip losses* δ_m , which can be modeled with a limited reflectively R_2 of another resonator mirror:

$$R_2 = 1 - \delta_m. \tag{IV.53}$$

For a laser cavity running in a stable regime, all these contributions have to be balancing each other and therefore we obtain the lasing condition:

$$R_1 R_2 \cdot e^{(g-\alpha)d} = 1$$

 $\Rightarrow gd = \alpha d - \ln(R_1 R_2) \text{ with } \ln(1-x) \approx -x$
 $gd \approx \alpha d + \delta_m + T$
 $gd \approx \delta + T \text{ with } \delta := d\alpha + \delta_m.$ (IV.54)

As δ_m and T can be assumed to be small we can approximate $\ln(R_1)$ and $\ln(R_2)$ by using the according Taylor series up to the linear term. Furthermore, we replace the loss terms with a common variable δ .

Cavity time constant

We can derive the common parameters that describe a resonator's feedback. The first one is the cavity's time constant τ_c , which is defined as the ratio of the resonators round-trip time $t_r = 2L/c$ and the relative loss per round-trip $\varepsilon = T + \delta$:

$$\tau_c = \frac{t_r}{\varepsilon} = \frac{2L}{c \cdot (T + \delta)}.$$
 (IV.55)

Quality factor

Another often used parameter is the so called quality factor Q defined as 2π times the ratio of energy stored in the cavity E_{store} and the energy dissipated in a round-trip E_{diss} :

$$Q = 2\pi \cdot \frac{E_{\text{store}}}{E_{\text{diss}}} = \frac{2\pi}{1 - \exp\left(-\frac{t_r}{\tau_c}\right)}, \quad \text{for } t_r \ll \tau_c \quad Q \approx 2\pi\tau_c \nu. \tag{IV.56}$$

For us the most interesting thing is how to dimension the output coupling of our laser cavity. There are two competing mechanisms:

- The efficiency of our laser is strongly linked with the relation of losses δ to the output coupling T. The higher T is in comparison to δ the more of the actual gain is transferred into output power.
- Increasing either losses or output coupling demands a higher gain coefficient *g*. According to (IV.51) this again requires a higher inversion density, which is proportional to the emitted fluorescence power. Due to this the portion of extracted power is reduced.

We cannot infinitely increase the output coupling to get a higher efficiency. Hence, there has to be an optimum output coupling level. To analyze this, we need to introduce the saturated gain coefficient in CW operation (compare with (III.16)) [Koe06, p.109]

$$g = \frac{g_0}{1 + I_{\text{in}}/I_{\text{sat}}} \quad \text{with} \quad I_{\text{sat}} = \frac{h\nu}{(\sigma_a + \sigma_e)\tau_f}.$$
 (IV.57)

Combining this equation with the lasing condition (IV.54) and solving for I_{in} gives us a formula for the intracavity intensity

$$I_{\text{in}} = I_{\text{sat}} \left(\frac{g_0}{g} - 1 \right) \stackrel{\text{(IV.54)}}{=} I_{\text{sat}} \left(\frac{g_0 \cdot d}{\delta + T} - 1 \right). \tag{IV.58}$$

Then we can calculate the output intensity I_{out} by noting that I_{in} at the output coupler consists of a forward and backwards propagating wave, where the forwards propagating intensity $I_{\text{forward}} := I$ is impinging on the output coupler and the backwards propagating wave $I_{\text{backward}} := I \cdot R$ is reflected. Then we find by using the exact relation for the output-coupling $T \to -\ln R$

$$I_{\text{in}} = I + I \cdot R = (1+R)I \quad \Rightarrow \quad I_{\text{out}} = (1-R)I = \left(\frac{1-R}{1+R}\right)I_{\text{in}} \stackrel{\text{(IV.58)}}{=} \left(\frac{1-R}{1+R}\right)I_{\text{sat}}\left(\frac{g_0 \cdot d}{\delta - \ln R} - 1\right). \tag{IV.59}$$

In figure IV.8 a general plot of the intra-cavity and output intensity can be seen. The optimum reflectivity of the output coupler could be calculated by differentiating (IV.59) and setting it to zero. The resulting equation is not solvable, however, by using the approximation $\frac{1-R}{1+R} \approx -\frac{1}{2} \ln R$ we can find the maximum as [Koe06, p.121]:

Equation: Optimum output coupling of a CW oscillator

$$\ln(R_{\text{opt}}) = \left(1 - \sqrt{\frac{g_0 \cdot d}{\delta}}\right) \cdot \delta. \tag{IV.60}$$

As inversion and gain are pinned to a fixed value by the laser condition (IV.54), an increase in the pump-rate above the laser level will (at least in the first approximation) not alter the inversion. Hence, the intra-cavity and output intensities will increase proportional to the pump rate (of course, this is disturbed by thermal effects for high powers). The slope of the output power vs. input is the so called slope efficiency of a laser.

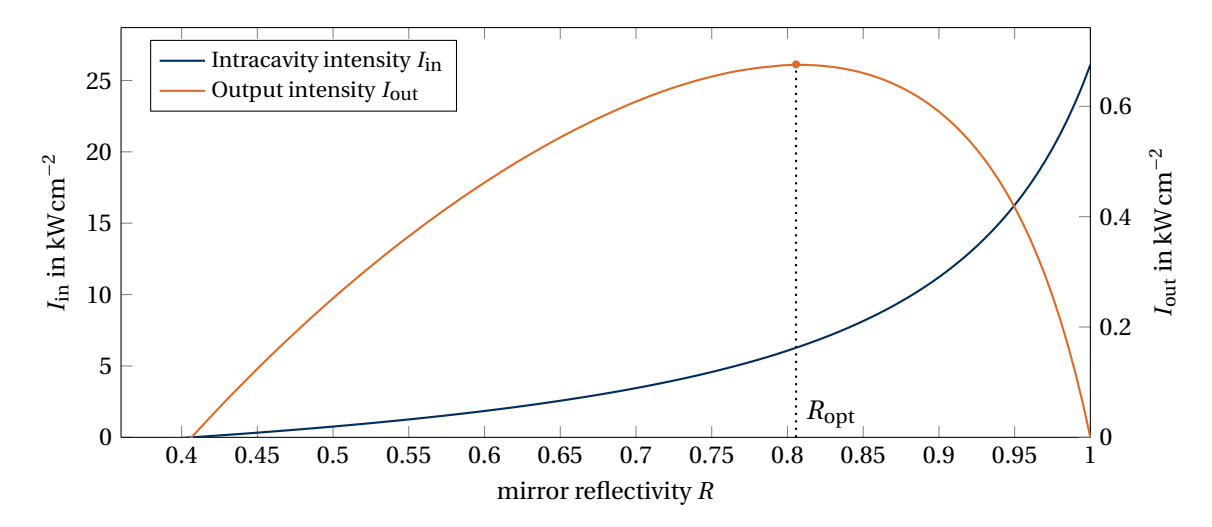


Fig. IV.8.: Laser output intensity I_{out} (IV.59) and internal flux I_{in} (IV.58) as function of output coupler reflectivity for $I_{\text{sat}} = 2.9 \, \text{kW cm}^{-2}$, $g_0 \cdot d = 1, \delta = 0.1$.

Relaxation Oscillations

So far we have only discussed the steady-state behaviour of laser oscillation. Now, we want to discuss the temporal evolution of the intensity within the cavity before the just discussed stable operation is achieved:

- When the pump is switched on, the inversion (and gain) starts to increase, but still is insufficient to allow laser oscillation.
- As soon as the threshold (the inversion for stable operation) is reached, the fluorescence light caught in the cavity starts to oscillate and is amplified. Hence, the intra-cavity intensity rises exponentially.
- As the intra-cavity intensity is still to low to balance the pump excitation due to extraction the inversion increases beyond the equilibrium inversion.
- The intra-cavity intensity reaches its level for stable operation, but as the inversion is higher as in the stable mode, the intensity increases further.
- As the intra-cavity intensity is now higher than in the balanced case, more energy is extracted and the inversion reduced.
- As soon as the inversion threshold value is reached, the intra-cavity intensity no longer increases.
- As the intensity is now above the balance value, the inversion is further reduced below the threshold, resulting also in a reduction of the intra-cavity intensity as δ and output coupling are not sufficiently compensated by the gain.
- As soon as the extraction is again low enough, the inversion is again increased by the pump.
- Now this process repeats itself with decreasing amplitude giving a time-pattern as shown in figure IV.9 which is called *spiking*.

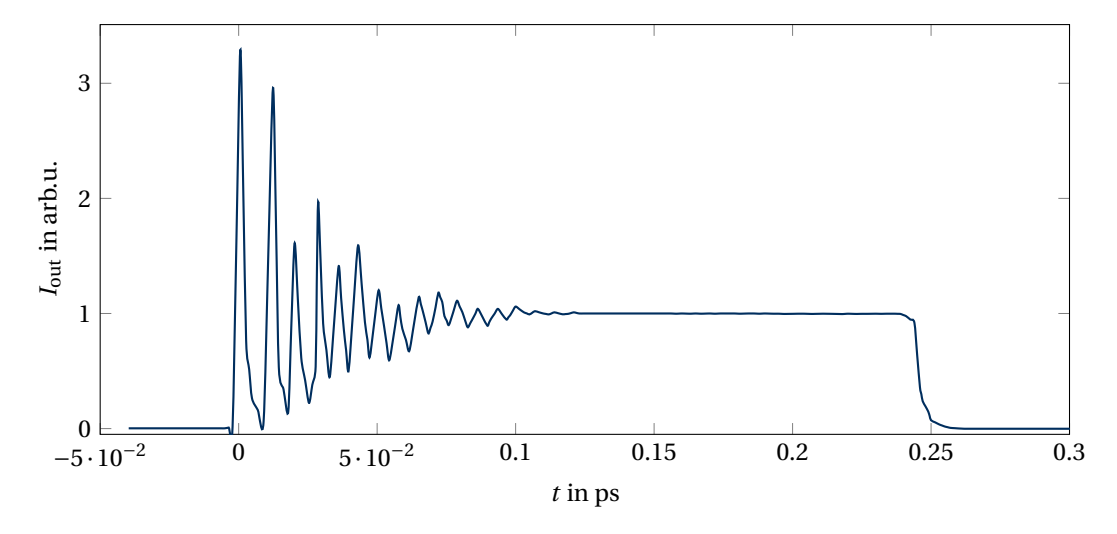


Fig. IV.9.: Spiking behaviour of a laser resonator recorded with a photo diode, detecting the leakage of the intracavity intensity.

IV.4.1. Q-switch operation

So far the oscillators we discussed do not generate high intensities. This is because continuous operation will limit the peak output power. Nevertheless the spiking, namely the first spike is already pretty interesting. As the intensity is higher the larger the initial inversion overshoot is, we can proceed by stopping our cavity from starting a laser oscillation, until we achieved the highest inversion we can get. Then we let the spiking begin and only use the first spike, which will be a giant impulse. But how can we achieve this? If we do nothing, the inversion is limited by the threshold (and a bit by the available pump power). We need something that blocks our cavity (i. e. reduces the quality factor Q by increasing losses) until we are ready. This can be done by:

• Mechanical elements:

We could either use a shutter or rotating chopper wheel to mechanically block the beam or use a rotating optic, e.g. prism to control the cavity losses.

Though this seems rather simple, it is very complicated to achieve a stable and predictable operation. Furthermore, mechanical devices are mostly way to slow.

• Electric Polarization switching and polarizer:

Using a polarizer, only one polarization is allowed to travel around in the cavity.

The switching element controls whether the polarization is turned (resulting in high losses at the polarizer) in every round-trip or not (low loss cavity).

Switching is typically realized with a *Pockels cell*: This is a birefringent crystal, who's refractive index difference in the two axes is dependent on an external electric field. Hence, by setting an external voltage to the cell, we can determine whether it does nothing, or induces a phase shift according to the applied voltage. As a phase shift of $\lambda/2$ corresponds (with according alignment of the crystal axis) to a polarization rotation of 90°. A schematic example can be seen in figure IV.10. Such electro-optical switches allow a very fast switching (nanosecond range) in a very controlled manner, which is mainly linked to an external trigger system. The drawbacks are the needed active synchronization, and high voltages involved which make these approach rather expensive and complicated.

• Acousto Optical Modulator (AOM):

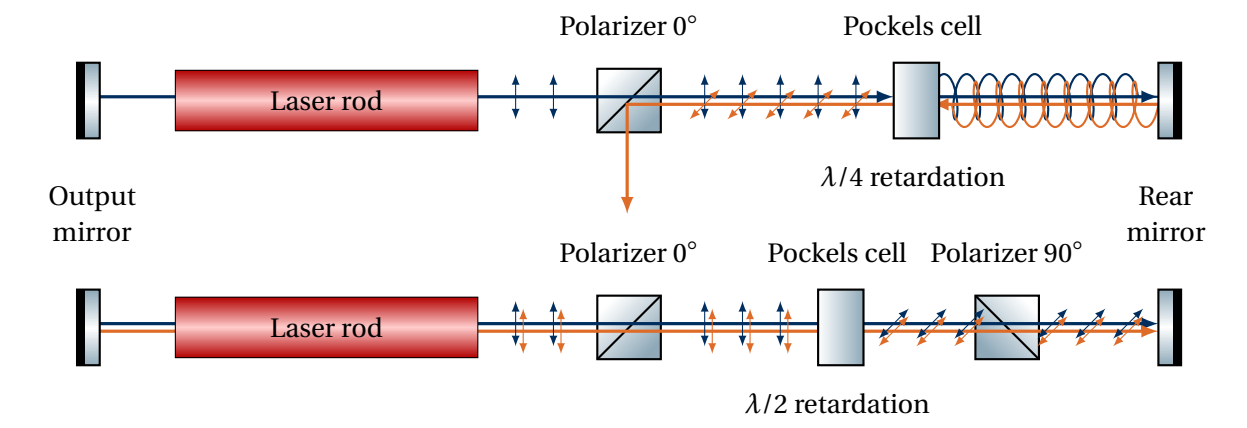


Fig. IV.10.: Q-switch operated linear cavities using an electro-optic Pockels cell in quarter wave (top) and half wave configuration (bottom). The polarizer under 0° is not necessary for polarized laser radiation. Top: *Pulse-off Q-Switch*. The Pockels cell is located between a polarizer and a rear mirror. During the pump process, the quarter-wave voltage is applied, such that any radiation is ejected by the polarizer. Finally, the cell is switched off, permitting a build up of oscillation within the cavity. Bottom: *Pulse-on Q-Switch*. The Pockels cell is located between crossed polarizers. During the pump process, no voltage is applied to the cell. Finally, the half-wave voltage is applied, which causes a 90° rotation and thus allowing oscillation.

Here, the modulator redirects parts of the beam out of the stable cavity by defraction on a volume grating that is generated by a standing acoustic wave in a transmissive optical element. This generates a density modulation and finally a refractive index modulation that acts like a grating, which induces refraction.

The advantages are similar to the ones of a Pockels cell, though instead of a high voltage, a frequency has to be handled. Futhermore, no polarizers are needed as the beam is refracted by the AOM. Limitations are given by the speed of sound for larger apertures, which limits the switching speed. Also, the switching efficiency is lower.

• Passive elements:

This is typically realized with a so called *saturable absorber*, which absorbs lower intensities and gets transparent for higher intensities. Therefore, the losses are higher for lower intensities. Materials used for such elements are e. g. Cr:YAG.

The main advantage is that such an element needs no active synchronization, but therefore it has to be accurately dimensioned from the beginning on, as there is no real way of adjusting. Additionally, the passive synchronization leads to temporal jitter.

Q-Switching procedure

For a standard *Q*-switch the temporal procedure is as follows (c. f. figure IV.11):

- 1. The cavity is in a blocked state (Pockels cell is off) and the pump is switched on.
- 2. The inversion β increases, but no photon field is present.
- 3. When the maximum (or desired) inversion is reached, the Pockels cell is switched on. The cavity is now open and has a predefined corresponding output coupling level.

Now, the process is identical with the spiking process, only, that as the gain is much higher, the overshoot and hence the output pulse is much bigger. According to this, we can find some characteristics for the *Q*-switch pulse:

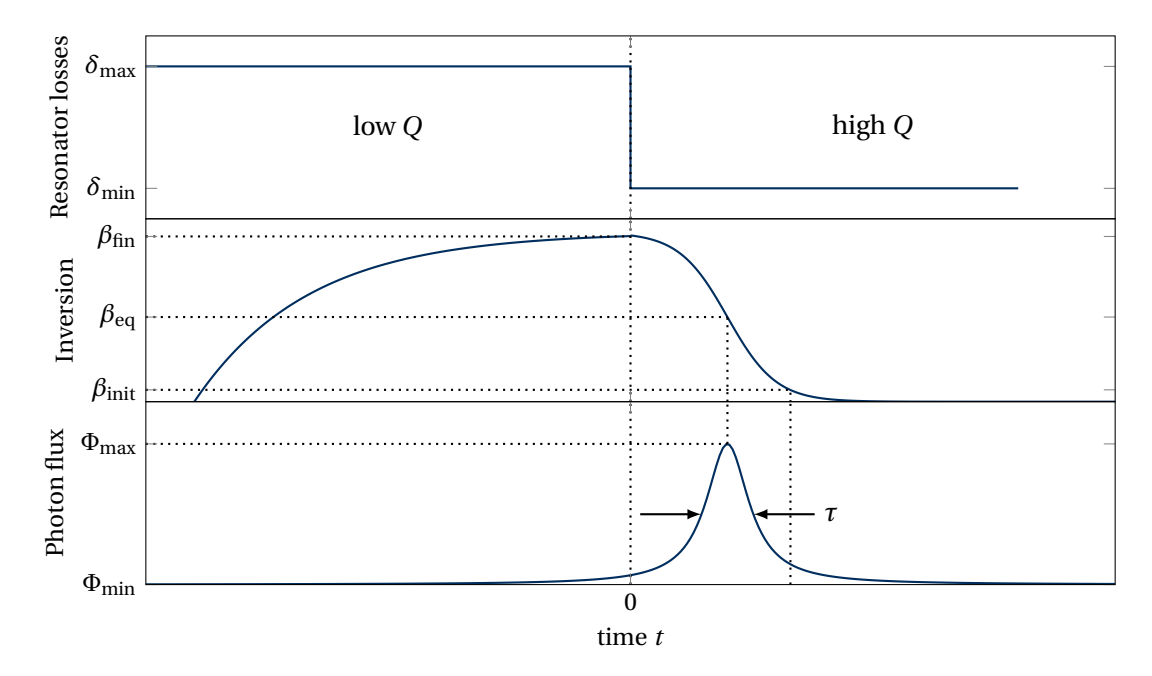


Fig. IV.11.: Temporal procedure in a Q-switch laser (adapted from [Koe06, p.489]).

- The leading edge is increasing exponentially according to the gain achieved in the laser medium.
- The trailing edge decreases exponentially, according to the combined output coupling and losses.
- Hence, the pulses will be shorter the higher the gain of the active medium and the shorter the cavity (round trip time, or amplification steps per time) is.

IV.4.2. Cavity Dump

Another way to achieve a nanosecond pulse is the so called cavity dump which is very similar to the normal *Q*-switch, but needs two switching operations (on and off) from the switching element. It works as follows:

- In the beginning of the pump cycle the cavity is blocked (Pockels cell is off).
- When the target inversion is achieved, the Pockels cell is switched on, which in contrary to the classical *Q*-switch results in a "perfect" cavity, i. e. that the output coupling will be zero.
- As there is no output coupling, the power evolving in the cavity according to the spiking procedure is trapped in the cavity, while only the losses reduce the stored energy.
- When the highest amount of stored energy in the cavity is achieved, the Pockels-cell is switched off, which leads to a 100 % output coupling, releasing the stored energy from the cavity at once.

Pulses generated by this method typically have the same length as the cavity round trip time (as long as the switching of the Pockels-cell is fast enough). The pulse shape also reflects this as the edges are given by the falling edge of the Pockels cell switch, while the plateau of the pulse is rather constant.

IV.4.3. Mode Locking

So far the lower limit for pulse lengths generated by a laser oscillator is merely the length of the cavity. For achieving ultrashort pulses shrinking the cavity length is not enough when we talk about sub picosecond pulses. Therefore, we need a another scheme to generate such pulses. The basic principle is that we will reduce the round-trip losses for shorter or more intense pulses either actively or passively.

Key point: Types of mode locking

- active modulation:
 - We can use a fast switch, e. g. an AOM that switches with a repetition rate that corresponds to the round trip time of our cavity, with an opening time as short as possible.
 The cavity will only be a low loss cavity for a short pulse traveling around in the cavity.
- passive modulation:
 - A saturable absorber with a short time constant (less than the round trip time) is used which provides a lower loss, if the energy in the cavity concentrated in a short pulse.
 - *Kerr lens*: Due to the dependence of the refractive index on intensity $(n = n_0 + n_2 \cdot I)$ this effect can be used to introduce a lens in the cavity that is only there for high intensities (short pulses). If the cavity exhibits lower losses with this lens as without, we achieved our goal.
 - With some fantasy also other nonlinear optic effects can be employed to modulate the losses in dependence of the intensity (e.g. second harmonic generation).

In most ultra short pulse lasers passive methods are used, as they are much faster than an active modulation, and hence allow for shorter pulses.

So now we know how we can build a cavity, that is essentially better suited for an ultra short pulse than for continuous operation, but how can we obtain such a pulse? The answer is pretty simple: It will just happen. A disturbance of such a laser e.g. by small knock on one of the mirrors, will lead to intensity fluctuations, which will finally develop to an ultra short pulse, which gets the higher gain per round-trip compared to the continuous operation, and hence, will win against it (c. f. Kerr lens mode-locking). As soon as this has happened, an ultra fast pulse is travelling in your cavity and a part of it can be coupled out in every round-trip. In contrary to the nano-second sources such a laser source is operated continuously, as the once generated pulse should be preserved. The repetition rate of such a laser is given by the round-trip time in the cavity. Hence, a longer cavity with the same average output power will result in a higher pulse energy.

In the final step to an ultra fast laser we consider that the pulse length is connected to the spectrum via Fourier Transform (FT), meaning the shorter the pulse length the broader the spectrum has to be, which is represented by the bandwidth limit (assuming a Gaussian with pulse duration Δt (FWHM) and spectral width Δv (FWHM) here):

Equation: Time-bandwidth product

$$\Delta t \Delta v = \frac{2 \cdot \ln 2}{\pi} \quad \Rightarrow \quad \Delta t = \frac{0.441}{c} \frac{\lambda^2}{\Delta \lambda} = 1468 \, \text{fs} \frac{\lambda^2 [\mu \text{m}^2]}{\Delta \lambda [\text{nm}]}.$$
 (IV.61)

Furthermore, two things have to be considered:

• To achieve a short pulse from the bandwidth available, the different wavelength have to be in phase, otherwise interference would prohibit any short pulse (cf. figure IV.12).

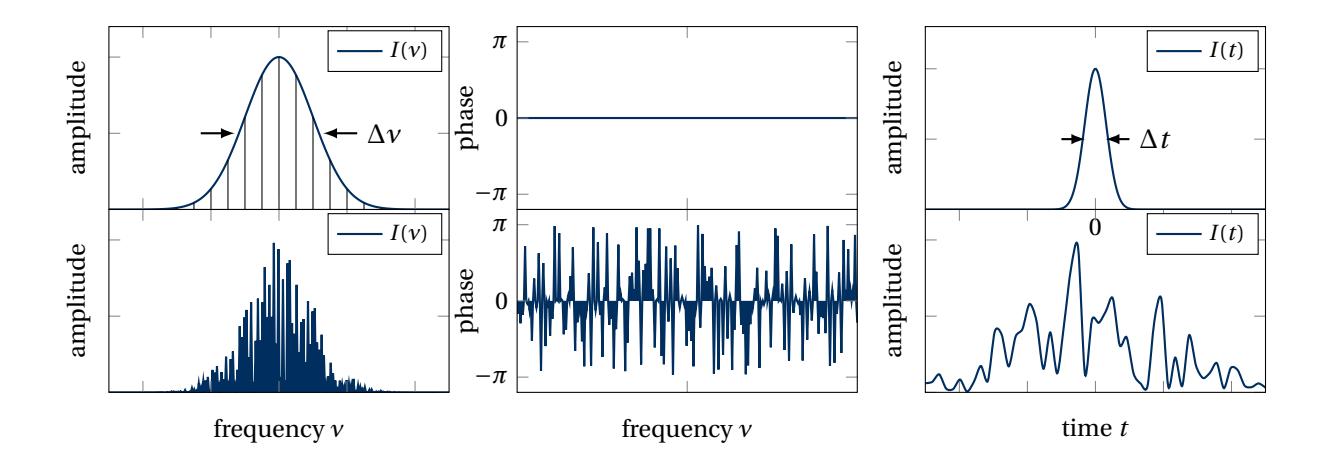


Fig. IV.12.: Top: Phase lock dependence for a mode locked pulse. The spectral intensities have a Gaussian distribution, while the phase is zero. This results in a fourier limited gaussian pulse in the time doimain. Bottom: Signal of a non-modelocked laser. The spectral intensities I(v) are Rayleigh distributed around the Gaussian mean, the phases are random. This results in a temporal structure characteristic to thermal noise.

• As we will have a considerable bandwidth for an ultra short pulse, every material will introduce an optical path difference due to dispersion. This would lead to a de-phasing of our ultra short pulse and therefore destroy it. Hence, compensating measures have to be taken in the cavity. This can either be a prism pair (e.g. see figure IV.13) or chirped mirrors. The latter are thinfilm optical systems with layers of different thickness, allowing the reflection of different wavelengths at various depths in the optical system.

Today, the preferred manner of femtosecond pulse generation is passive mode-locking via the Kerrlens effect or by means of a SEmiconductor Saturable Absorber Mirror (SESAM). Figure IV.13 depicts the setup of a Kerr-lens mode-locked Ti:sapphire laser. Mode-locking can either be achieved by hard or soft aperturing. For hard aperturing we insert a simple slit inside the cavity which blocks light which is not located on the optical axis. If the intensity is higher, the light is focused in the Kerr-medium which leads to a smaller beam diameter. For soft aperturing we design the cavity in such a way that the beam overlaps only with the spatial gain profile of the active medium when we have a pulse inside the cavity.

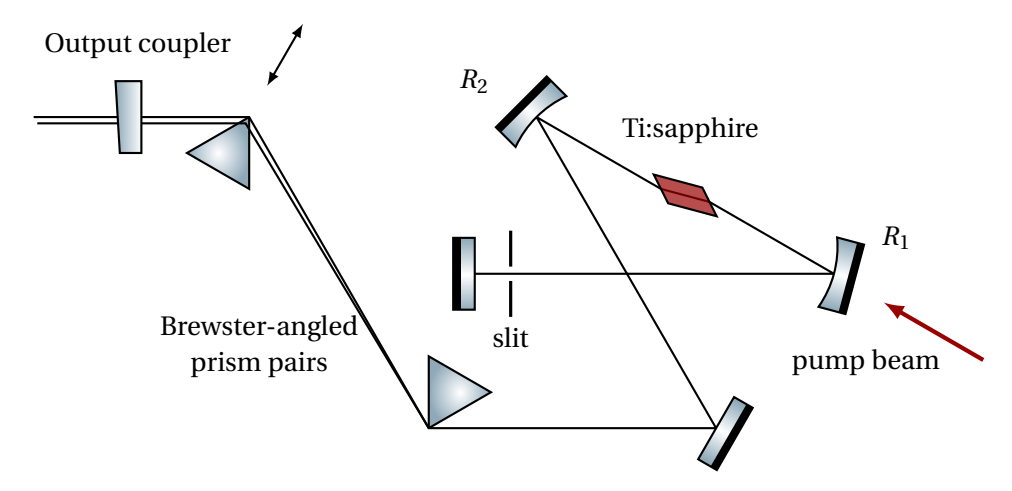


Fig. IV.13.: Example layout for a Ti:Sapphire femtosecond oscillator using (hard edge) Kerr lens mode locking and a prism pair for compensation of Group Velocity Dispersion (GVD) in the Ti:Sa crystal. (adapted from [Kra+92]).

IV.4.4. Single Mode Operation

After discussing short pules lasers as seeds for an amplifier system, it might at first sound a bit awkward to discuss single mode lasers, which are more linked to continuous wave operation. But there is one thing we have not included so far: If we have a nanosecond oscillator the emitted pulse is not a spectral single mode, in most cases it is a very large number of single modes. Now all these modes are not locked in phase to each other, but are at least partly coherent. This means that these modes will interfere with each other resulting in modulations in the temporal pulse shape. This can be avoided using a single mode laser either in pulsed form or as continuous wave laser where one cuts out a nanosecond pulse from the laser beam which is then amplified.

So how does it work? At first we should understand how longitudinal multi-mode operation is generated within a laser:

• The mode separation in a laser is given by the accepted modes of the cavity, where the constraint is that the wave is reconstructed after one round trip (otherwise there will be destructive interference):

$$\lambda_n = \frac{2L}{n}$$
 or $v_n = \frac{cn}{2L}$. (IV.62)

Hence the separation of two neighboring modes is:

$$\Delta v = \frac{c}{2L}.\tag{IV.63}$$

In an cavity of 1m length and a wavelength of $1\,\mu m$ this is an approximate separation in wavelength of only $0.5\,pm$.

- As the mode separation is so low, there are typically many modes having approximately the same gain according to the spectral characteristics of the laser medium, which is hence not sufficient to select out a single mode.
- This is why several modes are above laser threshold, resulting in a multi-mode operation. This is further worsened as due to interference with itself in a standard cavity, a single mode can spatially only use part of the inversion (spatial hole burning).

Hence to achieve single mode operation we have to select out a single mode and increase losses for all other modes:

- Using extremely short cavities, e.g. micro chip lasers: This increases the mode spacing and may, if the gain curve of the material is tight enough be sufficient to achieve single mode operation. For most Ytterbium materials this is not sufficient because of a wide bandwidth, but it works e.g. for Nd:YAG.
- Dispersive elements can be included in the cavity as Prisms or gratings, though the spectral separation is often not sufficient and the losses e.g. in case of the grating are rather high. Such techniques are used e.g. for diode lasers.
- Etalons (see e.g. https://lightmachinery.com/optical-design-center/etalon-designer/)
- Lyot filters (using the wavelength dependence of the birefringence to select out a wavelength that is not influenced by this element, while other wavelength get a phase shift, which in combination with a polarizer results in losses)

As single mode sources are often more stable if operated in a continuous mode, one has to think of how to obtain a nanosecond pulse for amplification. Here the switching devices discussed for *Q*-switching, especially electro-optic and acousto-optic devices allow to cut out a pulse. Nowadays, more sophisticated electro-optic modulators even allow to shape arbitrary pulse shapes with a temporal resolution of down to 100 pico-seconds.

V. Amplifiers

In the past chapter we learned how to generate basically any type of pulse. Nevertheless, the achievable output energy is limited for short pulses. In case of pulse pumped nanosecond operation the energy is limited by the feasibility of large cavity modes and the reduced efficiency because of the losses introduced by the mandatory switching elements. In case of ultra fast operation (mode locking) the high average power introduced by the intrinsic high repetition rate also limits the available single pulse energy. Hence, the only way to achieve high energetic pulses is to amplify the pulses coming from a seed source in an amplifier. In the following we will discuss several solid state amplifier layouts. Though most of the things described can be generalized, we will assume end pumped lasers.

V.1. Regenerative amplifiers

In case of lower output energies and where high gain is needed, a so called *regenerative amplifier* is the type of choice. Such amplifiers are typically identical to a cavity dumped oscillator (c. f. figure IV.10). Instead of using the cavity to generate a pulse starting from the fluorescence light, a seed pulse is coupled into the cavity.

In the example in figure V.1, a pulse is coupled into the cavity via a Thin Film Polarizer (TFP). Using

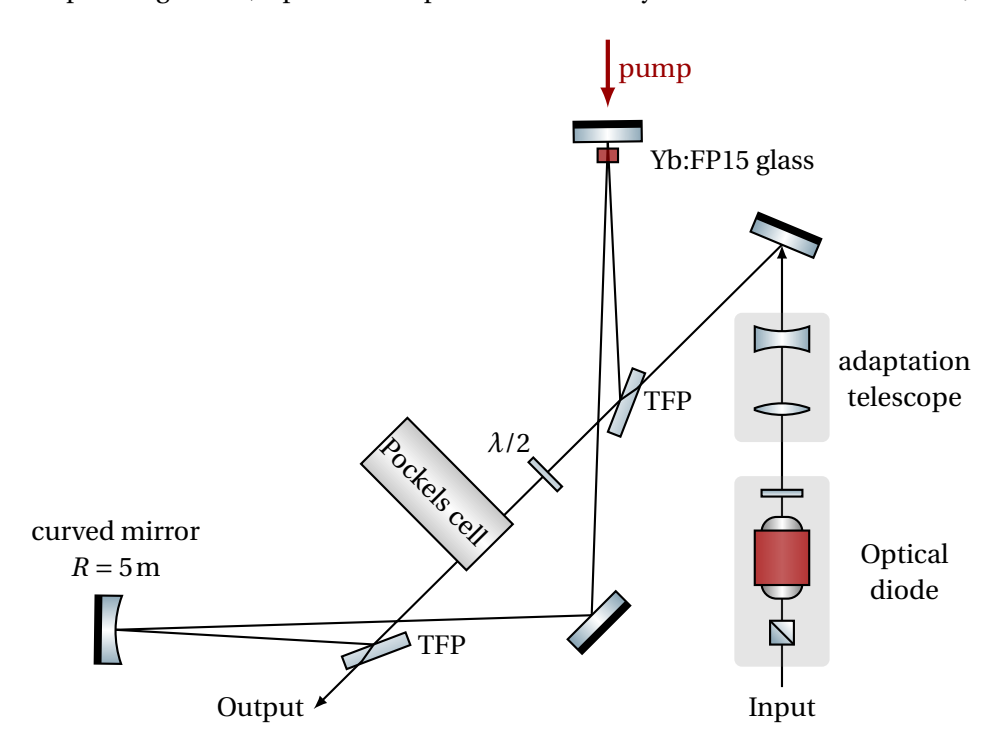


Fig. V.1.: Schematic layout of a typical regenerative amplifier. The input and output coupling is done via reflective TFPs which reflect s-polarized light (at 66° angle of incidence) and transmit p-polarization. The angle to the curved mirror is as small as possible to minimize astigmatism effects. The angle towards the pump mirror is also small such that pump beam and amplified pulse travel nearly collinearly. To match the size of the cavity mode, an adaptation telescope is inserted. Furthermore, back reflections are suppressed by an optical diode where the role of the second polarizer is fulfilled by the input TFP.

reflective polarizers like TFPs is preferable to polarizing beam splitters like Glan-Taylor polarizers, as there is no material dispersion in the reflection case. Due to a pass through the half wave plate the polarization is turned 90° and the pulse is reflected at the second TFP proceeding to perform one round trip. Then, the polarization is turned again by passing the half wave plate and the pulse is coupled out. If the Pockels cell is switched on while the pulse is within the cavity, the effect of the half wave plate is canceled. Hence, the pulse will be trapped within the cavity. Now the pulse can do an in principal infinite number of round trips extracting energy from the active medium. As soon as the Pockels cell is switched off again, the amplified pulse is coupled out. The off switching of the Pockels cell is typically synchronized to the point in time where the round trip losses are balancing the amplification to achieve maximum output energy (in pulse pumped mode for single pulse operation).

Comment: General remarks on regenerative amplifiers

- Cavity length:
 - To avoid truncating the pulse, the cavity length has to be at big enough to accommodate the pulse length and the switching time of the Pockels cell.
 - For a femtosecond oscillator as a seed source it might be useful to match the cavity length to the repetition rate of the oscillator to mitigate pre- and post-pulses.
- *Mode matching*: The input pulse has to be matched with the cavity mode. This can be achieved e.g. with an adaption telescope (c. f. figure V.1).
- *Mode aperture*: In order to obtain the TEM₀₀-mode with a symmetric profile, an aperture can be placed in the cavity to suppress higher order modes.
- *Optical diode*: Input and output beams have to be separated (otherwise we will destroy the seeder). One way to achieve this is a cavity where in- and output are separated, e.g. a ring cavity as in our example. If in- and output are not separated by the cavity layout, an optical diode can be used:
 - An optical diode consists of two polarizers with a Faraday rotator for 45° polarization rotation and a $\lambda/2$ -plate in between.
 - The polarizers are aligned to each other, such that each transmits the same polarization, whereas the other polarization is reflected.
 - As the polarization is always turned into the same direction independent from the propagation direction by the Faraday rotator, this setup transmits light in one direction, while in the other direction it is reflected by one of the two polarizers.

Key point:

We want to mention some advantages and drawbacks of regenerative amplifiers:

Advantages

- high gain/number of passes
- good beam quality (TEM₀₀)
- saturation can be easily achieved
- easier to align than Multi-pass amplifiers

- Q-switch operation possible

Disadvantages

- limited beam size and output energy
- losses due to optical switches in every round trip
- beam profiles other than TEM_{00} are hard to maintain

Hence: When we proceed to higher energies, we need another approach.

V.2. Multi-pass amplifiers

A multi-pass amplifier is an amplifier which redirects the laser beam several times through the laser medium on a predefined path to achieve the desired amplification.

V.2.1. Butterfly

The butterfly setup is the most simple variant of a multi-pass amplifier realized by several plane mirrors redirecting the beam. An example is shown in figure V.2.

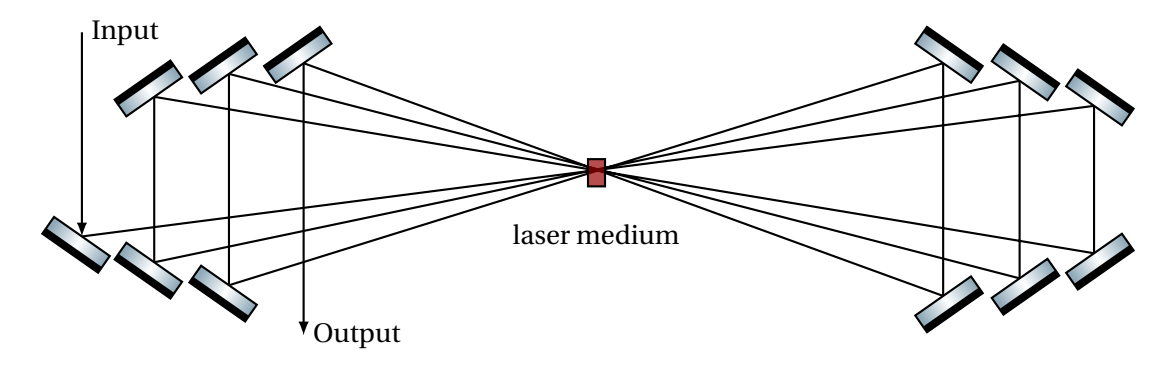


Fig. V.2.: Schematic layout of a butterfly style multi-pass amplifier.

As there is no imaging involved in such an amplifier the beam profile is influenced by propagation effects, which will lead for example to diffraction of shape features (e.g. edges) of the beam or a change in beam size. Hence this amplifier setup is mainly applicable to large beams with soft edges.

V.2.2. Imaging amplifiers

In many high energy amplifiers sharp features on the beam cannot be avoided, e.g. if a tophat beam is to be used to operate efficiently. In such case the basic principle is to image the laser medium with every pass, to maintain the beam profile (and the angular distribution).

A straight forward solution for this problem is to use a telescope in between every pass through the laser active medium. The drawback for this solution is, that for a large number of material passes a high number of optics is needed which also leads to a high effort for aligning the amplifier.

By intelligent folding it can be achieved that those imaging optics can undergo multiple uses during the round-trips, which allows compact setups with a high number of imaging round-trips. In the following a theoretical derivation for such systems taken from [KHK16] is given.

We assume that a round-trip in an imaging multi-pass amplifier is described by alternating free space propagation L (IV.4) and ideal imaging elements L (IV.3). Hence, the matrix representing one round-trip in a system of n elements is given by:

$$G_n = T_{n+1} \cdot L_n \cdot T_n \cdot L_{n-1} \cdot \dots \cdot L_1 \cdot T_1 \tag{V.1}$$

A suitable imaging system has to restore both the spatial and the angular distribution after each round-trip. Hence, the optical system matrix must equal either the unity matrix $\mathbb{1}$ or in the case of a symmetric profile, the negative unity matrix $-\mathbb{1}$. However, we can omit the latter solution by the fact that in a real world application we need to separate the different beam passes geometrically by introducing a little tilt of the flat optics in the image plane and only the asymmetric solution will prevent a summation.

Under these constraints, we proceed by solving the matrix equation $G_n = 1$. In the following, we will give the results for n = 1...3. Solutions for systems of more than three elements are no longer distinct, as there are too many degrees of freedom.

Starting with a system containing only one imaging element (n = 1) per round-trip, there is no solution, as the focusing or de-focusing effect of the single optic cannot be mitigated and will always alter the collimation state of the input beam.

Type I systems

In the case of n = 2 a solution is found for the negative unity matrix. Hence, double passing such a system back and forth will result in a unity matrix again. This is in a narrower sense a special case of four imaging elements. The solution in this case is:

$$d_1 = \frac{f_1 f_2 \cdot (f_1 + f_2) - d_3 f_1^2}{f_2^2}$$

$$d_2 = f_1 + f_2$$
(V.2)
(V.3)

$$d_2 = f_1 + f_2 (V.3)$$

$$f_1 = f_2 \tag{V.4}$$

Here, d_1 to d_3 are the corresponding free space propagation distances, and f_1 and f_2 are the focal lengths of the imaging elements. We will refer to such a kind of system in the following as a Type I system. Schematic setups for optical systems of this type accomplishing three round-trips are exemplarily given in Figure V.3a.

As this system needs to be double passed to fulfill the constraints, it is not really necessary to have a unity magnification, as was originally requested by the constraints used for deriving this solution. This renders Equation (V.4) unnecessary, but since all distances have to be ≥0, it follows from Equations (V.2) and (V.3) that f_1 and f_2 must be at least positive.

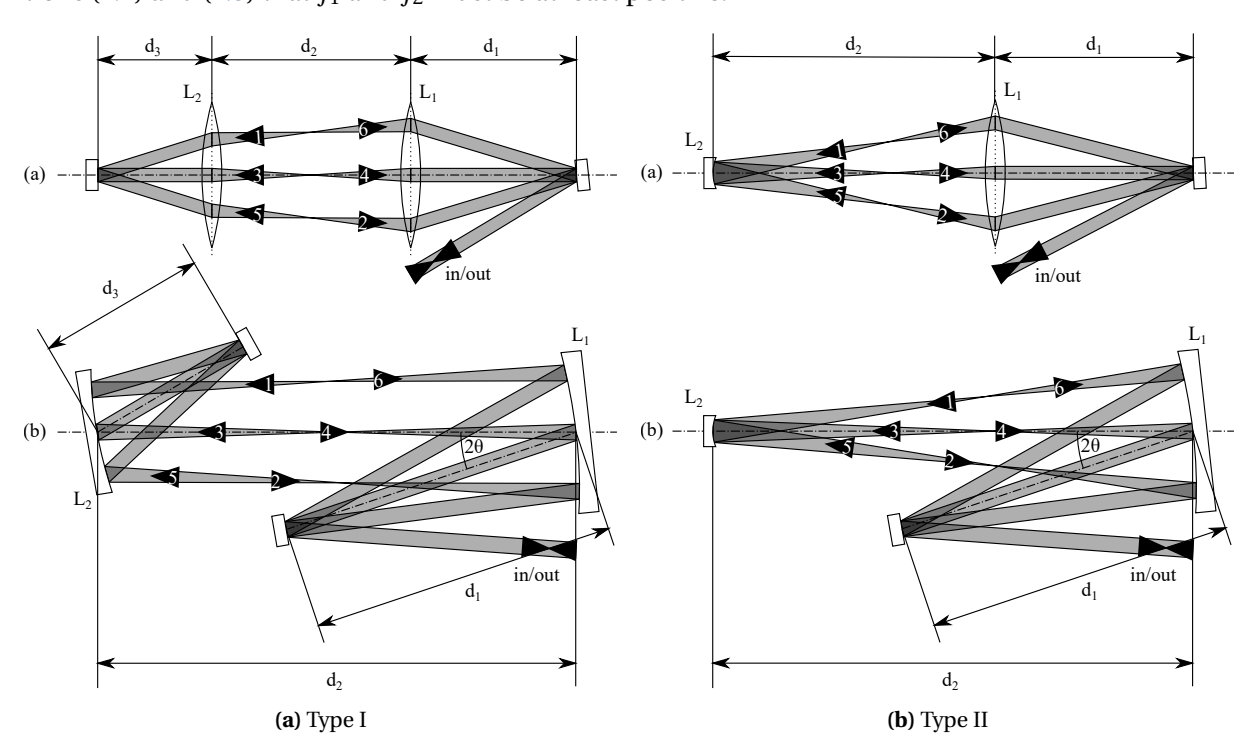


Fig. V.3.: Schematic drawings of (a) Type I and (b) Type II systems with three round-trips based on lenses (top) and on mirrors (bottom) as imaging elements. The numbers in the arrows denote the sequence of passing beams. Taken from [KHK16].

Type II systems

For a system with three imaging elements (n = 3), there are already too many degrees of freedom with respect to the four different distances to get a closed solution for each distance. Therefore, we concentrate on the special case of a symmetrical system, where the layout is mirrored at the second imaging element. Hence, the additional constraints $f_3 = f_1$, $d_4 = d_1$ and $d_3 = d_2$ reduce the degrees of freedom. Furthermore, in a practical setup, such a layout is very advantageous, as it only requires two different imaging elements. In this case, the ABCD-model results in the following constraints:

$$d_1 = \frac{f_1^2 + 2f_1f_2}{2f_2}$$

$$d_2 = f_1 + 2f_2.$$
(V.5)
(V.6)

$$d_2 = f_1 + 2f_2. (V.6)$$

Similar to the Type I system, both f_1 and f_2 have to be positive to obtain positive distances. Furthermore, solving these results for $1/f_1$, one obtains the imaging equation for an ideal lens:

$$\frac{1}{f_1} = \frac{1}{d_1} + \frac{1}{d_2} \tag{V.7}$$

Hence, this system will generate an image of the original beam on the second optical element. This reverses the angular distribution, and the beam is then imaged back to the original image plane by the first element. The diameter of the second element only has to be large enough for supporting the beam itself, as the individual round-trips will not be spatially separated on this optic. Such a system will be referred to as Type II in the following. Schematic examples are given in Figure V.3b for three round-trips also. It should be mentioned that Type I systems are identical to Type II systems for $d_3 = 0$ and half the focal length of the second element, to consider the double pass on this element.

Comment: Spherical mirrors vs. lenses

In the amplifier, using spherical mirrors instead of lenses as the imaging element has several advantages [KHK16, p.8]. The mirror-based layout enables smaller length scales, as the setup can be folded. Additionally, lenses induce higher losses and add additional material path into the setup. Furthermore, residually reflected light from the surface of the lens generates ghost foci which may damage the amplifier. Any transmitted light in a mirror-based design is de-focused. Nevertheless, a mirror-based design features one major drawback, which is that the incoming and outgoing beams have to hit the spherical mirrors under an angle θ as shown in figure V.3. This adds *astigmatism* to the beam, which increases for every roundtrip. The meridional f_m and sagittal f_s foctal lengths are given by

$$f_m = f \cdot \cos(\theta), \quad f_s = \frac{f}{\cos(\theta)}.$$
 (V.8)

V.3. Design limitations

Up scaling the output energy of our amplifier system is not straightforward, as additional effects have to be considered such as nonlinear effects like the intensity dependent refractive index of the laser medium leading to a break up of the beam profile at high energies. Other phenomena like Amplified Spontaneous Emission (ASE) have to be accounted for as well. Therefore, we will discuss different limitations of our amplifier system in the following sections.

V.3.1. Amplified spontaneous emission (ASE)

In a typical high energy laser system, the energy of the laser beam is amplified in various steps by using different amplifiers in succession. Besides the fact that certain types of amplifiers operate at different laser energies (e.g. regenerative amplifiers at mJ level, whereas multipass amplifiers are needed for J-level pulses), one might ask the question, why the usage of more than one amplifier is a common scheme for high energy lasers. We could argue that by scaling the number of material passes, the gain of an amplifier can be scaled as needed. To understand this, we should remember that an inverted active medium emits energy in form of fluorescence light:

$$\frac{\mathrm{d}\beta}{\mathrm{d}t} = \frac{\beta}{\tau_f} = \frac{1}{N_{\mathrm{dop}}} \frac{\mathrm{d}\Phi}{\mathrm{d}t} \tag{V.9}$$

As these photons are emitted in all directions, only a fraction is captured by the amplifier optics. But if this fraction is in the same order of magnitude as the input laser beam, one can no longer neglect it, as this radiation will be amplified, too. This is called Amplified Spontaneous Emission (ASE). This phenomenum occurs especially in regenerative amplifiers, as they can exhibit *Q*-Switching behaviour. Hence, in such cases a non-negligible amount of energy is within the underlying fluorescence light. Furthermore, if the amplified spontaneous emission significantly alters the inversion, the self lasing will ultimately limit the amount of storable energy in the laser medium.

First, we want to calculate an estimation of the generated ASE power in a regenerative amplifier [Kep+16]. We start by modifying the small signal gain formula (III.34) with a loss term L as

$$G = (1 - L) \exp(N_2 \cdot d(\sigma_e + \sigma_a)) \quad \text{with} \quad L = 1 - \exp(N_{\text{dop}} d(\sigma_e + \sigma_a)). \tag{V.10}$$

The total power of the fluorescence light P_f is the number of pumped photons $N_2(d \cdot A)$ de-exciting per second multiplied by their photon energy. Then, for $t \ll \tau_f$ we can write this as

$$P_{f} = \frac{hv \cdot N_{2}(d \cdot A)}{\tau_{f}} = \frac{hv}{(\sigma_{e} + \sigma_{a})\tau_{f}} \cdot A \cdot \ln\left(\frac{G}{1 - L}\right) = I_{\text{sat}} \cdot A \cdot \ln\left(\frac{G}{1 - L}\right). \tag{V.11}$$

We can now consider the evolution of the ASE during the amplification. In every roundtrip, more fluorescence light is added to the total ASE and the already existing ASE of the k-th roundtrip is amplified by G^{n-k} . With a total number of n-passes, we can approximate the accumulated ASE power with a geometric series [IMM03]:

$$P_{\text{ASE}} = P_f G^{n-1} \cdot \underbrace{\left[1 + \frac{1}{G} + \frac{1}{G^2} + \dots + \frac{1}{G^{n-1}}\right]}_{= P_f G^{n-1}} = P_f G^{n-1} \sum_{k=0}^{\infty} \frac{1}{G^k} = P_f G^{n-1} \frac{1}{1 - \frac{1}{G}}$$

$$= \sum_{k=0}^{n-1} \frac{1}{G^k} \approx \sum_{k=0}^{\infty} \frac{1}{G^k}$$

$$= P_f \frac{G^n}{G - 1} = I_{\text{sat}} \cdot A \cdot \underbrace{\ln\left(\frac{G}{1 - L}\right) \frac{G^n}{G - 1}}_{G_{\text{ASE}}}.$$
(V.12)

Now, in order to see how the contrast between the original seed laser energy (which is amplified by $G_{\text{pulse}} = G^n$) and the ASE deteriorates, we can plot $G_{\text{ASE}}/G_{\text{pulse}}$ as shown in figure V.4 for different amounts of losses L due to re-absorption or other cavity losses. We observe that higher losses significantly deteriorate the ASE-contrast especially for low small signal gain values.

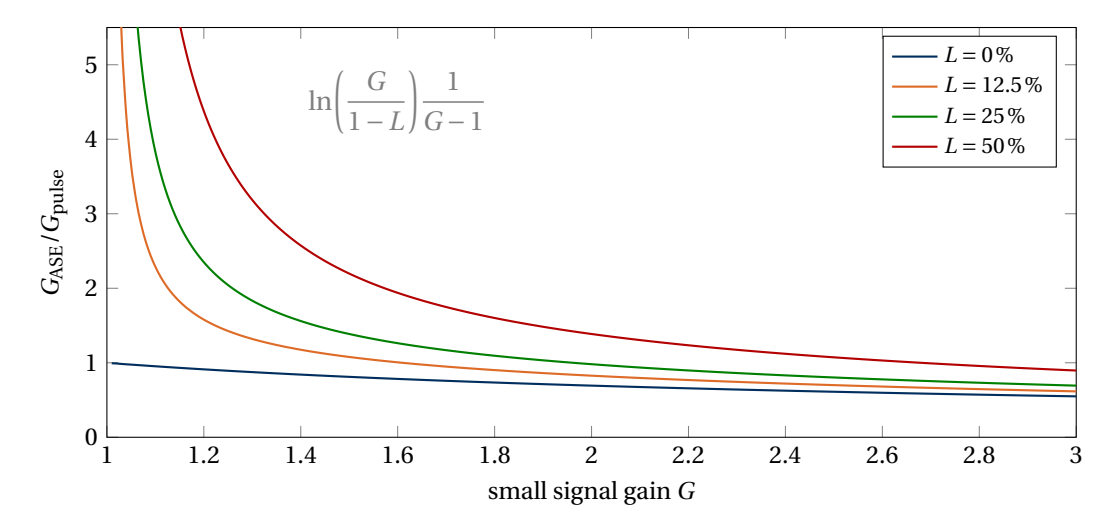


Fig. V.4.: Plot of the contrast between the gain of the ASE and the laser pulse depending on the small signal gain for different re-absorption losses *L*.

However, we must note that the calculated ASE power (V.12) is only valid by assuming that every fluorescence photon is amplified in the resonator, which unrealistic. Therefore, we need to introduce additional factors to accommodate for the spectral, angular and polarization acceptance of the amplifier:

Angular acceptance $K_{\Delta\Omega}$

Only the part of the fluorescence light emitted along the laser axis has to be considered for ASE. There are several ways of describing the Spatio-angular acceptance:

• Multipass-Amplifiers using laser rods [Koe06, p.195]: A high gain medium with a long path length is prone to exhibit strong ASE. Here, the acceptance solid angle $\Delta\Omega$ of the ASE is given by the geometry of the laser rod $\Delta\Omega = \frac{A}{d^2}$, where d and A describe the rod length and cross-sectional area, respectively (c. f. figure V.5). Due to refraction at the end-faces of the laser medium, the acceptance angle is further increased by the refractive index n^2 .

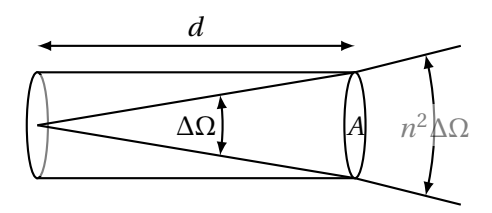


Fig. V.5.: Geometry for the derivation of the acceptance solid angle of a laser rod.

• Regenerative amplifier with a thin amplifier disc [Kep+16] ($d < z_R$): The acceptance angle depends only on the amplifier mode size and is independent of the amplifier geometry. Furthermore, there is no refraction at the surface, since the laser beam is perpendicular to the surface.

We can calculate a lower bound of the ASE by using the divergence of the TEM_{00} -mode which is given by the minimum Beam Parameter Product (BPP)

$$BPP = w_0 \cdot \theta \quad \text{and} \quad BPP_{\min} = \frac{\lambda}{\pi} \quad \Rightarrow \theta = \frac{\lambda}{\pi w_0}.$$
 (V.13)

With the divergence angle θ of the beam we can calculate the acceptance solid angle (under small angle approximation)

$$\Delta\Omega = 4\pi \sin^2\left(\frac{\theta}{2}\right) \approx \pi\theta^2 = \frac{\lambda^2}{A} \quad \Rightarrow \quad K_{\Delta\Omega} = \frac{\Delta\Omega}{4\pi} = \frac{\lambda^2}{4\pi A}.$$
 (V.14)

Note that this simplification is only valid if the amplifier accepts the TEM₀₀-mode only. For higher order Gaussian modes, we have to multiply this result by the M^2 factor of both spatial directions $M_x^2 \cdot M_y^2$. The factor $K_{\Delta\Omega}$ describes the share of the acceptance solid angle to the total solid angle.

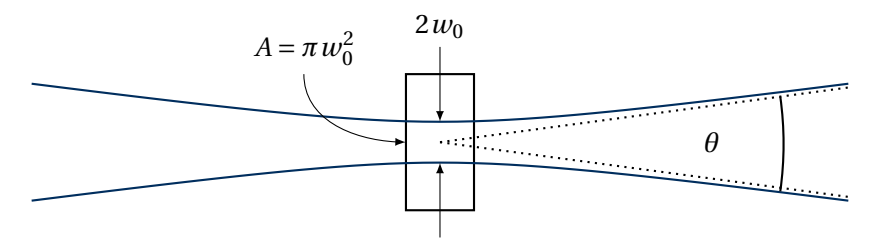


Fig. V.6.: Geometry for the derivation of the acceptance solid angle of a thin laser disc.

We can minimize the accepted solid angle by using e.g. spatial filters (pinholes), therefore only allowing spatial frequencies used in the beam profile. The accepted solid angle is most critical in large aperture imaging systems with high order super-Gaussian beams.

Spectral acceptance $K_{\Delta \nu}$

The spectral acceptance describes the part of the emitted fluorescence spectrum which can be amplified within the amplifier, as the optics of the system (e. g. dielectric mirrors in the cavity) only reflect a certain wavelength range at high reflectivity. Hence, reducing the spectral acceptance of the amplifier improves the contrast between the laser pulse power and the ASE. The share of accepted fluorescence $I_{\rm nu}$ to the fluorescence emitted over the full spectrum is calculated by

$$K_{\Delta \nu} = \frac{\int_{\Delta \nu} I_{\nu}(\nu) \, \mathrm{d}\nu}{\int_{0}^{\infty} I_{\nu}(\nu) \, \mathrm{d}\nu}.$$
 (V.15)

Polarization acceptance K_p

As most amplifiers are polarization sensitive, only fluorescence light with the correct polarization state is accepted by the cavity and thus amplified. The probability of a photon matching the correct polarization state is described by K_p . For isotropic laser glasses like Yb:FP15, the generated fluorescence light is unpolarized, hence $K_p = 0.5$. However, for anisotropic materials like Ti:Sa the emission and absorption cross sections are different for π - and σ -polarization (c. f. figure II.14).

We can now summarize all these factors into a single formula to describe the generation of ASE. We can now multiply the acceptance parameters to equation (V.12), which yields

Equation: Generated ASE power

$$P_{\text{ASE}} = \overline{I}_{\text{sat}} \cdot K_{\Delta\Omega} A \cdot K_{\Delta\nu} \cdot K_p \cdot \ln \left(\frac{\overline{G}}{1 - L} \right) \frac{\overline{G}^n}{\overline{G} - 1}. \tag{V.16}$$

We want to note that the saturation intensity and the small signal gain have been replaced by their averaged values over the accepted spectral range Δv .

Comment: Design of a laser material

Besides the forward directed self-lasing, ASE can also occur on other paths, e.g. within the laser medium itself. This is especially significant for large aperture amplifiers with a high single pass gain. Therefore, several design ideas are to be kept in mind:

- Laser medium aspect ratio
 - Very thin high doped discs will exhibit a huge transversal gain compared to the laser axis.
 - This is even more problematic as (unavoidable) total internal reflections guide a huge amount of the emitted fluorescence.
 - Measures: Bonding with un-doped material, increased material thickness with doping accordingly reduced (as far as possible in point of cooling and pumping scheme).
- The sides shall not reflect fluorescence (avoid whispering gallery modes). Here, we can utilize:
 - absorbing cladding (e.g. Cr:YAG for Yb:YAG)
 - special crystal shape
 - index matching + absorber

V.3.2. Laser Induced Damage Threshold

All optics have a certain Laser Induced Damage Threshold (LIDT), that describes the maximum allowable laser fluence that the optic can tolerate without being destroyed. This parameter is dependent on many factors and always includes a considerable variation. In actual laser amplifiers the most sensible part of the optics are the surfaces and coatings, as bulk LIDT is typically much higher, as long as there are no inclusions.

When we want to compare the specified LIDT of an optic to our laser system, we have to keep in mind the following parameters:

• *wavelength*: For a different wavelength than the specification, the damage threshold must be scaled appropriately. A good approximation for this is

$$LIDT = LIDT_{ref} \sqrt{\frac{\lambda}{\lambda_{ref}}},$$
 (V.17)

which means that the LIDT decreases for shorter wavelengths. However, a small distance to absorption bands can change the behaviour drastically [CRD03]. Furthermore, when a dielectric multi-layer coating, the position of the maximum electric field strength relative to the material boundaries can change the LIDT depending on the wavelength.

- Energy density of the laser beam (total energy divided by $1/e^2$ area).
- *Pulse duration* of the laser. For pulsed lasers, the LIDT decreases for shorter pulse duration and is roughly constant in the ultrashort regime.
- repetition rate | average power
- *Beam diameter* of the laser. A larger beam diameter (at a constant energy density) decreases the LIDT for longer pulse durations, since there is a higher chance of a defect occurring in the illuminated area, thus increasing the probability of damage.
- *Intensity profile* of the laser (e.g. Gaussian).

Generally we can distinguish the LIDT measurement between continuous wave (cw) lasers and pulsed lasers:

- *CW lasers*: The damage of an optic by a CW laser (or lasers with pulse lengths $\tau > 1\,\mu s$) is usually caused by the melting of the surface as a result of absorbing the laser energy or a damage to the optical coating. The scaling of LIDT to pulse length is linear.
- *Pulsed lasers*: Pulsed laser do not supply enough heat to the optic to induce thermal damage. However, the strong electric fields are capable of inducing dielectric breakdown in the material. This happens if the electric field density is high enough to remove electrons from their lattice position. For even higher electric fields, the free electrons are accelerated by the laser field and excite neighbouring bound electrons, which leads to avalanche ionization and multi-photon ionization for ultrashort laser pulses.

The dependence of the LIDT on the pulse length and beam diameter of a transparent material is shown in figure V.7 for the example of fused silica at 1064 nm [Woo98]. For long pulses and CW light the components temperature rises and thermal mechanisms take place.

For nanosecond pulse durations (dielectric breakdown), the ionization rate of freed electrons is proportional to $\sqrt{\tau}$.

For picosecond pulse durations (avalanche-ionization), the stronger ionization rate limits the build-up of the electron avalanche, as the electrons move out of the beam center during the characteristic

time t_i of ionization. For longer pulses and larger beam radius w, the chance of avalanche breakdown is higher and the LIDT scales with $\exp(-\tau/t_i)/w$.

At ultra short pulse duration ($\tau < 1 \times 10^{-13}$ s), multi-photon avalanche ionization can occur, as the interaction takes place in a time frame, where the freed electron absorbs several incident photons without intermediate movement. Here, the LIDT scales linearly with the pulse duration τ .

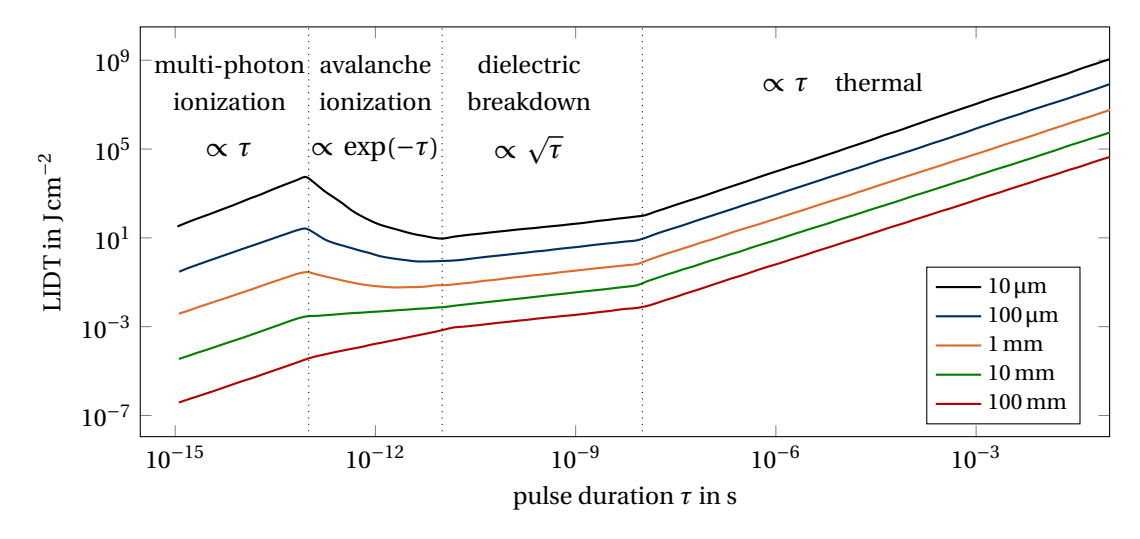


Fig. V.7.: Laser induced damage threshold in fused silica at 1064 nm as a function of pulse duration and spot size. Data taken from [Woo98].

Additionally, the actual coating, surface and choice of material has a large influence on the LIDT. Typically, the LIDT of laser materials and their coating lies in the range of 2 to $10\,\mathrm{J/cm^2}$ for $100\,\mathrm{ps}$ pulses. At the Polaris laser system the LIDT of the Yb:FP15 laser material lies at about $3\,\mathrm{J/cm^2}$, while the saturation fluence is around $30\,\mathrm{J/cm^2}$. Therefore, most of the time, it is not possible to operate Yb-doped laser media at the saturation fluence F_{sat} .

Other typical damage thresholds of typical metal films lie at around $1\,\mathrm{J/cm^2}$. Therefore, these mirrors are typically not used in amplifier systems (also due to their lower reflectivity at around 98 %) and are exchanged by coated dielectric mirrors.

Key point: Best parameters

In order to achieve a high damage threshold our laser should have the following properties:

- long wavelength
- long pulse duration
- small beam diameter at constant energy density
- smooth transversal profile (e.g. Gaussian)

In general, dielectric coated surfaces have a higher damage threshold and reflectivity than metal surfaces (e.g. silver mirrors). However, they are more expensive and have a smaller spectral acceptance window.

V.3.3. Nonlinear effects

A direct amplification of ultrashort pulses towards high pulse energies/intensities is not just limited by the LIDT, but also the manifestation of nonlinear interactions of the laser with the optical elements of the laser system (e. g. laser-active materials, Pockels cell crystals, lenses, polarizers, etc.). The refractive index of any material is not a constant with regard to the pulse intensity. When we consider a medium with a non-zero third order nonlinear susceptibility $\chi^{(3)}$, the solution of the wave equation with a polarization source term yields an additional phase contribution, which depends on the intensity I(t) of the laser pulse. In first approximation, this can be described as a linear scaling of the material's refractive index which is called the *optical Kerr effect* [Boy07, p. 375]:

Equation: Optical Kerr effect

$$n(t) = n_0 + n_2 I(t)$$
 with $n_2 = \frac{3\chi^{(3)}}{4\varepsilon_0 n_0^2 c}$. (V.18)

Here, n_2 is called the nonlinear refractive index, which is directly proportional to the nonlinear susceptibility $\chi^{(3)}$, c is the vacuum speed of light and ϵ_0 the permittivity of vacuum.

A practical approach to describe this effect is the so called *B-integral*, which describes the *total intensity induced phase shift* in radians¹. The path difference can be calculated by integrating over the additional optical way induced by the nonlinear refractive index [Sie86, p.386]

Equation: B-Integral
$$B = \frac{2\pi}{\lambda} \int\limits_0^L n_2 \cdot I \, \mathrm{d}z \,. \tag{V.19}$$

If we consider for example a *Gaussian-like* spatial profile, the magnitude of the *B*-integral is higher in the center of the beam than on its edges, this results in a *nonlinear phase distribution* generating a *lens*. The beam will experience a focusing effect called *self focusing*. As this further increases the intensity, the lens inscribed by this effect will get even stronger and leads to further focusing of the beam until the diffraction limits the focusing.

For large beams employing e.g. a tophat beam profile the effect leads to an intensification of modulations on the beam profile, as regions of higher intensity will generate their own lenses and thus get more intense. This leads to a *small scale break up* of the beam as seen in figure V.8.

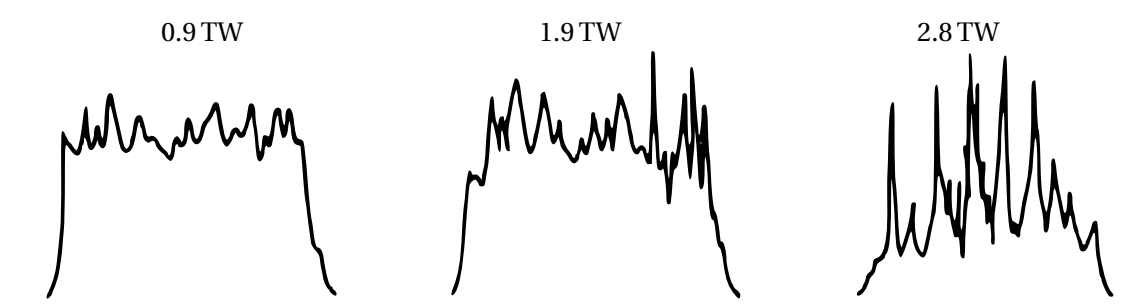


Fig. V.8.: Transversal beam profiles of a Nd:glass laser amplifier system (Argus laser) showing small scale beam break as the power is increased. Small modulations of the intensity profile get enhanced by self focusing of certain parts of the beam. Figure taken from [SHW81].

As a rule of thumb the B-integral should never be *greater than 2* to avoid nonlinear small scale beam break up. However, this should be treated as an empirical value, as there might be systems with high

¹Remember: The phase shift is $\varphi = k \cdot L$, *k*-wave vector, *L*-length of the medium

specifications where this value is already too high.

Example: Fused silica

In order to get an intuition of nonlinear effects, let us consider fused silica which has a nonlinear refractive index of $n_2 = 2.74 \times 10^{-16} \, \mathrm{cm^2/W}$ [Mil98] with $n \approx 1.5$ at 1053 nm. For a 1 ns long square pulse at $10 \, \mathrm{J/cm^2}$ we have a beam intensity of $1 \times 10^{10} \, \mathrm{W/cm^2}$. Then, the ratio of the nonlinear part of the refractive index to the linear part is

$$\frac{\Delta n}{n} = 1.8 \cdot 10^{-6} \quad \text{with} \quad \Delta n = n_2 \cdot I. \tag{V.20}$$

This results in a value of B = 1.13 for L = 10 cm of fused silica at $\lambda = 1$ μ m.

In an amplifier a calculation of the B-integral is typically sufficient for the output energy of the last passes.

V.3.4. Beam Distortions

In this section we want to discuss the effects on the spatial (thermal lensing, clipping) and temporal (gain saturation) profile of the beam.

Temporal effects - Edge steepening

Back in chapter III.3.3 when we presented the Frantz-Nodvik solution of pulse amplification, we were able to compute the inversion and temporal pulse shape of our seed pulse, when it gets amplified in the active material. When we consider a high gain material like Yb:YAG, we can achieve single pass gain-factors well beyond one. Then the pulse will change the inversion during its propagation through the material. Therefore, the rising edge of the pulse will *see* a higher inversion than the trailing edge, which will lead to a distortion of the temporal profile. This process is called edge steepening and is shown in a simulation displayed in figure V.9 for a high gain material (Yb:YAG) and a lower gain material (Yb:CaF₂) for roughly the same total gain. Due to edge steepening in saturated amplifiers the effective pulse length and temporal shape might be strongly changed.

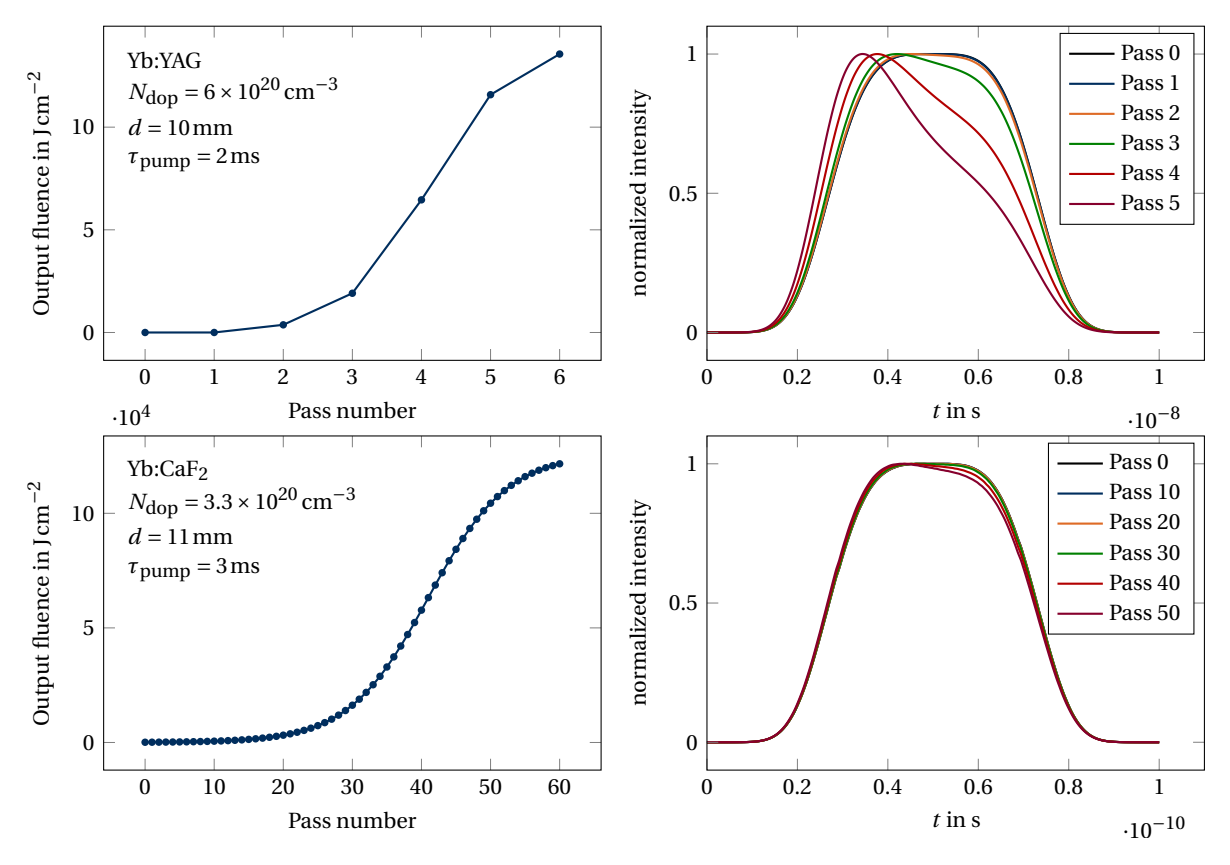


Fig. V.9.: Simulated temporal profile of a seed pulse in an amplifier using Yb:YAG (top) and Yb:CaF₂ (bottom) pumped at 940 nm with an emission wavelength at 1030 nm with a pump intensity of $30 \, \text{kW cm}^{-2}$. For the seed, a high order Gaussian pulse (GO = 2) with an input fluence of $10 \, \text{mJ cm}^{-2}$ was chosen. The high gain material (Yb:YAG) shows significantly higher distortions of the beam profile than the lower gain material (Yb:CaF₂), even though the total gain was similar.

Comment: Spectral edge steepening

Edge steepening may also occur in a CPA-system with a broadband, stretched pulse. Here, the wavelengths of the beam are separated in time, thus edge steeping can also affect the spectral profile of the beam. Since broadband gain media often have lower cross sections (c. f. FL-

equation), this effect is rather small.

Spatial effects

There are several effects that can alter the spatial profile of the beam:

- Shape of the pump beam: Modulations in the pump beam will directly transfer into the beam profile. However, the adaptation of the shape is nonlinear. Thus, a Gaussian pump beam will not generate a Gaussian output. Hence, for efficiency and LIDT considerations, mostly tophat beams are used.
- Clipping of the beam profile: Especially for tophat beams diffraction during propagation has to be considered. Optics with an aperture smaller than the beam size will lead to clipping, which introduces ripples onto the beam profile. Those high spatial frequencies may be filtered by pin-holes.
- Temperature gradients:
 - thermal lensing n(T) (c. f. section V.3.5)
 - temperature dependent amplification $\sigma(T)$ (c. f. section II.10)

V.3.5. Thermal lensing

The beam quality is influenced by the wavefront of the amplified laser pulse. Here, the active medium may induce aberrations which are a consequence of a spatially different Optical Path Difference (OPD) $\varphi(r)$. This path differences may be induced (similar to the description in section V.3.3) by a change of the refractive index due to pump induced thermal load or changes of the electronic configuration [Tam+18]. These spatial distortions will reduce the focusability of the output beam, thus limiting the available peak power and intensity.

Determining the thermal profile

For Yb_3^+ -doped materials the small quantum defect of approximately 9 % leads to reduced thermally-induced OPD of the pumped material. Therefore, electronic contributions are more important and cannot be neglected in the description of wavefront aberrations. However, for this section we want to study the thermal contributions. This can be done by solving the heat equation [Ché+06]

$$\varrho C_p \frac{\partial T(\boldsymbol{r}, t)}{\partial t} - K_c \nabla^2 T(\boldsymbol{r}, t) = \frac{P_{\text{th}}(\boldsymbol{r}, t)}{V}.$$
 (V.21)

 $T(\mathbf{r}, t)$ Temperature in K.

 ϱ Density in kg/cm³

 C_p Specific heat capacity in J/(kgK). It only affects the temperature variation in the pulse regime. For quasi CW laser pump diodes the temporal variation can be ignored.

 K_c Thermal conductivity in W/(mK). This governs the temperature gradient inside the crystal

 $P_{\rm th}$ Absorbed pump power $P_{\rm th} = \eta \cdot P_{\rm abs}$ which is converted into heat. The ratio is given by the heat fraction η .

V Volume, in which the pump radiation is absorbed.

We can simplify the equation by assuming a steady state condition $\left(\frac{\partial T}{\partial t} = 0\right)$, a radially symmetric pump profile T(r,t), a scalar and temperature independent thermal conductivity K_c^2 . Then the heat equation becomes

$$\frac{1}{r}\frac{\partial}{\partial r}\left(r\frac{\partial T}{\partial r}\right) + \frac{\partial^2 T}{\partial z^2} = -\frac{\eta P_{\text{abs}}(r,z)}{V \cdot K_c}.$$
 (V.22)

An analytical solution of this equation is only calculable in rather simple systems. Assuming a cylindric laser rod with length L and radius R, one obtains a parabolic temperature profile [Koe06, p.97]

$$T(r) = T(R) + \frac{\eta P_{\text{abs}}}{4\pi R^2 \cdot L \cdot K_c} (R^2 - r^2),$$
 (V.23)

where T(R) is the temperature on the crystal surface, which can be calculated by a proper choice of boundary conditions. The temperature difference between the center and the surface of the rod is given by

$$\Delta T = T(0) - T(R) = \frac{\eta P_{\text{abs}}}{4\pi \cdot L \cdot K_c},$$
(V.24)

which is, surprisingly, independent of the radius R and the surface temperature T(R), but scales inversely with L. This means that external cooling will not decrease the thermal gradient inside.

²This restricts our discussion to glasses and cubic crystals

The heat transfer between the laser crystal and the flowing cooling agent leads to a temperature difference between the surface T(R) and coolant T_c . A steady state is reached when the absorbed pump power is equal to the power removed from the rods surface

$$P_{\text{th}} = A \cdot H(T(R) - T_{\text{c}})$$
 with $A = 2\pi R \cdot L$, (V.25)

where *H* is the heat transfer coefficient which can be calculated by the geometry and flow rate of the cooling agent [Koe70]. The total temperature profile is shown in figure V.10.

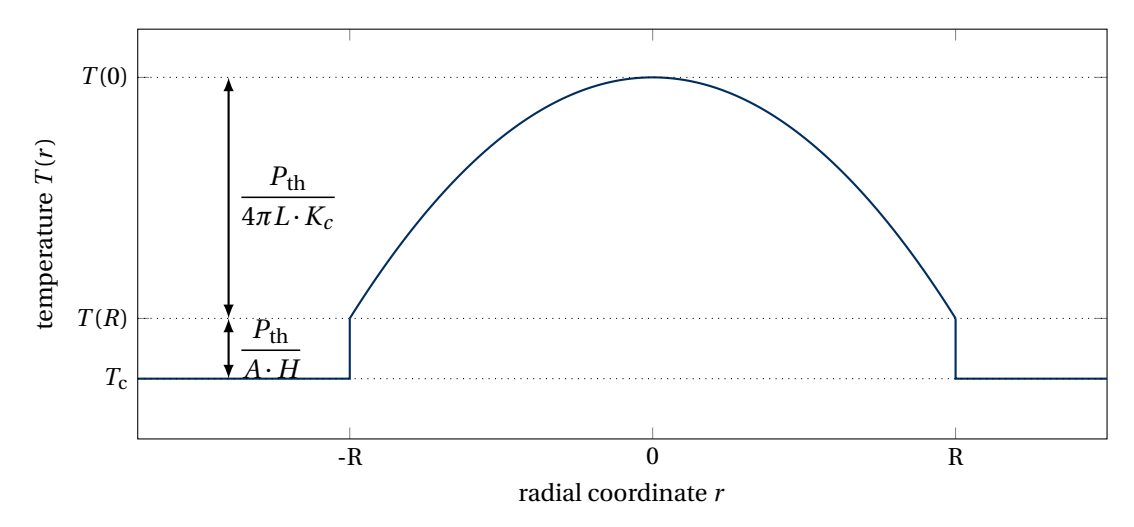


Fig. V.10.: Steady-state temperature profile of a homogeneously pumped laser rod of length L and radius R.

Comment:

This solution is only valid for a homogeneously pumped laser rod and is therefore not applicable to end-pumped geometries. For spatially restricted pump profiles the solution is given in the literature for top-hat shaped pump profiles [SGW00] and gaussian shaped profiles [Inn+90].

Determining the OPD profile

When we have a suitable model to describe the temperature profile of the laser material, we can calculate the OPD profile using [Ché+06, p.119]

Equation: Optical path density profile

$$\Phi(\mathbf{r},t) = \left[\frac{\mathrm{d}n}{\mathrm{d}T} + \underbrace{2n_0^3\alpha_T C_r}_{\text{Photoelastic effect}} + \underbrace{(n_0 - 1)(1 + \nu)\alpha_T]}_{\text{thermal expansion}}\right] \cdot (T(\mathbf{r},t) - T_0)L. \tag{V.26}$$

 $\frac{dn}{dT}$ thermo-optic coefficient

 n_0 refractive index of the unpumped material

 α_T coefficient of thermal expansion

v Poisson's ratio. It measures the ratio of deformation in axial and transversal direction

 C_r Photoelastic constant in radial direction

We observe three contributions to the thermal OPD profile of the laser material. First we have the temperature dependence of the refractive index, which can be either positive (Yb:YAG) or negative

(YbCaF₂) c. f. table V.1. Thermo-optical stress is described by the photoelastic effect which induces a birefringence in the crystal. As most beams are perpendicular to the rod's surface, only the radial part C_r contributes. The thermal expansion describes the deformation of the end faces of the laser rod.

Table V.1.: Thermo-optical coefficients for three different Yb-doped laser materials. Taken from [Tam+18].

material	unit $[1 \times 10^{-6} \mathrm{K}^{-1}]$	Yb:YAG	Yb:CaF ₂	Yb:FP15
thermo-optic	$rac{\mathrm{d}n}{\mathrm{d}T} \ 2n_0^3 lpha_T C_r$	9.0	-10.1	-8.3
photoeleastic	$2n_0^3\alpha_TC_r$	0.3	-4.0	0.2
thermal expansion	$(n_0 - 1)(1 + v)\alpha_T$	7.1	10.0	9.6

V.3.6. Air breakdown

At very high laser beam intensity, i. e. when focusing in an imaging amplifier, the local laser intensity can be large enough to trigger inoization effects in the surrounding gas before the pulse reaches its focal plane. This creates a plasma with a non-uniform electron density distribution, because the typically gaussian-shaped transversal intensity distribution is not uniform. This leads to a higher electron density $n_e(r)$ close to the laser axis which affects the refractive index $\eta(r)$ of the plasma

$$\eta(r) = \sqrt{1 - \frac{n_e(r)}{n_{\text{crit.}}}}, \text{ with } n_{\text{crit}} = \frac{\omega^2 \varepsilon_0 m_e}{e^2}.$$
(V.27)

Here, $n_{\rm crit}$ is the critical plasma density which depends on the wavelength $\lambda = 2\pi\omega/c$ of the laser beam. This leads to an increase of the phase velocity $v_{\rm ph}(r) = c/\eta(r)$ in regions of higher electron density which results in a diverging behaviour. Thus, the maximum achievable intensity of the laser beam is reduced. As this defocusing behaviour depends on the density of electrons, reducing the ambient pressure increases the threshold of the ionization induced-defocusing effect as shown in figure V.11 (right). Furthermore, the threshold of breakdown increases for decreasing pulse durations (c. f. figure V.11 (left)). In summary, the threshold intensity depends on the wavelength, pulse duration and

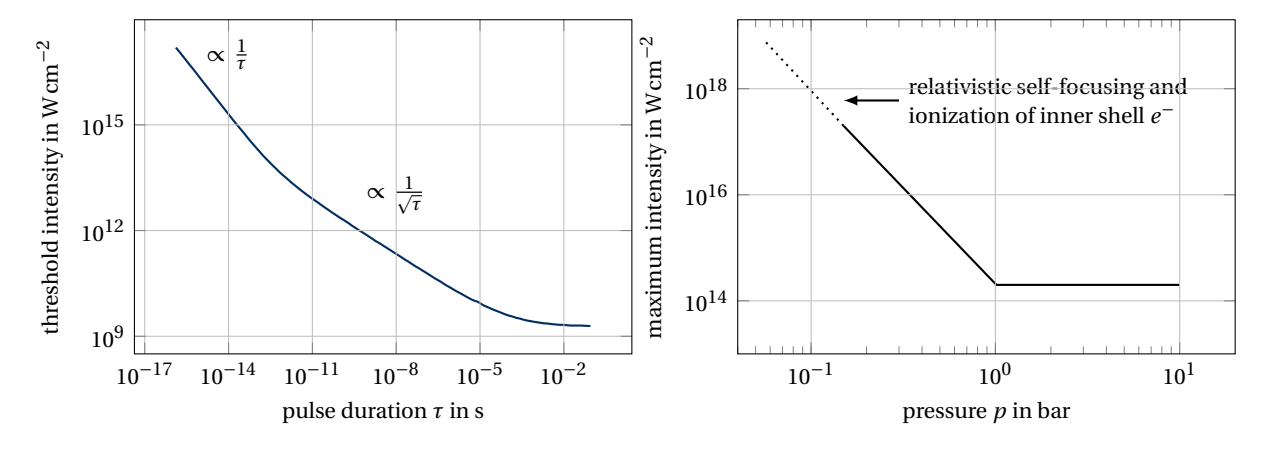


Fig. V.11.: Scaling of the laser breakdown intensity I in air (nitrogen gas) as a function of pulse duration (left) [Nie95] and pressure p (right) [Mäu19, p.80]. For short pulse durations (4 ps to 8 μ s) an inverse square root dependence is observed. The scaling law on the right side was obtained using a laser pulse at $\lambda = 1030\,\mathrm{nm}$ at room temperature. The maximum reachable laser intensity decreases for increasing air pressure until the barrier for tunnel-ionization is reached, then the threshold stays constant.

pressure. This leads to the need of placing imaging amplifiers in vacuum chambers to prevent breakdown in air.

VI. Diode lasers as pump source

To achieve higher pulse energies, as well as to increase the repetition rate, it is important to maximize the efficiency of the conversion of applied electric energy to extracted optical energy. In contrast to broadband excitation of the laser medium using flash lamps, diode lasers with a narrow emission bandwidth have also been established, ensuring selective excitation of the absorption lines and thus effective utilization of the used radiation. Commercially available InGaAs high-power diode lasers achieve more than 60 % conversion efficiency from electrical to optical power [Pil+14].

VI.1. Laser diode basics

A LD is a semiconductor device similar to a Light Emitting Diode (LED), which is made of a negative (n) and positive (p) doped layer of the same semiconductor material and an undoped intermediate layer (i). At high input currents, a sideways emitting zone builds up in the p-i-n-junction of the semiconductor. Due to the geometrical layout and the coating of the facets, a feedback allows the generation of a laser beam in a cavity of 1 to 2 mm length.

A homo-junction using a single semiconductor material for the p-i-in-structure suffers from leakage of electrons and the lack of a guiding structure of the generated light [Trä12]. Therefore, a double heterostructure is required which was a Nobel prize winning idea invented by Kroemer and Alferov. Here, the intrinsic layer-material is chosen, such that it has a lower band-gap than the surrounding doped areas. The intermediate layer then confines the electrons/holes in the conduction/valence band and acts as an optical 2D-waveguide since the lower bandgap corresponds to a higher refractive index n. In order to insure confinement of the laser emission in a single axis, the active material is embedded in a semi-insulating material for force the current to move only through the intermediate layer. An example of the geometry of a single emitter is shown in figure VI.1.

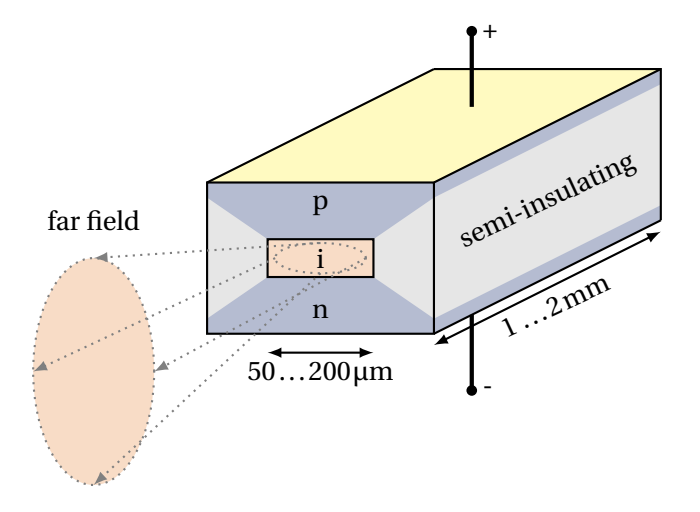


Fig. VI.1.: Schematic of a single semiconductor laser emitter with a double hetero structure. A single laser emitter has an output power of $P \approx 1 \, \text{W}(< 2 \, \text{V}, < 10 \, \text{A})$. Since the intermediate layer is very thin in the horizontal axis, the output profile in the far field is elliptical with a large vertical opening angle. Adapted from [Trä12, p.760].

VI.1.1. Electrical characteristic

The electrical characteristics follows a normal diode:

- in backward direction it has a high resistance. If a sufficient voltage is applied there will be a breakthrough, which leads to the destruction of the diode.
- in forward direction there will be a high resistance until the threshold is reached, than the current increases very fast (low differential resistance).

Since the characteristic of a laser-diode is highly non-linear, we need a special driver to control the laser diode.

- The current has to be regulated.
- Current spikes and backward voltage have to be avoided.

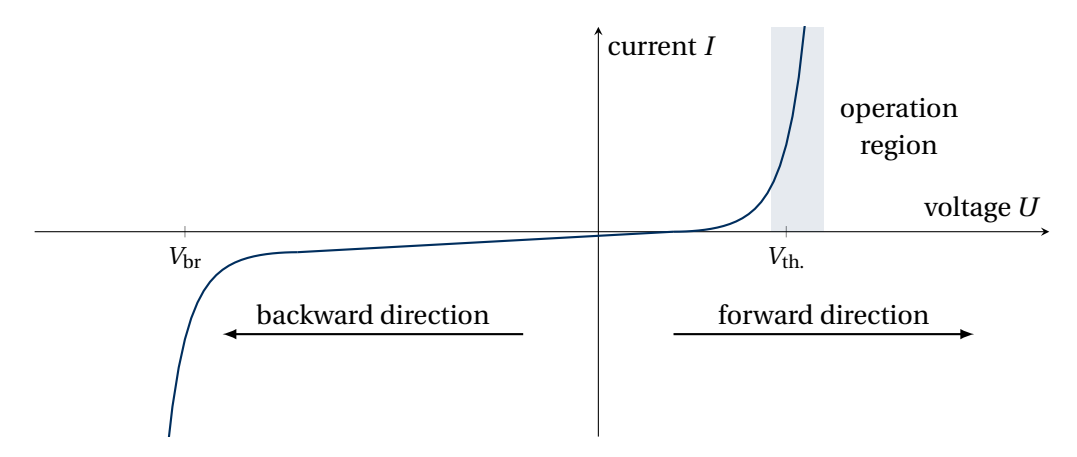


Fig. VI.2.: Current-voltage characteristic of a pn-junction.

VI.1.2. Output spectrum

The actual output spectrum of a laser diode is defined by the used semiconductor material, the coating and its dimensions. For high power laser diodes in the range 900-1000 μ m typically InGaAs-diodes are used.

- Standard high power laser diodes will exhibit a spectral width of some nm, dependent on the current (higher current higher width)
- the central wavelength shifts with temperature (typically approx. 0.3 nm/K)
 - induced by cooling temperature
 - average power
 - might change over pulse
- A regulation of the output wavelength is possible by controlling the heat sink temperature using a cooling liquid like water or applying a bias-current.

Furthermore, the spectrum of a laser diode can be pinned to a certain wavelength by generating feedback, which also allows for reduction in its bandwidth:

- Use a special coating of the end facets of the single emitter, to reflect only a small bandwidth.
- Within the layers of the semiconductor material a volume bragg grating (VBG) can be applied which leads to output bandwidths down to $\Delta\lambda < 0.5$ nm.

VI.2. Power scaling

A single emitter, as shown in figure VI.1, allows for an output power in the range of 10 W. Such diodes are usually provided as fiber coupled modules for oscillator or pre-amplifier pumping. Typical high power laser diodes are stripe emitters, i. e. they have different dimensions in horizontal and vertical direction. Due to the aspect ratio we can differentiate between two different emission axes:

• Fast Axis (FA): In the thin direction, stripe emitters offer a close to Gaussian shaped Transverse Electro-Magnetic (TEM)₀₀ distribution, with a rather large divergence angle

$$\theta = \frac{\lambda}{\pi w_0} \approx 70^{\circ},\tag{VI.1}$$

with w_0 being the mode size. Due to the high beam quality in this axis, the beam can be collimated efficiently by attaching a small cylindrical lens (fast axis collimation FAC) on the front facet of the emitter.

• Slow Axis (SA): In the other direction, the material is much broader resulting in non-Gaussian beam distribution, but with lower divergence angle ($\approx 10^{\circ}$). Due to the multi-mode structure of the slow axis, a beam collimation is hard to achieve.

Higher output powers are generated by combining multiple stripe emitters. This is done conveniently in form of a bar, where several diodes are used in parallel. Hence the the current is scaled up by the number of single emitters. Currently, bars of 1 cm length can generate more than 500 W. A photo and sketch of a diode bar is shown in figure VI.3.

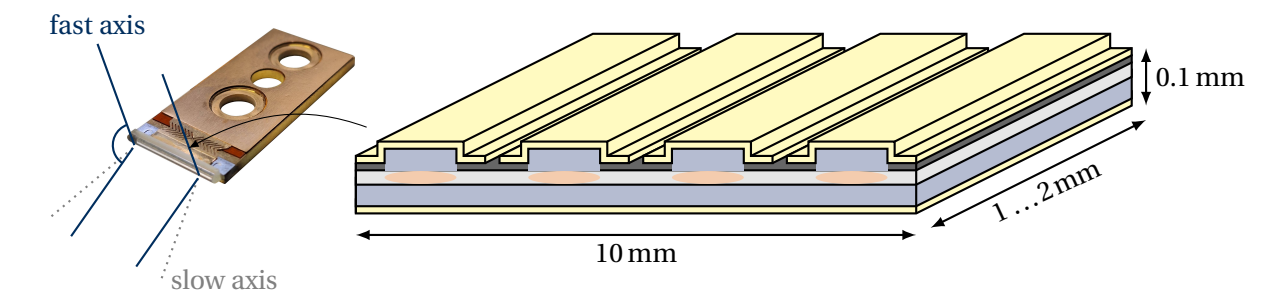


Fig. VI.3.: Left: Photo of a laser diode bar with dimensions of 1.5 mm × 3 mm. With a cylindrical lens to collimate the fast axis beam. The largest part of the bar is the heat sink which is connected to a water cooling system (the water flows through the two outer holes of the heat sink). Right: Sketch of a laser bar with several parallel stripe lasers. Figure adapted from [EE10, p.190]

To further increase the output power, several single bars are arranged in series to a stack (e.g. 20 Bars) as shown in figure VI.4. This allows a power output of $2.5 \dots 10 \,\mathrm{kW}$ of continuous output power. As the high-power laser diode stack has an efficiency of $< 60 \,\%$, a lot of power is transferred into heat, which has to be dissipated via a metallic heat sink (typically copper). The heat sink is coated by a corrosion resistant gold-alloy material and cooled with water flowing through a simple tube in the middle as shown in figure VI.3 (left). The cooling can be improved by using micro-channels within the heat sink or peltier elements [EE10, p.191].



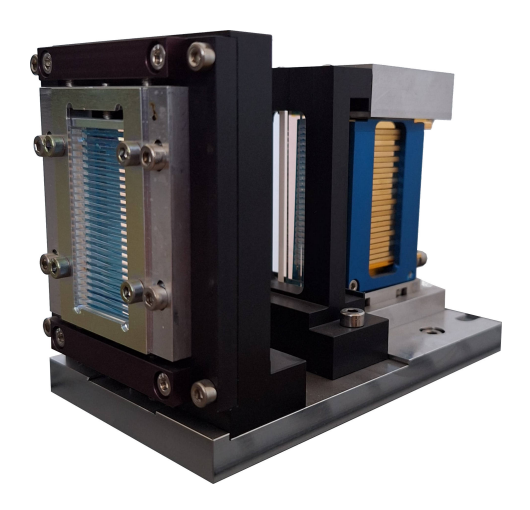


Fig. VI.4.: Left: Photo of a laser diode stack used at the POLARIS laser system in Jena with an output power of 2.5 kW. The left images shows 20 stacked diode bars with cylindrical fast axis collimation lenses. The right side shows the entire laser diode stack including its beam shaping components.

Table VI.1.: Power scaling of the different components of a laser diode stack.

	single diode	diode bar	diode stack
current I	510A	1001000A	1001000A
voltage U	< 2V	< 2 V	< 20 V
power P	10W	150W	2.5 10 kW

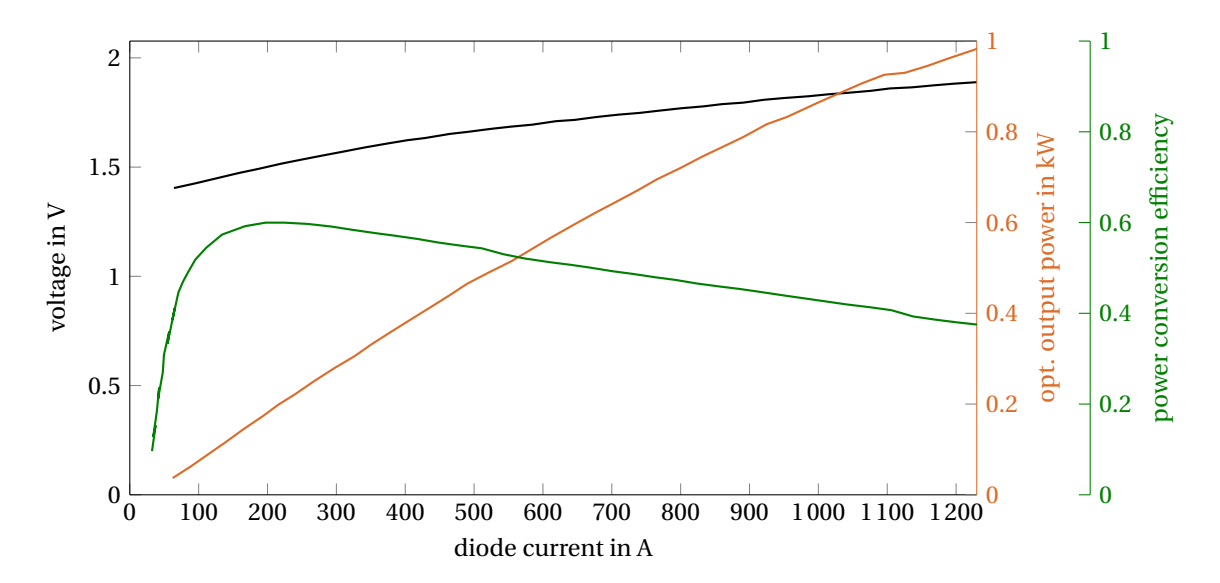


Fig. VI.5.: Performance of a single laser bar. Bias voltage, optical output power and efficiency as a function of the quasi continuous wave current for a repetition rate of $f=10\,\mathrm{Hz}$ and duration of $\tau_p=0.1\,\mathrm{ms}$. Adapted from [Cru+15].

VI.3. Beam shaping

As the profile generated in laser diode modules is not suitable for pumping, beam shaping is a crucial part. In most applications it is desirable to use a tophat shaped pump distribution, which will avoid the spatial distortion of a beam profile during amplification.

For small modules with just a few emitters, the homogenization of the beam can be achieved by using a fiber coupled approach. This allows for intrinsic homogenization, as the beam adapts automatically to the fiber core shape, which is typically multi-mode.

- The fiber coupling can be demanding, as the beam divergence of a single diode emitter is large.
- The coupling can be realized directly for small divergence lasers or by using a focusing lens.
- The output power is limited, given by the beam parameter product (BPP) of the diode source, the fibers core diameter and numerical aperture and the allowed maximum power.

Hence, a more scale-able homogenization version is highly desirable. Besides *homogenizing rods*, here micro optic homogenizers are most promising. For this a so called *imaging micro-lens array* (MLA) is used:

VI.3.1. Homogenization with an imaging micro-lens array (MLA)

A Micro Lens Array (MLA) is a periodic structure of mostly square or hexagonal lenslets. Typically, spherical lenses are used at the entrace and exit surface of the lenslets.

For homogenization purposes two types of micro lens based homogenization techniques exist, imaging and non imaging homogenizers. The latter one is mostly not suitable, as the achievable uniformity is worse than for imaging homogenizers. Therefore, we will only discuss imaging homogenizers here.

In the following, we will focus on monolithic micro lens arrays, meaning arrays that are designed in a way that both faces, entrance and exit surface, have a lens array. This is an often used simplification for the actual setup, as otherwise a six axis (all rotations and relative distances!) alignment is necessary and additional surfaces are involved (meaning additional losses, additional coating, etc.). Nevertheless, if no monolithic arrays are available, also air spaced homogenizer can be used.

Working principle of the homogenization

For now we will also assume that the length of the array is identical with the internal focal length, meaning the second lens surface is placed in the focus of the first one.

The homogenization setup consists of our monolithic array and a fourier lens as indicated in figure VI.6. In the focal length distance behind the lens, our homogenized beam profile will be generated. This is what happens:

- We assume that our input beam consist of many collimated single beams, each larger than the aperture of a single lens.
- Now each of these beams is focused onto the surface of the second lens (in the end we see the angular distribution of our input beam here!). This already defines an *acceptance angle*: only the lens directly across should be hit. If other lenses are hit, this will lead to so called *ghosting*, which are spatial echoes of the original flat-top profile. This will be analyzed later.
- Then, the second MLA-lens surface transforms the spatial illumination pattern of the first lens into its angular distribution, as the lenses are in their respective focal length distance.
- Now the Fourier lens transforms the sum of all single angle distributions back into a spatial distribution in its focal length distance.

- This corresponds now to an average of the illumination pattern of the individual micro lenses, which resembles a homogeneous distribution (if enough lenses are illuminated and the spatial frequencies are not too high), which is tailored by the aperture of the single lens.
- Therefore, the beam in the final image plane resembles a top-hat, where the shape is identical with the shape of the micro lenses. Thus, only two shapes are possible without blocking parts of the aperture, as these have to be aligned, to result in a closed surface: rectangular/square or hexagonal.

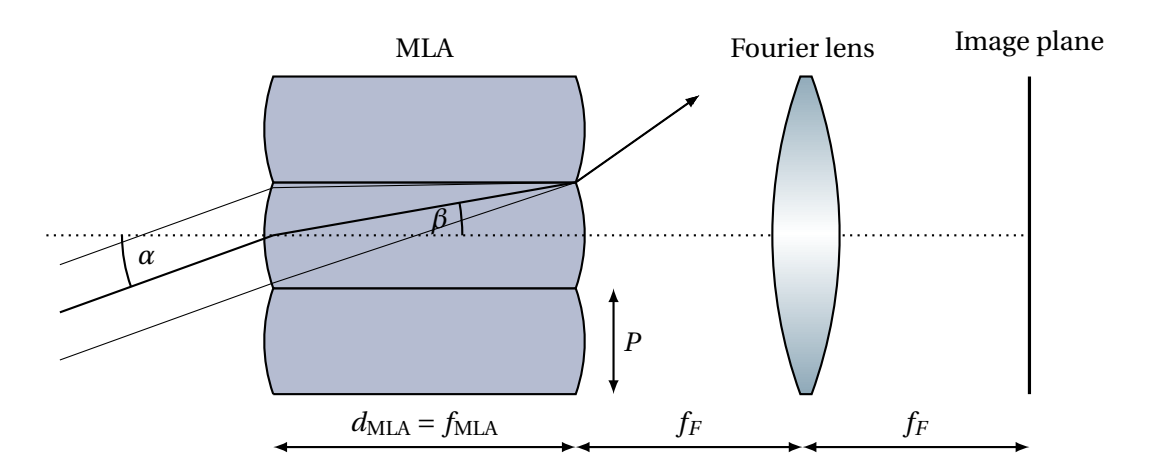


Fig. VI.6.: Schematic drawing of the beam homogenization setup with a MLA with spherical lenslets at the entrance and exit surface. There are three rays with the acceptance angle α sketched in the case of d = f.

Focal length / MLA-thickness

The refraction at a spherical boundary was given by (IV.6) and can be modified for the transition from air $n_1 = 1$ to

$$R_S = \begin{pmatrix} 1 & 0 \\ \left(\frac{1}{n} - 1\right) \cdot \frac{1}{R} & \frac{1}{n} \end{pmatrix}. \tag{VI.2}$$

Here n is the refractive index of the lens material, and R the radius of curvature (ROC) of a single lens. An incoming collimated beam ($\alpha = 0$) with a distance x_0 to the optical axis is transformed to

$$\mathbf{x_2} = R_S \cdot \begin{pmatrix} x_0 \\ 0 \end{pmatrix} = \begin{pmatrix} 1 & 0 \\ \left(\frac{1}{n} - 1\right) \cdot \frac{1}{R} & \frac{1}{n} \end{pmatrix} \cdot \begin{pmatrix} x_0 \\ 0 \end{pmatrix}$$
$$= \begin{pmatrix} x_0 \\ \left(\frac{1}{n} - 1\right) \cdot \frac{x_0}{R} \end{pmatrix} \equiv \begin{pmatrix} x_1 \\ \beta \end{pmatrix}$$
(VI.3)

Within the small angle approximation we can derive the focal length in the medium using trigonometry under the small angle approximation:

Equation: focal length of a MLA
$$f_{\rm MLA} = \frac{x_1}{\beta} = \frac{R}{\left(\frac{1}{n}-1\right)}. \tag{VI.4}$$

Therefore, this should be the thickness d_{MLA} of the MLA.

Acceptance angle

In the following calculation we use the small angle approximation again. The maximum angle β of a mid beam (after refraction) within the MLA that still hits the opposite lens is (cf. figure VI.6):

$$\beta = \frac{P}{2d_{\text{MLA}}} \tag{VI.5}$$

Here, P is the so called pitch of the MLA, noting the diameter of a single lens, and $d_{\text{MLA}} = f_{\text{MLA}}$ the thickness of he MLA which in our case is identical with the focal length of a single micro lens.

Including the refraction, the input acceptance angle α can be calculated using Snell's law $(n_1\alpha = n_2\beta)$ with $n_1 = 1, n_2 = n$

$$\alpha = n\beta = \frac{nP}{2d} \tag{VI.6}$$

Image size

The size of the final flat top beam just depends on the angular distribution and the focal length of the final lens, as it is just the far field. We remember the conversion of a spatial coordinate x into an far field angle ϕ from the single lens focusing with ABCD matrices (see equation (IV.11)):

$$\phi = \frac{x}{f_{\text{MLA}}} \tag{VI.7}$$

Therefore, we obtain our image size x (since $\phi = \alpha$):

$$x = \alpha \cdot f_{\text{MLA}} = \frac{nPf_{\text{MLA}}}{2d} \tag{VI.8}$$

It is interesting to note that in principle the distance of the Fourier lens has no impact on the generated image. Nevertheless, it should be placed in focal length distance to optimize for beam divergence. Due to this, it will be ensured that the angular distribution in the image is minimal, as it is the Fourier transform of the smallest spot size, which lies on the MLA back-surface.

VI.3.2. compaction

see exercise. Basic rules:

- The diode beam should always be adapted to the acceptance angle of the homogenizer.
 - too low: good image quality but loss in brightness
 - too high: ghosting
- To preserve brightness the MLA should be placed either in the near or far-field of the stacks (the angular distribution shall not depend on space)
- Strong intensity modulations on the MLA should be avoided.

VII. Beam Characterization

For the understanding and optimization of a high-power, high-energy class laser system, precision in the output parameters and efficiency are critical. A comprehensive beam characterization is important, as we need to optimize its spatial, temporal and spectral shape to achieve high intensities which determines its effectiveness in the desired applications.

Therefore, in this chapter we will explore key aspects and methods to characterize a beam, focusing on three fundamental properties:

- Spatial: The beam's intensity distribution, divergence and quality of the wavefront are crucial for the focus-ability, propagation and design of optical components in the amplifier chain.
- Temporal: The pulse length is an important part for high-power applications. Furthermore, the analysis of the contrast between the main pulse and amplified spontaneous emission or pre-/post-pulses is important.
- Spectral: In order to achieve short pulses, the spectral shape of the laser beam needs to be controlled carefully. In order to ensure the compressibility of the amplified laser beam in compressor unit, the spectral intensity and phase profile need to be characterized and tailored.

VII.1. Spatial characterization

In order to achieve a small focus in our high-intensity laser application, the wavefront and beam quality have to be analyzed and optimized. This is done via different measurement techniques using wavefront sensors. First, we will introduce different parameters that are used to characterize the quality of a beam.

VII.1.1. Beam parameter product

The Beam Parameter Product [mm mrad] is given by the product of the laser beam's divergence angle θ in the farfield and the beam waist radius w_0

$$BPP = \theta \cdot w_0. \tag{VII.1}$$

In the case of a diffraction limited Gaussian beam, we can calculate the divergence angle in the farfield (c. f. figure IV.3). Using the definition of the beam width (IV.23), the divergence angle can be written as

$$\theta = 2\arctan\left(\lim_{z\to\infty}\frac{w(z)}{2z}\right) = 2\arctan\left(\frac{w_0}{2z_r}\right) = 2\arctan\left(\frac{\lambda}{2\pi w_0}\right) \approx \frac{\lambda}{\pi w_0},$$
 (VII.2)

where λ is wavelength of the laser beam. Then, the BPP is given by

Equation: Beam parameter product

$$BPP = \theta \cdot w_0 = \frac{\lambda}{\pi}.$$
 (VII.3)

It is important to note that the BPP is unchanged when the beam propagates through an optical system without aberrations. As the beam diameter decreases, the divergence increases.

VII.1.2. Radiance

The Radiance L [kW/cm²sr], which is often also called "brightness", is a parameter commonly used to describe beams from laser diode pump engines. It describes the power content P of a beam parameter product, and hence cannot be increased by normal optical means (excluding e.g. amplification or polarization combining):

$$L = \frac{P}{A\Omega} \tag{VII.4}$$

Here A is the area, from which P is emitted and Ω the solid opening angle in [sr]. For practical reasons Ω is typically assumed to be either rectangular (pyramid shape) or circular (cone shape). In these cases it can be calculated by:

- rectangular [Kha68]¹: $\Omega = 4 \cdot \arcsin(\sin(\varphi_x)\sin(\varphi_y))$
- circular: $\Omega = 2\pi \cdot \sin^2(\varphi)$

Here φ is the half opening angle of the cone and φ_x , φ_y the half-opening apex angles of the pyramid.

Example: Laser bar

We can apply the formula of the radiance to a laser bar with the specifications mentioned in chapter VI.2 ($2\varphi_x = 10^\circ$, $2\varphi_y = 70^\circ$, P = 150 W) which results in

$$L = \frac{150 \,\mathrm{W}}{1 \,\mathrm{cm} \times 1 \,\mathrm{\mu m}} \frac{1}{4 \,\mathrm{arcsin}(\sin(5^\circ) \cdot \sin(35^\circ))} = 7.5 \,\frac{\mathrm{MW}}{\mathrm{cm}^2 \,\mathrm{sr}}. \tag{VII.5}$$

However, for a standard laser diode stack, the radiance is typically a bit lower as the homogenization scheme introduces losses. Typical values ranging from 1 to $5\,\mathrm{MW/cm^2sr}$ can be commonly found today. A principal problem arising with the definition of the radiance is that it should be clearly stated how area and angle should be defined with respect to the beam diameter (e.g. FWHM, $1/e^2$) or power content (typically 95%).

VII.1.3. Beam quality factor - M²

Coming to actual laser beams the radiance is a rather uncommon value. For oscillator beams rather the M^2 - value is used instead to describe the beam quality. This value describes the opening angle of a beam in comparison to a TEM_{00} Gaussian beam of the same size:

$$M^2 = \frac{\varphi}{\varphi_{\text{TEM00}}} \tag{VII.6}$$

Here similar problems arise as for the radiance with the definition of beam size and opening angle, as soon as the analyzed beam is no longer a clean Gaussian one (e.g. tophat). In the ISO 11146-1 for that purpose the RMS width of the intensity distribution is used.

some facts:

- \bullet As the TEM_{00} Gaussian has the lowest possible divergence, the M^2 value is always greater than 1
- tophat beams have high M² values

¹We refer to equation 3 of the paper, where the apex angles are given by $\sin(\varphi_x) = a \cdot \sqrt{a^2 + h^2}^{-1}$.

VII.1.4. Wavefront analysis

For most high energy lasers the determination of the beam quality factor M^2 is not sufficient for a description of the spatial profile. Due to thermal load of the pump, mechanical stress in the amplified medium, corresponding birefringence and nonlinear effects, the wavefront of the beam can be deformed. This has to be corrected in order to efficiently focus the beam to high intensities. Therefore, the wavefront analysis is an important tool to characterize the beam, as it helps us to identify the origin of certain beam distortions. This helps to determine the influence of tilted lenses, astigmatism, mirror quality issues or effects of thermal lensing.

Wavefront measurement

The measurement of the wavefront in the visible and near-infrared spectrum is done via the detection of intensity variations using a Shack-Hartmann wavefront sensor. The sensor is made up of a microlens array which is positioned in front of a CCD-sensor as shown in figure VII.1. A plane wavefront impinging on the microlens array is divided by the microlens apertures and generates a spot pattern on the CCD-camera. The centroid-position is then recorded and can be compared to the spot pattern of a distorded wavefront. The shift of the spots compared to the plane wave corresponds directly to the average slope of the wavefront over the lenslet of the microlens array. The information of the wavefront slope can then be used to reconstruct the wavefront of the whole beam profile, where the resolution is given by the pitch of the microlens array.

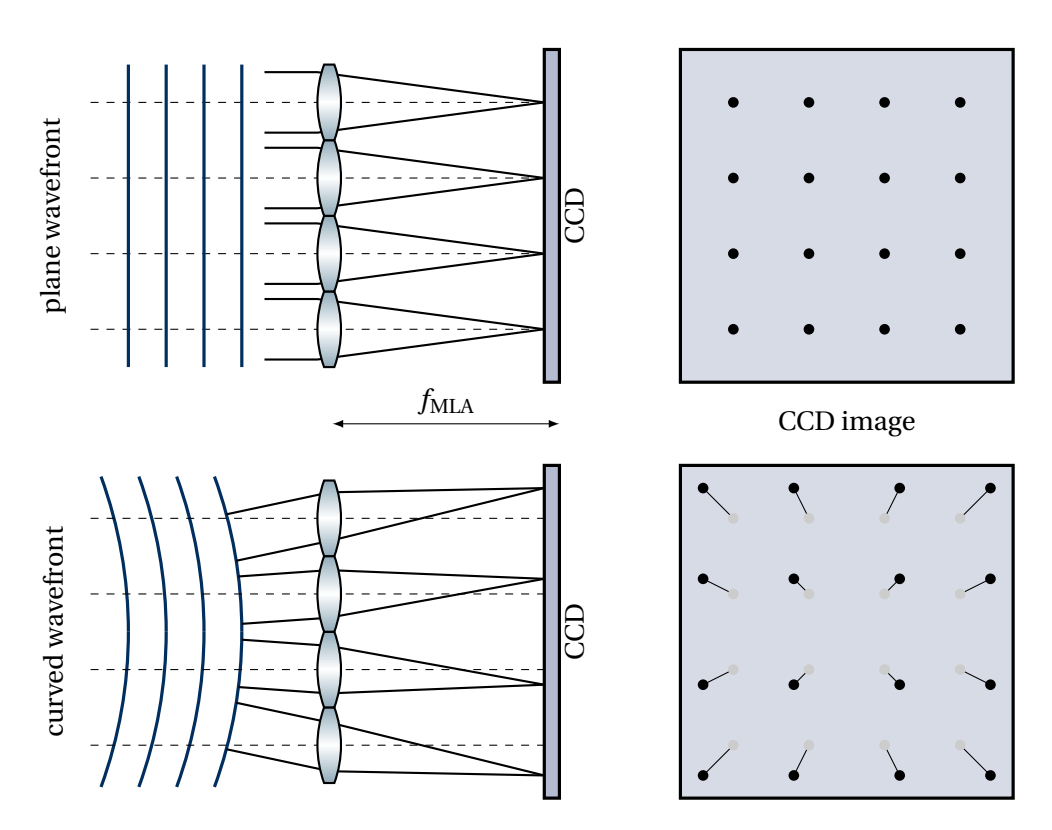


Fig. VII.1.: Setup of a Shack-Hartmann wavefront sensor. On the top, a plane wavefront enters the sensor and a spot pattern is generated as shown on the sketch of the CCD image. On the bottom, a curved wavefront results in a variation of the spot pattern compared to the plane wavefront.

The measured wavefront is finally decomposed into into the orthogonal Zernike polynomials which

are given as

$$Z_n^m(r,\varphi) = R_n^m(r)\cos(m\varphi) \qquad \text{(even)}$$

$$Z_n^m(r,\varphi) = R_n^m(r)\cos(m\varphi) \qquad \text{(even)}$$

$$Z_n^{-m}(r,\varphi) = R_n^m(r)\sin(m\varphi) \qquad \text{(odd)}$$
(VII.8)

$$R_n^m(r,\varphi) = R_n^m(r)\sin(m\varphi) \quad \text{(odd)}$$

$$R_n^m(r) = \sum_{k=0}^{\frac{n-m}{2}} \frac{(-1)^k (n-k)!}{k!(\frac{n+m}{2}-k)!(\frac{n-m}{2}-k)!} r^{n-2k} \quad \text{if} \quad n-m \quad \text{is even.}$$
(VII.9)

non-negative integers with $n \ge m \ge 0$ m, n

azimuthal angle φ

radial distance $0 \le r \le 1$

 R_n^m for n - m odd, the radial polynomial is zero.

The amplitudes of the eigenfunctions tell us, which part of beam distortions dominate the final wavefront profile, as aberrations can be attributed to different Zernike polynomials. The lower order Terms of the Zernike polynomials are shown in figure VII.2. As the polynomials are orthogonal, no cross influence of individual terms is observed.

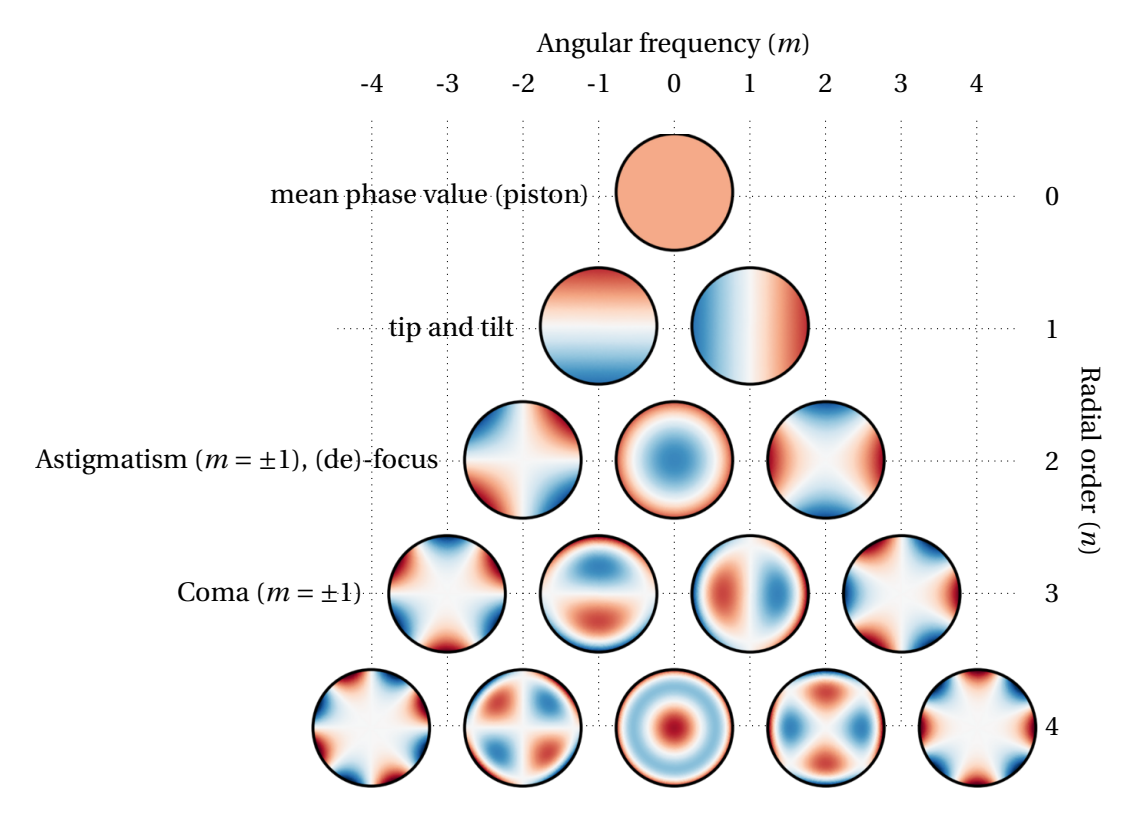


Fig. VII.2.: The first 15 Zernike polynomials, ordered vertically by radial degree and horizontally by azimuthal degree. The different forms of aberrations can be attributed to different Zernike polynomials. Taken and adapted from [Com20].

Wavefront adaptation

After the measurement and characterization, the wavefront can be manipulated using adaptive optics. This is typically a deformable mirror that changes shape by an external control. Some important parameters that characterize a deformable mirror are listed below:

- *Surface type*: A deformable mirror can either be continuous or segmented as shown in figure VII.3. Continuous membrane mirrors are made up of a single surface which can be deformed at several positions using actuators. Segmented mirrors consist of smaller mirror sections which provide individual control.
- *Actuators*: The mirror segments are positioned by tip-tilt actuators. For continuous surface deformable mirrors use actuators under the reflective surface to deform the surface. This can be realized by mechanical actuators, magnets or piezoelectric elements. The number of used actuators relates to the quality of the output profile, the adaptive optics can produce. Typical numbers of actuators range between ten to hundreds.

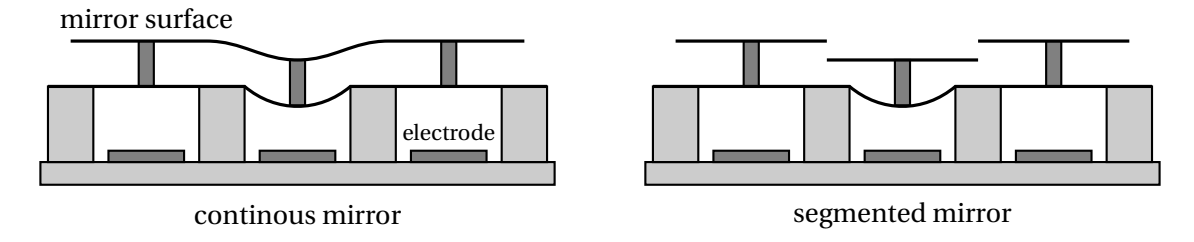


Fig. VII.3.: Different types of deformable mirrors as adaptive optics.

VII.2. Temporal characterization

For high-power laser applications the characterization and optimization of the temporal pulse profile is important. Here, the shape of the main pulse peak is important, as well as the picosecond contrast to the background (amplified stimulated emission, pre-pulses). We will start with a description of the pulse length measurement.

VII.2.1. Pulse length

The temporal length of an ultra short laser pulse is usually accomplished by scanning auto-correlation, which will be discussed in the next section. However, for a low repetition rate system, such a measurement takes a long time and is not ideal for alignment purposes. Thus, a single shot autocorrelator can be used to obtain the pulse length within a single shot.

Here, the pulse enters the measurement device and is split into two parts and recombined under an angle in a frequency-doubling crystal, which leads to Sum Frequency Generation (SFG), if both pulses overlap in time. The sum frequency is captured on a CCD camera and the generated image can be used to determine the pulse length.

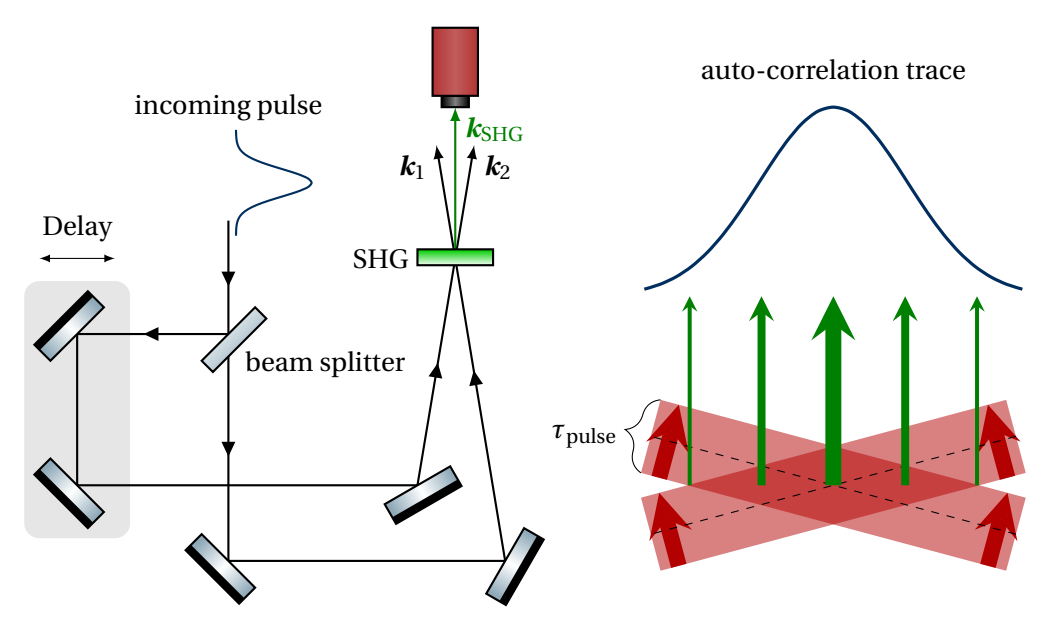


Fig. VII.4.: Setup for a single shot auto-correlation measurement. The incoming pulse is split into two pulses and recombined in a Second Harmonic Generation (SHG) crystal. The right side shows the spatial mapping of the two thin disks of light, spatially overlapping in the SHG crystal. The shorter the pulse length, the thinner the autocorrelation trace will be.

The measured intensity distribution recorded by the CCD camera is described by a convolution of the intensity distribution I(t) of the pulse with itself

$$A^{(2)}(\tau) = \int_{-\infty}^{\infty} I(t) \cdot I(t-\tau) \,\mathrm{d}t. \tag{VII.10}$$

Since we cannot resolve this temporal distribution with a photodiode, the crossing of the beams maps the delay τ between both pulses onto a transverse position which can be recorded by the CCD camera. The width of the recorded second-order autocorrelation trace is not identical to the pulse width. However, the Root Mean Square (RMS) of the autocorrelation trace can be related to the RMS pulse width

$$\tau_{\text{pulse}} = \frac{1}{\sqrt{2}} \tau_{\text{AC}}.$$
 (VII.11)

Therefore, knowledge of the temporal pulse shape is not needed to measure the pulse length. However, the intensity auto-correlation is not sufficient for a full characterization of the pulse shape, as the generated signal is symmetric $A(\tau) = A(-\tau)$, thus different pulse shapes can yield identical auto-correlation traces.

VII.2.2. Pulse contrast

The issue of a second order autocorrelation measurement is the resulting symmetry in the determined pulse shape which leaves ambiguity when we want to determine the actual pulse shape. We can break the symmetry of autocorrelation by using a third-order nonlinear process. There are several methods of measuring the third-order autocorrelation trace using polarization gating or self-diffraction in a nonlinear medium [Tre12, p.77], but it can be also achieved by combining a SHG-crystal with a third-order nonlinear medium as shown in VII.5.

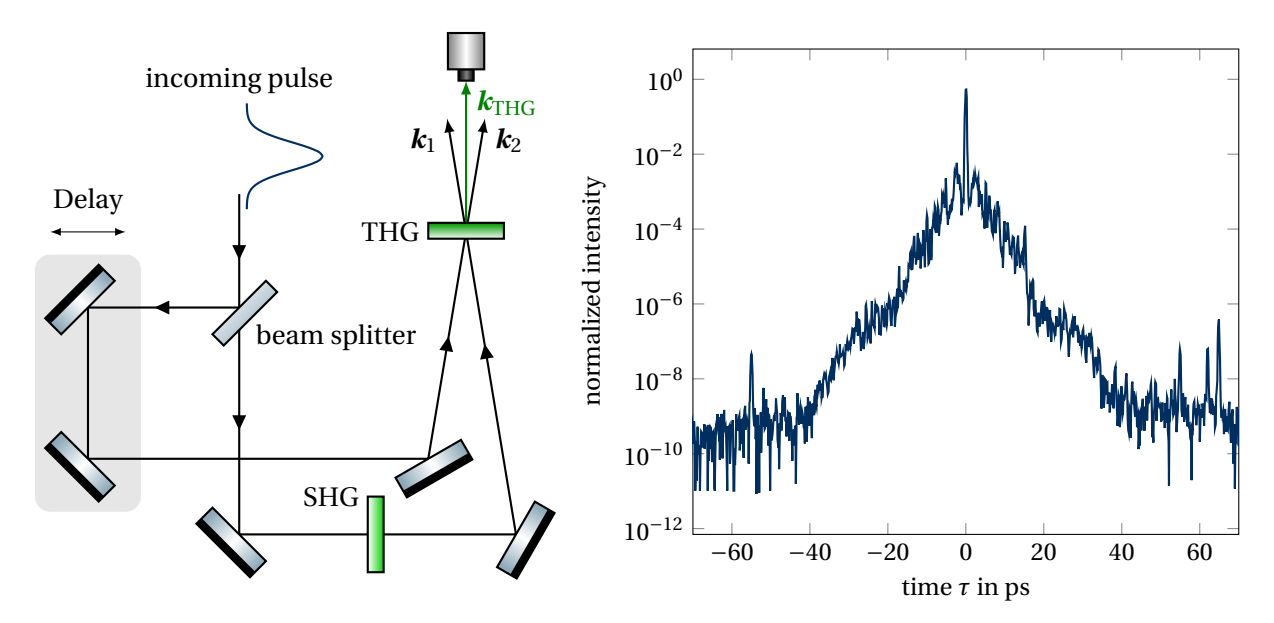


Fig. VII.5.: Left: Setup for a third-order scanning auto-correlation measurement. The incoming pulse is split into two pulses, one arm is converted to the SH and both are recombined in a Third Harmonic Generation (THG) crystal. The previously used camera is replaced by a photomultiplier. For a measurement, the pulse delay is scanned and the generated THG intensity is recorded for each step. Right: Exemplary contrast measurement of a mJ pulse at the POLARIS laser system recorded with a Sequoia third-order autocorrelator.

In order to measure the pulse contrast over a large range, a single-shot measurement via spatial mapping is not feasible. Therefore, instead of a camera, a photo multiplier is installed to measure the generated third harmonic intensity. Then, the delay τ can is changed and the measurement repeated with another pulse. This generates the third order autocorrelation signal

$$A^{(3)}(\tau) = \int_{-\infty}^{\infty} I^{2}(t) \cdot I(t - \tau) \, \mathrm{d}t,$$
 (VII.12)

which can be evaluated to obtain the temporal contrast profile of the laser pulse as shown in figure VII.5 (right). As the measurement requires a scanning of the pulse delay τ , several thousand of pulses are needed to obtain the measurement. This restricts the application to stable laser conditions, where the pulse shape is reproducable. Furthermore, third-order nonlinearities are weaker than second-order ones, hence they require a higher initial pulse energy (> 1 mJ).

VII.3. Spectral characterization

For a precise control of the temporal pulse shape, its spectral components have to be characterized first. A FT of the temporal electric field E(t) yields a complex quantity $\tilde{E}(\omega)$ which can be separated into its spectral *intensity* $S(\omega)$ and *phase* $\varphi(\omega)$

$$\tilde{E}(\omega) = \sqrt{S(\omega)} \exp(-i\varphi(\omega)).$$
 (VII.13)

We will discuss in the following two sections how two measure these two quantities in order to obtain a full description of the pulse.

VII.3.1. Spectral intensity

Performing a measurement of the intensity of a laser pulse is straightforward, as we only need a photo-sensitive detector like a photodiode or a Charge-Coupled Device (CCD). Now, in order to spectrally resolve the intensity, we need to spatially separate the wavelengths by utilizing dispersion and assigning different positions of the detector to a certain wavelength range. The separation is typically done via gratings or prisms. In the following, we want to discuss the working principle of a prism and grating spectrometer.

Prism spectrometer

In a spectrometer the entrance aperture of the apparatus is usually imaged onto the CCD chip via two lenses/curved mirrors. The dispersive element is then placed in between those two imaging elements as shown in figure VII.6.

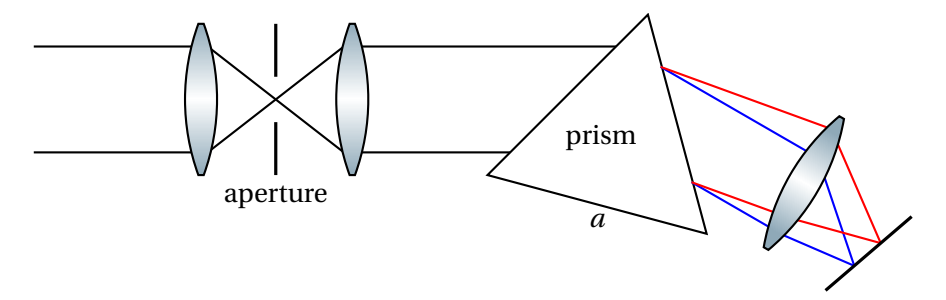


Fig. VII.6.: Sketch of a prism spectrometer. The aperture represents the input hole of the apparatus, which is imaged onto the CCD-chip using two lenses. The prism is then positioned in the minimum deviation angle position, i.e. the position, where the input and output angle of the central wavelength are equal with respect to the prism base of length *a*.

The resolution of such a spectrometer can be determined using the refractive index dispersion as a function of wavelength

Equation: Resolution of a prism spectrometer
$$\frac{\lambda}{\mathrm{d}\lambda} = a \cdot \left| \frac{\mathrm{d}n}{\mathrm{d}\lambda} \right|, \tag{VII.14}$$

where a is the prism base length. The larger the frequency dispersion of the refractive index n is, the larger is the resolution of the spectrometer.

Grating spectrometer

The grating spectrometer has a similar working principle. Instead of refraction at the interfaces, the wavelengths are separated via diffraction. In contrast to prism spectrometers, zero-order and higher order diffraction can occur, which limits the sensitivity and spectral range of these spectrometers. The resolution of this spectrometer can be determined by counting the number of illuminated grating

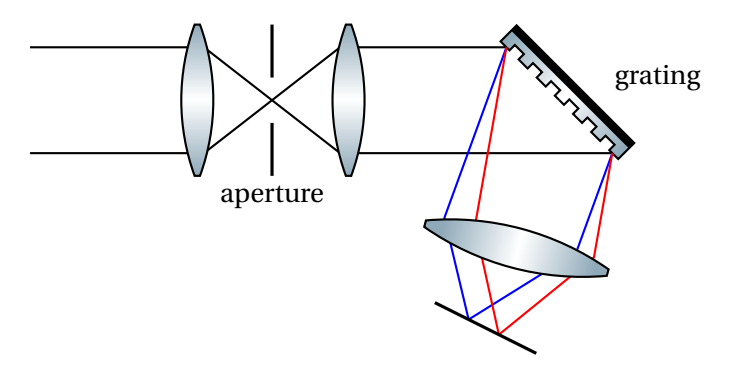


Fig. VII.7.: Sketch of a Grating spectrometer. As before, the input aperture is imaged onto the CCD-chip using two lenses.

lines N and multiplying that with the diffraction order

Equation: Resolution of a grating spectrometer
$$\frac{\lambda}{\mathrm{d}\lambda} = m \cdot N. \tag{VII.15}$$

As the efficiency of the diffraction is wavelength dependent, the spectrometer has to be intensity calibrated using a well characterized broadband light source.

Finally, we want to compare both types of spectrometers as shown in table VII.1. We want to note that these days, grating spectrometers are used more commonly for the detection of visible and near-infrared laser radiation. This is due to the fact that the resolution of the spectrometer scales with the size of the optical element and gratings are cheaper than prisms of similar size.

Grating spectrometer Prism spectrometer in most cases higher resolution lower resolution limited free spectral range due to the overfree spectral range only limited by the lap of high order diffraction. However, the prism material and its absorption bands spectral range can be increased by adding color filters polarization sensitive polarization insensitive wavelength dependent diffraction effihigher output intensity as there is only one ciency lower damage threshhold (issue for pulsed lasers)

Table VII.1.: Comparison of the grating and prism spectrometer

VII.3.2. Spectral phase

The information how a medium affects the laser pulse can be found in the refractive index $n(\omega)$ and the wave vector $\mathbf{k}(\omega)$. The pulse accumulates phase according to $\varphi(\omega) = k(\omega) \cdot L$ in a medium of length L. Therefore, the dispersion effects are contained in the spectral phase. Since the phase cannot be extracted directly from the intensity spectrum $S(\omega)$, an interference method can be utilized. The spectral components of two time-shifted pulses can interfere with each other, whereby the spectral phase is imprinted on the intensity spectrum. The interference occurs as fringes in the spectrum, which is shown schematically in figure VII.8. Analyzing the spectral fringes can be used for a determination of the delay t_0 and the spectral phase.

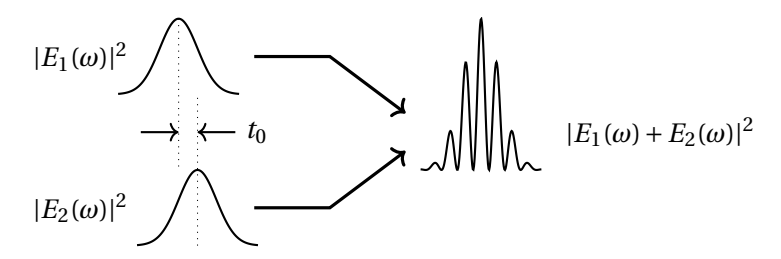


Fig. VII.8.: Sketch of spectral interference between two laser pulses with a GAUSSIAN spectrum, one of which is delayed by t_0 . Taken from [Bey20].

Spectral interferometry

The method of Spectral Interferometry (SI) is mainly used to obtain the spectral phase difference of two gaussian pulses. In this method, two single pulses $E_1(t)$ and $E_2(t)$ interfere to form an interference pattern, which can be described mathematically as a superposition of two single pulses. Since the fourier transform is linear, the spectrum $\tilde{S}(\omega)^2$ can be written as

$$\tilde{S}(\omega) = |E_1(\omega) + E_2(\omega)|^2$$

$$= |\sqrt{S_1(\omega)} e^{-i\varphi_1(\omega)} + \sqrt{S_2(\omega)} e^{-i\varphi_2(\omega)}|^2$$

$$= S_1(\omega) + S_2(\omega) + 2\sqrt{S_1(\omega)S_2(\omega)} \cdot \cos(\varphi_1(\omega) - \varphi_2(\omega)). \tag{VII.16}$$

It is assumed that the spectral intensity of both pulses is the same $S_1(\omega) = S_2(\omega) = S(\omega)$. By introducing a delay t_0 and using the Fourier transform shift theorem a time delayed pulse $E(t-t_0)$ transforms to $E(\omega) \exp(-i\omega t_0)$. The delay can be separated from the phase $\varphi_1(\omega)$ and therefore the spectrum can be written as

$$\tilde{S}(\omega) \stackrel{\text{(VII.16)}}{=} 2 S(\omega) \left[1 + \cos\left(\Delta\varphi(\omega) + \omega t_0\right)\right] \quad \text{with} \quad S(\omega) = \exp\left(-\frac{\omega^2 \tau^2}{2}\right)$$
 (VII.17)

where $\Delta \varphi(\omega) = \varphi_1(\omega) - \varphi_2(\omega)$ is the phase difference of the two GAUSSIAN pulses. The cosine indicates that depending on the delay t_0 of the pulses, a periodic change in the amplitude can be observed. These spectral fringes are the key for SI. The fringe distance is inversely proportional to the delay t_0 . An example of an interference spectrum is depicted in figure VII.9.

The key to characterize dispersion effects of the medium is the spectral phase, but only the intensity spectrum can be measured by a spectrometer. However, the interference spectrum can be used to retrieve the spectral phase difference $\Delta \varphi(\omega)$ by performing an inverse FT on (VII.17) into a pseudo time domain (without temporal phase information)

$$\mathscr{F}^{-1}[\tilde{S}(\omega)](t) = \frac{1}{\tau} \left(2e^{-\frac{t^2}{2\tau^2}} + e^{-\frac{(t-t_0)^2}{2\tau^2}} e^{-i\Delta\varphi} + e^{-\frac{(t+t_0)^2}{2\tau^2}} e^{i\Delta\varphi} \right)$$
(VII.18)

²The frequency ω describes the shift $\omega = \omega' - \omega_0$ to the central frequency ω_0 .

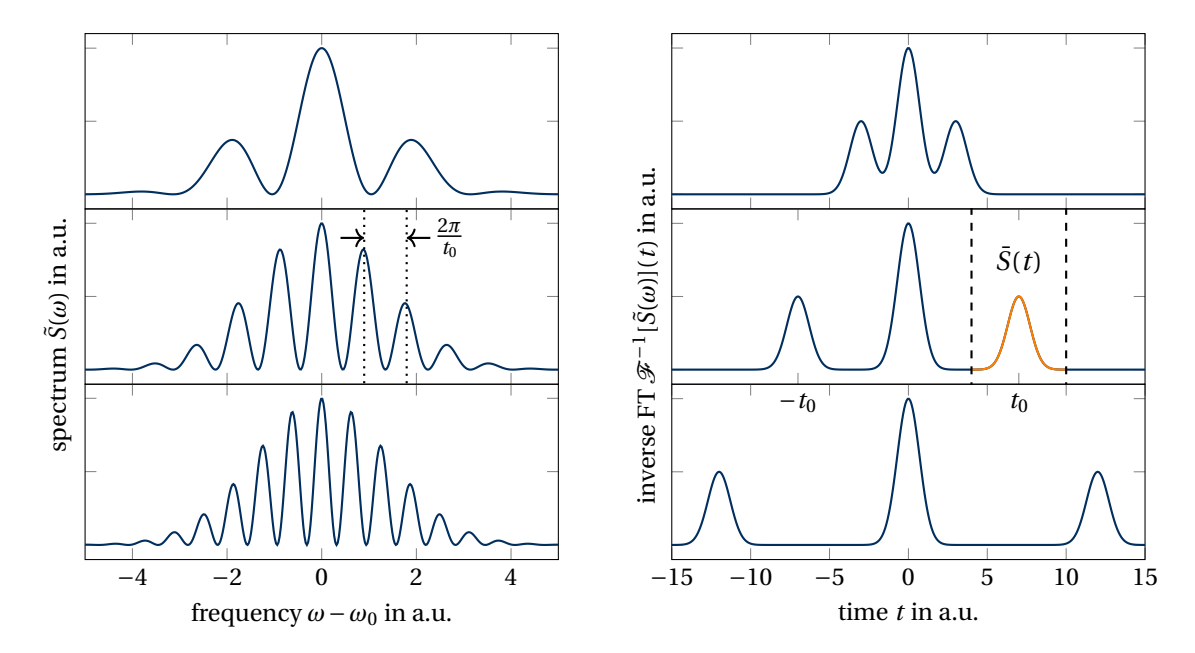


Fig. VII.9.: The left side shows the simulated spectrum of two interfering GAUSSIAN pulses for different delays t_0 . On the right the absolute value of the Fourier transform of the spectrum is depicted. Taken from [Bey20].

which is also depicted in figure VII.9. The fourier transform describes which frequencies lead to the course of the measured spectrum. The spectrum contains a central peak which describes the underlying Gaussian of the frequency spectrum and contains no phase information. The shifted side peaks are symmetrical and contain the spectral phase according to (VII.18). The phase can be extracted by isolating the side peak and performing a fourier transform of the chosen part of the spectrum. The phase $\Delta \varphi(\omega)$ contains the information of the Group Delay Dispersion (GDD) (second order dispersion) and higher order dispersions (TOD, FOD), which can be extracted via phase differentiation.

An experimental setup for performing spectral interferometry is shown in figure VII. 10 with a Michelson interferometric setup.

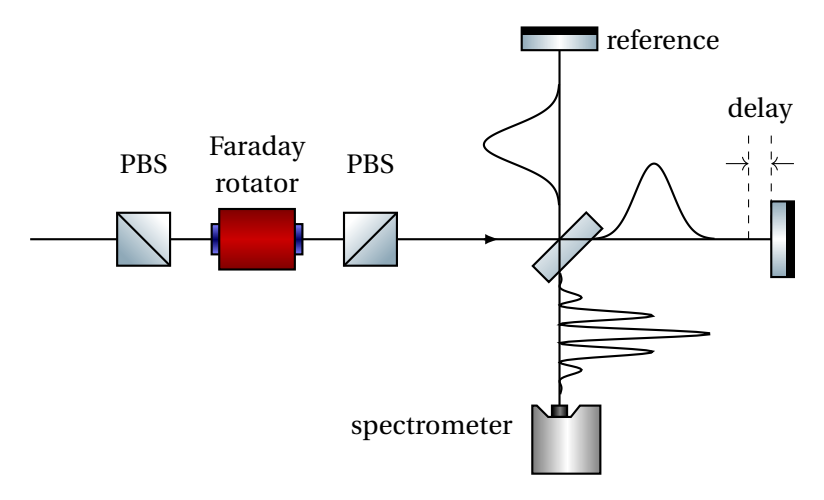


Fig. VII.10.: A Michelson interferometer is used to create a second pulse, which interferes with the first pulse leading to fringes in the spectral domain due to the delay between the two pulses.

A. Appendix - Frantz-Nodvik calculations

In this section we want to further discuss the Frantz-Nodvik solution of the system of rate equation we found for the amplification process. First, we derive the solution and then we proof that the solution is additive, i. e. the results are the same, whether we amplify a long pulse or several shorter pulses. This is particularly helpful to simulate the spectral amplification of a laser amplifier, by chopping a single pulse into many smaller pulses of different wavelength.

A.1. Derivation of the solution

We start with the rate equations (III.40) and (III.41)

$$\frac{\partial \Phi}{\partial z} = -\alpha \Phi \left(1 - \frac{\beta}{\beta_{eq}} \right) \quad \text{with} \quad \alpha = \sigma_a \cdot N_{\text{dop}}$$
 (A.1)

$$\Rightarrow \frac{\partial \beta}{\partial t} = \sigma_c \beta_{eq} \Phi \left(1 - \frac{\beta}{\beta_{eq}} \right) \quad \text{with} \quad \sigma_c = c \cdot (\sigma_a + \sigma_e). \tag{A.2}$$

First, we want to find the solution of the photon density $\Phi(z, t)$. For this, we need to eliminiate β from the equation system by solving (A.1) for $\beta(z, t)$

$$\left(1 - \frac{\beta}{\beta_{\text{eq}}}\right) = -\frac{1}{\alpha} \frac{1}{\Phi} \frac{\partial \Phi}{\partial z}
\Rightarrow \beta(z, t) = \beta_{\text{eq}} \left(1 + \frac{1}{\alpha} \frac{1}{\Phi} \frac{\partial \Phi}{\partial z}\right) = \beta_{\text{eq}} \left(1 + \frac{1}{\alpha} \frac{\partial}{\partial z} \ln \Phi\right)$$
(A.3)

and inserting the solution into (A.2)

$$\beta_{\text{eq}} \frac{\partial}{\partial t} \left(1 + \frac{1}{\alpha} \frac{\partial}{\partial z} \ln \Phi \right) = \sigma_c \beta_{\text{eq}} \Phi \left(1 - 1 - \frac{1}{\alpha} \frac{1}{\Delta} \frac{\partial \Phi}{\partial z} \right) \qquad \left| \cdot \frac{\alpha}{\beta_{\text{eq}}} \right|$$

$$\frac{\partial}{\partial t} \left(\frac{\partial}{\partial z} \ln \Phi \right) = -\sigma_c \frac{\partial}{\partial z} \Phi$$

$$\Rightarrow \frac{\partial}{\partial z} \left(\frac{\partial}{\partial t} \ln \Phi + \sigma_c \Phi \right) = 0. \tag{A.4}$$

$$:= f_1(t)$$

Here, we found a space invariant function $f_1(t)$ which we can use to solve for $\Phi(z,t)$. We take the derivative $\frac{\partial}{\partial t} \ln \Phi = \frac{1}{\Phi} \frac{\partial \Phi}{\partial t}$, divide the equation by Φ and find a differential equation for the inverse Φ^{-1}

$$\frac{1}{\Phi^{2}} \frac{\partial}{\partial t} \Phi + \sigma_{c} = \frac{1}{\Phi} \cdot f_{1}(t), \quad \text{with} \quad \frac{\partial}{\partial t} \Phi^{-1} = -\frac{1}{\Phi^{2}} \frac{\partial}{\partial t} \Phi \quad \text{follows}$$

$$\Rightarrow \quad -\frac{\partial}{\partial t} \Phi^{-1} + \sigma_{c} = \Phi^{-1} \cdot f_{1}(t)$$

$$\Rightarrow \quad \sigma_{c} = \frac{\partial}{\partial t} \Phi^{-1} + \Phi^{-1} \cdot f_{1}(t).$$
(A.5)

This is a first order linear, inhomogeneous differential equation. We start by solving the homogeneous part ($\sigma_c = 0$) by separation of variables

$$\Phi^{-1} = A(z)e^{-F_1(t)}$$
 with $F_1 = \int f_1(t) dt$. (A.6)

We proceed to solve the inhomogeneous part by inserting (A.6) into (A.5) with the ansatz A = A(z, t) (variation of constants) which yields

$$\sigma_c = \frac{\partial A}{\partial t} e^{-F_1(t)} - f_1(t) A(z, t) e^{-F_1(t)} + f_1(t) A(z, t) e^{-F_1(t)}$$
(A.7)

$$\Rightarrow A(z,t) = \int \sigma_c e^{F_1(t)} dt + f_2(z). \tag{A.8}$$

The function $f_2(z)$ is a possibly space dependent integration constant. Now we split off the time dependence of A(z,t) using a help function S(t) which is defined as

$$S(t) = \sigma_c \int e^{F_1(t)} dt + f_2(0) \quad \Rightarrow \quad \frac{dS}{dt} = \sigma e^{F_1(t)}. \tag{A.9}$$

Using this help function, we can find a compact expression for the solution $\Phi(z,t)$

$$\Phi(z,t) = \frac{e^{F_1(t)}}{A(z,t)} = \frac{\frac{1}{\sigma_c} \frac{dS}{dt}}{S(t) + f_2(z) - f_2(0)} = \frac{1}{\sigma_c} \frac{\partial}{\partial t} \ln(S(t) + f_2(z) - f_2(0)). \tag{A.10}$$

In the second step, we used again the chain rule to rewrite the time derivative. For a proper solution we have to include boundary conditions to determine the function S(t). We assume that before the interaction, the photon density is given as $\Phi_0(t) = \Phi(z=0,t)$, (z=0) denotes in this context that the input pulse has not entered the medium yet). Then we find

$$\Phi_0 = \frac{1}{\sigma_c} \frac{\partial}{\partial t} \ln(S(t)) \quad \Rightarrow \quad S(t) = \exp\left(\sigma_c \int_0^t \Phi_0(t') \, \mathrm{d}t'\right). \tag{A.11}$$

Using the explicit expression of S(t) we can insert it into the first part of equation (A.10), which yields

$$\Phi(z,t) = \frac{\Phi_0(t) \cdot S(t)}{S(t) + \tilde{f}_2(z)} \quad \text{with} \quad \tilde{f}_2(z) = f_2(z) - f_2(0). \tag{A.12}$$

We now proceed to insert our solution into the explicite equation of $\beta(z,t)$ (A.3) in order to find an expression for $\tilde{f}_2(z)$

$$\beta(z,t) = \beta_{\text{eq}} \left(1 + \frac{1}{\alpha} \frac{1}{\Phi} \frac{\partial}{\partial z} \Phi \right) = \beta_{\text{eq}} \left(1 - \frac{1}{\alpha} \frac{\widetilde{S(t)} + \widetilde{f}_2(z)}{\Phi_{\Phi}(t) - \widetilde{S(t)}} \frac{\Phi_{\Phi}(t) - \widetilde{S(t)}}{[S(t) + \widetilde{f}_2(z)]^2} \cdot \frac{\mathrm{d}\widetilde{f}_2}{\mathrm{d}z} \right)$$

$$= \beta_{\text{eq}} \left(1 - \frac{1}{\alpha} \frac{1}{S(t) + \widetilde{f}_2(z)} \frac{\mathrm{d}\widetilde{f}_2}{\mathrm{d}z} \right) = \beta_{\text{eq}} \left(1 - \frac{1}{\alpha} \frac{\partial}{\partial z} \ln[S(t) + \widetilde{f}_2(z)] \right). \tag{A.13}$$

Again, we can introduce boundary conditions with $\beta(z, t = 0) = \beta_0$ and S(t = 0) = 1

$$\beta_0(z) = \beta_{\text{eq}} \left(1 - \frac{1}{\alpha} \frac{\partial}{\partial z} \ln(1 + \tilde{f}_2(z)) \right). \tag{A.14}$$

We can now solve this equation for $\tilde{f}_2(z)$

$$\frac{1}{\alpha} \frac{\partial}{\partial z} \ln(1 + \tilde{f}_2(z)) = 1 - \frac{\beta_0(z)}{\beta_{eq}} \quad \Big| \quad \int_0^z \dots dz'$$

$$\Rightarrow \quad \tilde{f}_2(z) = \exp\left(\alpha \int_0^z \left(1 - \frac{\beta_0(z')}{\beta_{eq}}\right) dz'\right) - 1. \tag{A.15}$$

We have now introduced the *z*-dependent gain G(z) in the laser medium. Before we can summarize our solutions, we have to find an expression for the derivative $\frac{d\tilde{f}_2}{dz}$

$$\frac{\mathrm{d}\tilde{f}_2}{\mathrm{d}z} = \frac{1}{G^2(z)} \cdot \left(1 - \frac{\beta_0}{\beta_{\mathrm{eq}}}\right) \alpha \cdot G(z) = \left(1 - \frac{\beta_0}{\beta_{\mathrm{eq}}}\right) \frac{\alpha}{G(z)}.$$
 (A.16)

Finally, we can write down the solution by substituting $\tilde{f}_2(z)$ with G(z)

Equation: Frantz-Nodvik solution

$$\Phi(z,t) \stackrel{\text{(A.12)}}{=} \Phi_0(t) \frac{\Phi_0(t) \cdot S(t)}{S(t) + \frac{1}{G(z)} - 1} = \frac{S(t) \cdot G(z)}{1 + [S(t) - 1]G(z)}$$
(A.17)

$$\beta(z,t) \stackrel{\text{(A.13)}}{=} \beta_{\text{eq}} - \frac{\beta_{\text{eq}}}{\alpha} \frac{\left(1 - \frac{\beta_0}{\beta_{\text{eq}}}\right) \frac{\alpha}{G(z)}}{S(t) + \frac{1}{G(z)} - 1} = \beta_{\text{eq}} + \frac{\beta_0(z) - \beta_{\text{eq}}}{1 + [S(t) - 1]G(z)}. \tag{A.18}$$

A.2. Additivity of the solution

In this section we will show that the solution can be also applied by chopping the original pulse into several parts and amplifying them separately. Consider a temporal profile $\Phi_0(t) \in (0, T)$ given as

$$\Phi_0(t) = \Phi_{0,a}(t) + \Phi_{0,b}(t) = \begin{cases} \Phi_{0,a}(t) & t \in (0, t_1) \\ \Phi_{0,b}(t) & t \in (t_1, T). \end{cases}$$
(A.19)

Now we have to show that the amplified pulse $\Phi(t)$ is given by

$$\Phi(t) = \Phi_0(t) \cdot \frac{G_0 \cdot S(t)}{G_0(S(t) - 1) + 1} \stackrel{!}{=} \Phi_a(t) + \Phi_b(t), \tag{A.20}$$

where $\Phi_a(t)$ and $\Phi_b(t)$ are the amplified parts of $\Phi_{0,a}(t)$ and $\Phi_{0,b}(t)$. For the first time interval $t \in (0, t_1)$, the saturation $S_a(t)$ is given by

$$S_a(t) = \exp\left(\sigma c \int_0^{t_1} \Phi_{a,0}(t) \, \mathrm{d}t\right) = \exp\left(\sigma c \int_0^{t_1} \Phi_0(t) \, \mathrm{d}t\right) = S(t). \tag{A.21}$$

Then, the expression for $\Phi_a(t)$ is simply given by

$$\Phi_a(t) = \Phi_{0,a}(t) \frac{G_0 \cdot S(t)}{G_0(S(t) - 1) + 1} \quad \text{for} \quad t \in (0, t_1).$$
(A.22)

Now we have to calculate the amplification of the second pulse $S_{0,b}(t)$, which is more complicated, as the inversion and gain are already changed by $\Phi_a(t)$. The new inversion is given by

$$\beta_1(z) = \beta_{\text{eq}} + \frac{\beta_0(z) - \beta_{\text{eq}}}{1 + [S(t_1) - 1]G_0(z)}.$$
(A.23)

Then, the corrected gain (at the end of the medium of length d) can be calculated analogously to

section III.3.5 by

$$G_{1}(d) = \exp\left[N_{\text{dop}}\sigma \int_{0}^{d} \left(\beta_{\text{eq}} + \frac{\beta_{0}(z) - \beta_{\text{eq}}}{1 + [S_{a}(t) - 1]G(z)}\right) - \beta_{\text{eq}} dz\right]$$

$$= \exp\left[N_{\text{dop}}\sigma \int_{0}^{d} \frac{\beta_{0}(z) - \beta_{\text{eq}}}{1 + [S_{a}(t) - 1] \exp\left(\int_{0}^{z} (\beta_{0}(z') - \beta_{\text{eq}}) dz'\right)} dz\right]$$

$$= \exp\left[a \int_{0}^{d} \frac{f(z)}{1 + b \cdot \exp(a \cdot F(z))} dz\right] \quad \text{with} \quad f(z) = \beta_{0}(z) - \beta_{\text{eq}}, a = N_{\text{dop}}\sigma, b = S_{a}(t) - 1. \quad (A.24)$$

This integral is analytically solvable (notice that f(z) is the derivative of F(z)) and the solution is given by

$$G_1(d) = \exp\left[-\ln\left(1 + \frac{1}{b}\exp(-a \cdot F(z))\right)\Big|_0^d\right] = \frac{G_0 S_a(t)}{1 + G_0[S_a(t) - 1]}.$$
(A.25)

Now, the amplified pulse $\Phi_b(t)$ can be calculated by

$$\begin{split} \Phi_{b}(t) &= \Phi_{0,b}(t) \cdot \frac{G_{1}(d) \cdot S_{b}(t)}{G_{1}(d)(S_{b}(t) - 1) + 1} \\ &\stackrel{(A.25)}{=} \Phi_{0,b}(t) \cdot \frac{1}{1 + G_{0}[S_{a}(t) - 1]} \frac{G_{0}S_{a}(t)S_{b}(t)}{\frac{G_{0}S_{a}(t)}{1 + G_{0}[S_{a}(t) - 1]}(S_{b}(t) - 1) + 1} \\ &= \Phi_{0,b}(t) \cdot \frac{G_{0}S_{a}(t)S_{b}(t)}{G_{0}S_{a}(t)(S_{b}(t) - 1) + 1 + G_{0}[S_{a}(t) - 1]} \\ &= \Phi_{0,b}(t) \cdot \frac{G_{0}S_{a}(t)S_{b}(t)}{G_{0}(S_{a}(t)S_{b}(t) - 1) + 1}. \end{split} \tag{A.26}$$

In the last step we have to analyze the product $S_a(t)S_b(t)$

$$S_{a}(t) \cdot S_{b}(t) = \exp\left(\sigma c \int_{0}^{t_{1}} \Phi_{a,0}(t) dt\right) \exp\left(\sigma c \int_{t_{1}}^{T} \Phi_{b,0}(t) dt\right)$$

$$= \exp\left(\sigma c \int_{0}^{T} (\Phi_{a,0}(t) + \Phi_{b,0}) dt\right) = \exp\left(\sigma c \int_{0}^{T} \Phi_{0}(t) dt\right) = S(t). \tag{A.27}$$

Now we can combine equations (A.26) and (A.22)

$$\Phi_a(t) + \Phi_b(t) = (\Phi_{0,a}(t) + \Phi_{0,b}(t)) \frac{G_0 \cdot S(t)}{G_0(S(t) - 1) + 1} = \Phi(t). \tag{A.28}$$

List of abbreviations

AOM Acousto Optical Modulator

ASE Amplified Spontaneous Emission

BPP Beam Parameter Product

CCD Charge-Coupled Device

CPA Chirped Pulse Amplification

CW Continuous Wave

FA Fast Axis

FL Füchtbauer-Ladenburg

FT Fourier Transform

FTL Fourier Transform Limit

FWHM Full Width at Half Maximum

GDD Group Delay Dispersion

GO Gaussian Order

GRM Graded Reflectivity Mirror

GVD Group Velocity Dispersion

HECDPSSL High Energy Class Diode Pumped Solid State Laser

LED Light Emitting Diode

LIDT Laser Induced Damage Threshold

LD Laser Diode

MC McCumber

MLA Micro Lens Array

OPD Optical Path Difference

RMS Root Mean Square

SA Slow Axis

SFG Sum Frequency Generation

SHG Second Harmonic Generation

SESAM SEmiconductor Saturable Absorber Mirror

A. Appendix - Frantz-Nodvik calculations

SI Spectral Interferometry

TEM Transverse Electro-Magnetic

TFP Thin Film Polarizer

THG Third Harmonic Generation

YAG Yttrium Aluminium Garnet

WLC White Light Continuum

ZPL Zero Phonon Line

Definition of symbols

A area

 $A(\tau)$ autocorrelation signal

 A_{21} Einstein coefficient of spontaneous emission

 B_{12}, B_{21} Einstein coefficients of absorption and stimulated emission

b image distance

 C_p specific heat capacity

 c, c_0 speed of light (in vacuum)

d thickness of the laser material

 d_1, d_2 degeneracies of the upper and lower manifold

 E_i, E_i sub level energy

 E_{ZPL} Energy at the zero phonon line

 $F_{\rm sat}$ saturation fluence

 $F, F_{\text{pump}}, F_{\text{eq}}$ fluence

f focal length g gain factor

g object distance

 g_1, g_2 resonator parameters

 g_L, g_G line shape of a Lorentz and Gaussian distribution

G(z), $G_0(z)$ gain, small signal gain

 $\mathcal{G}(z)$ total gain

H heat transfer coefficient

h Planck constantI intensity, current

 I, I_l, I_p intensity/power density of a laser beam

 $I_{
m sat}$ saturation intensity K_c thermal conductivity $k_{
m B}$ Boltzmann constant

k wave number

L resonator cavity length
L radiance (brightness)

M ABCD-matrix

 M^2 beam quality factor

 N_1, N_2 number density of ions in the lower (1) and upper (2) manifold

A. Appendix - Frantz-Nodvik calculations

 $N_{
m dop}$ doping concentration of the laser-active ion in the host medium

 \mathcal{N} total number of ions in a given volume

n refractive index

 n_2 nonlinear refractive index

 n_e electron density

 P, P_f, P_{ASE} power

P Pitch of a micro-lens array

p pressureQ quality factorq q-parameter

 q_{QD} quantum defect: energy difference between pump and laser wavelength

R(t,z) pump rate

 R, R_1, R_2 radius of curvature of resonator mirrors

 R_0 , R_{GRM} reflectivity

S(*t*) Saturation (c. f. Frantz-Nodvik)

 $S(\omega)$ spectral intensity

T temperature

 t_r cavity round-trip time

t time U voltage V volume

w beam radius of a Gaussian beam

 Z_u, Z_l partition functio of upper (u) and lower (l) manifold

 Z_n^m Zernike polynomials

 z_r Rayleigh length

 α absorption coefficient

 α_T coefficient of thermal expansion

 β inversion, given as the ratio $N_2/N_{\rm dop}$

 $eta_{
m eq}$ equilibrium inversion

 δ resonator roundtrip losses

 ε_0 dielectric permittivity of vacuum

 ζ Gouy phase $\eta_{
m QD}$ heat fraction

 θ beam opening angle

 λ_p, λ_l pump and laser wavelength v_p, v_l pump and laser frequency

v Poisson's ratio ρ material density

 $\rho(v)$ spectral energy density

 σ_{ij} cross section of a single cross section

 σ_a absorption cross section σ_e emission cross section

 σ_c $c(\sigma_a + \sigma_e)$ au pulse duration

 au_f fluorescence life time au_{rad} radiative life time au_p pump duration Φ photon density

 $\chi^{(3)}$ third order nonlinear coefficient

 Ω solid angle

 $\Delta\Omega$ acceptance solid angle ω angular frequency

Bibliography

Books

- [Boy07] Robert W Boyd. *Nonlinear optics*. Academic press, 2007.
- [Bro13] I.N. Bronštejn. *Taschenbuch der Mathematik*. Edition Harri Deutsch. H. Deutsch, 2013. ISBN: 9783808556719.
- [EE10] Hans Joachim Eichler and Jürgen Eichler. *Laser: Bauformen, Strahlführung, Anwendungen.* Springer-Verlag, 2010.
- [Koe06] W. Koechner. *Solid-State Laser Engineering*. Springer Series in Optical Sciences. Springer, 2006. ISBN: 9780387290942.
- [Kör14] Jörg Körner. Effizienzsteigerung Yb^{3+} -basierter Kurzpuls-Laserverstärker. Göttingen: Sierke Verlag, 2014.
- [Sie86] Anthony E Siegman. Lasers. University science books, 1986.
- [ST19] Bahaa EA Saleh and Malvin Carl Teich. *Fundamentals of photonics*. john Wiley & sons, 2019.
- [Trä12] Frank Träger. Springer Handbook of Lasers and Optics. Berlin, Heidelberg: Springer Verlag, 2012.
- [Tre12] Rick Trebino. *Frequency-resolved optical gating: the measurement of ultrashort laser pulses.* Springer Science & Business Media, 2012.

Articles

- [Aza+24] Yasmina Azamoum et al. "Optical probing of ultrafast laser-induced solid-to-overdense-plasma transitions". In: *Light: Science & amp; Applications* 13.1 (May 2024). ISSN: 2047-7538. DOI: 10.1038/s41377-024-01444-y.
- [BH16] R. Betti and O. A. Hurricane. "Inertial-confinement fusion with lasers". In: *Nature Physics* 12.5 (May 2016), pp. 435–448. ISSN: 1745-2481. DOI: 10.1038/nphys3736.
- [Bul+02] SV Bulanov et al. "Oncological hadrontherapy with laser ion accelerators". In: *Physics Letters A* 299.2-3 (2002), pp. 240–247. DOI: 10.1016/S0375-9601(02)00521-2.
- [Ché+06] Sébastien Chénais et al. "On thermal effects in solid-state lasers: The case of ytterbium-doped materials". In: *Progress in quantum electronics* 30.4 (2006), pp. 89–153. DOI: 10. 1016/j.pquantelec.2006.12.001.
- [CRD03] CWo Carr, HB Radousky, and SG Demos. "Wavelength Dependence of Laser-Induced Damage: Determining the Damage Initiation Mechanisms". In: *Physical Review Letters* 91.12 (2003), p. 127402. DOI: 10.1103/PhysRevLett.91.127402.
- [Cru+15] P. Crump et al. "Joule-Class 940-nm Diode Laser Bars for Millisecond Pulse Applications". In: *IEEE Photonics Technology Letters* 27.15 (Aug. 2015), pp. 1663–1666. ISSN: 1941-0174. DOI: 10.1109/lpt.2015.2434095.

- [CZC14] Michael Chini, Kun Zhao, and Zenghu Chang. "The generation, characterization and applications of broadband isolated attosecond pulses". In: *Nature Photonics* 8.3 (Feb. 2014), pp. 178–186. ISSN: 1749-4893. DOI: 10.1038/nphoton.2013.362.
- [FN63] Lee M. Frantz and John S. Nodvik. "Theory of pulse propagation in a laser amplifier". In: *Journal of Applied Physics* 34.8 (Aug. 1963), pp. 2346–2349. ISSN: 1089-7550. DOI: 10. 1063/1.1702744.
- [GR18] Shambhu Ghimire and David A. Reis. "High-harmonic generation from solids". In: *Nature Physics* 15.1 (Nov. 2018), pp. 10–16. ISSN: 1745-2481. DOI: 10.1038/s41567-018-0315-5.
- [Hei+06] Thomas Heinzl et al. "On the observation of vacuum birefringence". In: *Optics Communications* 267.2 (2006), pp. 318–321. ISSN: 0030-4018. DOI: 10.1016/j.optcom. 2006.06.053.
- [IMM03] Vladimir V Ivanov, Anatoly Maksimchuk, and Gerard Mourou. "Amplified spontaneous emission in a Ti: sapphire regenerative amplifier". In: *Applied optics* 42.36 (2003), pp. 7231–7234. DOI: 10.1364/A0.42.007231.
- [Inn+90] M. E. Innocenzi et al. "Thermal modeling of continuous-wave end-pumped solid-state lasers". In: *Applied Physics Letters* 56.19 (May 1990), pp. 1831–1833. ISSN: 0003-6951. DOI: 10.1063/1.103083.
- [Jam+13] Venkatesan Jambunathan et al. "Spectroscopic characterization of various Yb3+ doped laser materials at cryogenic temperatures for the development of high energy class diode pumped solid state lasers". In: *High-Power, High-Energy, and High-Intensity Laser Technology; and Research Using Extreme Light: Entering New Frontiers with Petawatt-Class Lasers*. Vol. 8780. SPIE. 2013, pp. 77–85. DOI: 10.1117/12.2016915.
- [Kar+15] Felix Karbstein et al. "Vacuum birefringence in strong inhomogeneous electromagnetic fields". In: *Physical Review D* 92.7 (Oct. 2015), p. 071301. ISSN: 1550-2368. DOI: 10.1103/PhysRevD.92.071301.
- [Kep+16] Sebastian Keppler et al. "The generation of amplified spontaneous emission in high-power CPA laser systems". In: *Laser & photonics reviews* 10.2 (2016), pp. 264–277. DOI: 10.1002/lpor.201500186.
- [Kha68] A. Khadjavi. "Calculation of Solid Angle Subtended by Rectangular Apertures". In: *J. Opt. Soc. Am.* 58.10 (Oct. 1968), pp. 1417–1418. DOI: 10.1364/JOSA.58.001417.
- [KHK16] Jörg Körner, Joachim Hein, and Malte Christoph Kaluza. "Compact Aberration-Free Relay-Imaging Multi-Pass Layouts for High-Energy Laser Amplifiers". In: *Applied Sciences* 6.11 (Nov. 2016), p. 353. ISSN: 2076-3417. DOI: 10.3390/app6110353.
- [Koe+12] Joerg Koerner et al. "Measurement of temperature-dependent absorption and emission spectra of Yb:YAG, Yb:LuAG, and Yb:CaF2 between 20C and 200C and predictions on their influence on laser performance". In: *J. Opt. Soc. Am. B* 29.9 (Sept. 2012), pp. 2493–2502. DOI: 10.1364/JOSAB.29.002493.
- [Koe70] W. Koechner. "Absorbed Pump Power, Thermal Profile and Stresses in a cw Pumped Nd:YAG Crystal". In: *Appl. Opt.* 9.6 (June 1970), pp. 1429–1434. DOI: 10.1364/AO.9.001429.
- [Kör+11] J Körner et al. "Temperature dependent measurement of absorption and emission cross sections for various Yb3+ doped laser materials". In: *Diode-Pumped High Energy and High Power Lasers; ELI: Ultrarelativistic Laser-Matter Interactions and Petawatt Photonics; and HiPER: the European Pathway to Laser Energy.* Ed. by Joachim Hein et al. Vol. 8080. SPIE. SPIE, May 2011, p. 808003. Doi: 10.1117/12.887410.
- [Kör+19] Jörg Körner et al. "Novel unstable resonator configuration for highly efficient cryogenically cooled Yb:YAG Q-switched laser". In: *Opt. Express* 27.15 (July 2019), pp. 21622–21634. DOI: 10.1364/0E.27.021622.

- [Kos+15] S Kostić et al. "Study of structural and optical properties of YAG and Nd: YAG single crystals". In: *Materials Research Bulletin* 63 (2015), pp. 80–87. DOI: 10.1016/j.materresbull. 2014.11.033.
- [Kra+92] F. Krausz et al. "Femtosecond solid-state lasers". In: *IEEE Journal of Quantum Electronics* 28.10 (1992), pp. 2097–2122. ISSN: 0018-9197. DOI: 10.1109/3.159520.
- [Lin+99] Phillip P. Lin et al. "Multiwavelength output from a Nd:YAG/Cr:LiSAF hybrid laser". In: *Appl. Opt.* 38.9 (Mar. 1999), pp. 1767–1771. DOI: 10.1364/A0.38.001767.
- [McC64] D. E. McCumber. "Einstein Relations Connecting Broadband Emission and Absorption Spectra". In: *Phys. Rev.* 136 (4A Nov. 1964), A954–A957. DOI: 10.1103/PhysRev.136. A954.
- [Mil98] David Milam. "Review and assessment of measured values of the nonlinear refractive-index coefficient of fused silica". In: *Appl. Opt.* 37.3 (Jan. 1998), pp. 546–550. DOI: 10. 1364/A0.37.000546.
- [Mor97] M. Morin. "Graded reflectivity mirror unstable laser resonators". In: *Optical and Quantum Electronics* 29.8 (Aug. 1997), pp. 819–866. ISSN: 1572-817X. DOI: 10.1023/A:1018569331235.
- [Nie95] M. H. Niemz. "Threshold dependence of laser-induced optical breakdown on pulse duration". In: *Applied Physics Letters* 66.10 (Mar. 1995), pp. 1181–1183. ISSN: 0003-6951. DOI: 10.1063/1.113850.
- [Pay+92] S. A. Payne et al. "Infrared cross-section measurements for crystals doped with Er³⁺, Tm³⁺ and Ho³⁺". In: *IEEE Journal of Quantum Electronics* 28.11 (1992), pp. 2619–2630. ISSN: 0018-9197. DOI: 10.1109/3.161321.
- [Pil+14] Jan Pilar et al. "Characterization of diode-laser stacks for high-energy-class solid state lasers". In: *High-Power Diode Laser Technology and Applications XII*. Vol. 8965. SPIE. 2014, pp. 218–226. DOI: 10.1117/12.2042058.
- [R+19] Sundar R et al. "Laser Shock Peening and its Applications: A Review". In: *Lasers in Manufacturing and Materials Processing* 6.4 (Oct. 2019), pp. 424–463. ISSN: 2196-7237. DOI: 10.1007/s40516-019-00098-8.
- [Rob+07] C. Robilliard et al. "No "Light Shining through a Wall": Results from a Photoregeneration Experiment". In: *Physical Review Letters* 99.19 (Nov. 2007), p. 190403. ISSN: 1079-7114. DOI: 10.1103/PhysRevLett.99.190403.
- [SC97] F Sánchez-Bajo and FL Cumbrera. "The use of the pseudo-Voigt function in the variance method of X-ray line-broadening analysis". In: *Journal of Applied Crystallography* 30.4 (Aug. 1997), pp. 427–430. ISSN: 0021-8898. DOI: 10.1107/s0021889896015464.
- [Sch+08] H-P Schlenvoigt et al. "A compact synchrotron radiation source driven by a laser-plasma wakefield accelerator". In: *Nature Physics* 4.2 (2008), pp. 130–133. ISSN: 1745-2481. DOI: 10.1038/nphys811.
- [SGW00] M. Schmid, Th. Graf, and H. P. Weber. "Analytical model of the temperature distribution and the thermally induced birefringence in laser rods with cylindrically symmetric heating". In: *J. Opt. Soc. Am. B* 17.8 (Aug. 2000), pp. 1398–1404. DOI: 10 . 1364 / JOSAB . 17 . 001398.
- [SHW81] W. Simmons, J. Hunt, and W. Warren. "Light propagation through large laser systems". In: *IEEE Journal of Quantum Electronics* 17.9 (1981), pp. 1727–1744. DOI: 10.1109/JQE. 1981.1071337.
- [Tam+18] Issa Tamer et al. "Spatio-Temporal Characterization of Pump-Induced Wavefront Aberrations in Yb3+-Doped Materials". In: *Laser & Photonics Reviews* 12.2 (2018), p. 1700211. DOI: 10.1002/lpor.201700211.

- [Woo98] RM Wood. "Laser induced damage thresholds and laser safety levels. Do the units of measurement matter?" In: *Optics & Laser Technology* 29.8 (1998), pp. 517–522. DOI: 10.1016/S0030-3992(97)00054-6.
- [Zhu+13] HY Zhu et al. "Highly efficient continuous-wave Nd: YAG ceramic lasers at 946 nm". In: *Laser Physics Letters* 10.7 (2013), p. 075802. DOI: 10.1088/1612-2011/10/7/075802.

Theses

- [Bey20] Martin Beyer. "Characterization of optical components of a laser amplifier via spectral interferometry". Bachelor's Thesis. 2020.
- [Mäu19] Max Mäusezahl. "Untersuchung lasergetriebener Protonenbe-schleunigung bezüglich Vorplasmaerzeugungund räumlicher Protonendetektion". Master's Thesis. 2019.

Online

- [Com07] Wikimedia Commons. *Tiefendosiskurven*. 2007. URL: https://upload.wikimedia.org/wikipedia/commons/c/c8/Tiefendosiskurven.svg (visited on 10/25/2008).
- [Com20] Wikimedia Commons. Zernike polynomials with read-blue cmap. 2020. URL: https://commons.wikimedia.org/wiki/File:Zernike_polynomials_with_read-blue_cmap.png.
- [Pas05a] R. Paschotta. YLF Lasers. 2005. DOI: 10.61835/ark. URL: https://www.rp-photonics.com/ylf_lasers.html (visited on 10/07/2025).
- [Pas05b] R. Paschotta. *Ytterbium-doped Laser Gain Media*. 2005. DOI: 10.61835/zdc. URL: https://www.rp-photonics.com/ytterbium_doped_laser_gain_media.html (visited on 11/09/2024).
- [Pas07] R. Paschotta. Laser Crystals. 2007. DOI: 10.61835/pw6. URL: https://www.rp-photonics.com/laser_crystals.html (visited on 11/09/2024).

Index

ABCD-matrix, 58	excited state absorption, 30
absorption	
coefficient, 9	Faraday roatator, 82
cross section, 9	fast axis, see laser diode
actuator, see deformable mirror	fluence
air breakdown, 98	extractable, 45
amplified spontaneous emission, 86	saturation, 49
angular acceptance, 87	fluorescence lifetime, 10
polarization acceptance, 88	Frantz-Nodvik, 51
spectral acceptance, 88	Füchtbauer-Ladenburg equation, 18
amplifier	
multipass	gain, 10
butterfly, 83	reduction, 55
imaging, 83	saturation
regenerative, 81	CW, 72
AOM, 74	saturation corrected, 54
autocorrelator, 112	small signal, 48
	Gaussian beam, 62
B-Integral, 46, 92	beam radius, 62
beam break up, 92	radius of curvature, 62
beam parameter product, 107	ghost focus, 85
beam quality factor, 108	glass, 28
	Gouy phase, 63
CaF ₂ , 28	
cavity dump, 76	heat fraction, 11
cavity time constant, 71	:
Cr:YAG, 75, 89	intensity
cross section	saturation, 41
absorption, 9	inversion, 39
temperature dependence, 35	equilibrium, 39
crystal, 27	kerr effect, 92
deformable mirror, 110	1011 011001, 02
degeneracy, 20	Lambert Beer, 9
doping concentration, 32	Lambert Beer's law, 24
doping concentration, 62	laser diode, 99
edge steepening, 94	current-voltage characteristic, 100
efficiency	fast axis, 101
storage, 45	output spectrum, 100
Einstein cofficients, 13	slow axis, 101
Einstein relations, 15	laser diode stack, 102
energy levels, 23	laser manifold, 38
etalon, 79	level scheme, 37

LIDT, 46, 90	refractive index
line broadening	nonlinear, 92
homogeneous, 16	relaxation oscillation, 73
inhomogeneous, 16	resonator parameters, 60
line function, 19	resonator stability diagram, 61
Lyot filter, 79	,
	saturable absorber, 75
M ² , see beam quality factor	saturation
matrix	fluence, 11, 49
inverse optical setup, 59	Frantz-Nodvik, 51
lens, 58	intensity, 41
propagation, 58	self focusing, 92
McCumber relation, 21	SESAM, 78
Michelson interferometer, 117	Shack-Hartmann sensor, 109
micro lens array, 103	single mode, 79
focal length, 104	slow axis, <i>see</i> laser diode
mode locking, 77	specific heat capactiy, 96
active, 77	spectral
Kerr lens, 78	intensity, 114
passive, 77	interferometery, 116
mode matching, 82	phase, 114, 116
multi phonon relaxation, 30	spectrometer
	grating, 115
Nd:YAG, 31	prism, 114
number density, 32	speed of light
	numerical value, 13
output coupling, 72	stability criterion, 60
par-axial approximation, 57	storage efficiency, 44, 45
partition function, 20	sum frequency generation, 112
photon density, 38, 51	
Planck constant, 13	TFP, 82
Pockels cell, 74	thermal conductivity, 96
POLARIS, 102	thermal lens, 95, 96
	optical path density, 97
polarizer, 82 pulse contrast measurement, 113	Ti:Sa, 31, 78
pulse length, 112	time bandwidth product, 77
-	
pump rate 30	unstable cavity, 66
pump rate, 39	gain modulation, 69
q-Parameter, 63	graded reflectivity mirror, 68
Q-switch, 74	hard edge, 66
quality factor, 71	magnification, 67
quantum defect, 11	Voigt profile 17
quantum efficiency, 30	Voigt profile, 17
<u>,</u>	wavefront adaptation, 110
radiance, 108	wavefront analysis, 109
rate equation	, 0.0, 200
Einstein, 14	YAG, 32
inversion, 39	Yb:CaF ₂ , 23, 31
laser cycle, 38	Yb:FP15, 23, 31, 91
pump rate, 40	Yb:LiMgAS, 23, 31

Yb:YAG, 23, 27, 31, 89, 94

Zernike polynomials, 110 zero phonon line, 21